Characterisation of two essential proteins for host cell egress and invasion identified by phenotypic screening in *Toxoplasma gondii*

von Wei Li

Inaugural-Dissertation zur Erlangung der Doktorwürde

(Dr. rer. biol. vet.)

der Tierärztlichen Fakultät der Ludwig-Maximilians-Universität München

Characterisation of two essential proteins for host cell egress and invasion identified by phenotypic screening in *Toxoplasma gondii*

von Wei Li

aus Sichuan (China)

München 2023

Aus dem Lehrstuhl für Experimentelle Parasitologie der Tierärztlichen Fakultät der Ludwig-Maximilians-Universität München

Lehrstuhl für Experimentelle Parasitologie

Arbeit angefertigt unter der Leitung von:

Univ.-Prof. Dr. Markus Meißner

Mitbetreuung durch: Dr. Elena Jimenez-Ruiz

Gedruckt mit Genehmigung der Tierärztlichen Fakultät der Ludwig-Maximilians-Universität München

Dekan:	Univ.-Prof. Dr. Reinhard K. Straubinger, Ph.D.
Berichterstatter:	Univ.-Prof. Dr. Markus Meißner
Korreferenten:	Univ.-Prof. Dr. Katrin Hartmann
	Univ.-Prof. Dr. Dr. h. c. Gerd Sutter
	Univ.-Prof. Dr. Eckhard Wolf
	Univ.-Prof. Dr. Marcia Ferraz

Tag der Promotion: 11. Februar 2023

My Love

For my parents

TABLE OF CONTENTS

TABLE OF CONTENTS

TABLE OF CONTENTS

LIST OF ABBREVIATIONS

Aa	Amino acid
AAMT	Apical annuli methyltransferase
ABA	Abscisic acid
ABPs	Actin-binding proteins
ACT1	Actin1
ADF	Actin depolymerising factor
AID	Auxin-inducible degron
AKMT	Apical complex lysine (K) methyltransferase
ALIX	Apoptosis-linked gene 2-interacting protein
ATc	Anhydrotetracycline
APH	Acylated pleckstrin homology domain–containing protein
APR	Apical polar ring
ARP2/3	Actin-related protein 2/3 complex
AMA1	Apical membrane antigen 1
BFD1	Myb-like transcription factor
BioID	Biotin identification
bp	Base pair
CAP	Cyclase-associated protein
Cb	Chromobody
CbEm	Chromobody-emeraldFP
CD2AP	CD2-associated protein
CDC50.1	Cell division control 50.1
cAMP	Cyclic adenosine monophosphate
cGMP	Cyclic guanosine monophosphate
Ci	Calcium ionophores
CIN85	CBL-interacting protein of 85 kDa
cKO	Conditional knockout
CLAMP	Claudin-like apicomplexan microneme protein
CGP	Conoid gliding protein
CRISPR Cas9	Clustered regularly interspaced short palindromic repeats and CRISPR-associated protein 9
CDPKs	Calcium-dependent protein kinases
DAG	Diacylglycerol
DAP1	Dispensable protein 1
dd	Destabilisation domain

LIST OF ABBREVIATIONS

DGK1	Diacylglycerol kinase 1
DGK2	Diacylglycerol kinase 2
DHFR	Dihydrofolate reductase
DIC	Differential interference contrast
DiCre	Dimerisable recombinase
DOC2.1	Double C2 domain-containing protein
DSB	Double-strand break
RlmN	rRNA large subunit methyltransferase gene N
Elp3	Elongator protein-3
ER	Endoplasmic reticulum
EM	Electron microscopy
FACS	Fluorescence-activated single cell sorting
F-actin	Filamentous actin
FDR	False discovery rate
FH	Formin homology
FPS	Frames per second
FRM1	Formin 1
FRMs	Formins
GABA	γ-aminobutyric acid
GAC	Glideosome-associated connector
G-actin	Globular actin
GAP40	Gliding-associated protein 40
GAP50	Gliding-associated protein 50
GAPM	Glideosome-associated protein with multiple-membrane spans
GIC	Gliding initiation complex
GC	Guanylate cyclase
GOI	Gene of interest
HFFs	Human foreskin fibroblasts
HiT	High-throughput
hpi	Hours post induction
HR	Homologous recombination
IAA	3-indoleacetic acid
ICAP16	Indispensable conserved apicomplexan protein 16
IFA	Immunofluorescence assay
Indels	Insertions and deletions mutations
IMC	Inner membrane complex
IP3	Inositol triphosphate
IVN	Intravacuolar network

LIST OF ABBREVIATIONS

KD	Knock-down
KO	Knock out
LC-MS/MS	Liquid chromatography with tandem mass spectrometry
mAID	Minimal auxin-inducible degron
MICs	Microneme proteins
MJ	Moving junction
MLC1	Myosin light chain 1
MTOC	Microtubule organisation centre
Mn	Microneme
MyoA	Myosin A
MyoH	Myosin H
N.A.	Numerical aperture
NCBI	National Institute for Biotechnology Information
ND	Non-discharge
NEB	New England Biolabs
NES	Nuclear export sequence
NHEJ	Non-homologous end joining
NIH	National Institutes of Health
NLSs	Nuclear localisation sequences
ORF	Open reading frame
ANOVA	One-way analysis of variance
PA	Phosphatidic acid
PAGE	Polyacrylamide gel electrophoresis
PAP	Phosphatidic acid phosphatase
PCKMT	Preconoidal lysine methyltransferase
Pcrs	Preconoidal proteins

LIST OF ABBREVIATIONS

PCRs	Preconoidal rings
PDE	Phosphodiesterase
PI(4,5)P2	Phosphatidylinositol 4,5-bisphosphate
PI-PLC	Phosphoinositide phospholipase
PKAc1	Protein kinase A catalytic 1 domain
PKAr1	PKA regulatory subunit
PKG	Protein kinase G
PLP1	Perforin-like protein 1
PLV	Plant-like vacuole
PM	Plasma membrane
POI	Protein of interest
pPM	Parasite plasma membrane
PV	Parasitophorous vacuole
PVM	PV membrane
rSAM	Radical S-adenosylmethionine
RB	Residual body
Rh	Rhoptry
ROI	Regions of interest
RONs	Rhoptry neck proteins
RoPs	Rhoptry bulb proteins
SAGs	Surface antigens
SAS6L	Spindle assembly abnormal 6-like
sCas9	Split Cas9
SD	Standard deviation
sgRNA	Single guide RNA
Shld1	Shield-1
SLF	Signalling linking factor

LIST OF ABBREVIATIONS

SPMTs	Subpellicular microtubules
ssDNA	Single-stranded DNA
TATi	Trans-activator trap identified
TBS	Tris-Buffered saline
TE	Toxoplasmic encephalitis
TFP1	Transporter facilitator protein
TPR	Tetratricopeptide
TSG101	Tumour susceptibility gene 101 protein
U1snRNP	U1 small nuclear ribonucleic particle
UGO	Unique GC organizer
uprt	*Uracil phosphoribosyltransferase gene*
VAC	Vacuolar compartment
WHO	World Health Organization
WT	Wildtype

LIST OF FIGURES

LIST OF FIGURES

LIST OF FIGURES

LIST OF TABLES

LIST OF TABLES

I. INTRODUCTION

1. The phylum of Apicomplexa and *T. gondii*

The phylum of Apicomplexa, as obligate intracellular parasites, consists of more than 6,000 described unicellular protozoa. Apicomplexa are divergent from mammalian cells but closely related to ciliates and dinoflagellates, which are classified as the superphylum Alveolata, characterised by the presence of alveoli (Sato 2011, Francia et al. 2015, Koreny et al. 2021). The Apicomplexa phylum consists of the families Hematozoa, Coccidia, Gregarines and Cryptosporidium, which are capable of infecting a variety of vertebrate and invertebrate hosts. Most apicomplexan parasites are pathogenetic to their host, and some cause serious diseases in poultry or livestock, such as coccidiosis (caused by Coccidia), babesiosis (caused by *Babesia* spp.), theileriosis (caused by *Theileria* spp.), and besnoitiosis (caused by *Besnoitia* spp.). These lead to economic loss and thus have both veterinary and economical importance (Zintl et al. 2003, Sato 2011, Gutiérrez-Expósito et al. 2016, Song et al. 2018, López-Osorio et al. 2020).

Regarding human health, *Cryptosporidium* spp. is an opportunistic parasite. It is regarded as a waterborne disease and the second most common cause of diarrhoea in children after rotavirus. People infected with *Cryptosporidium* spp. range from asymptomatic to experiencing diarrhoea and even death, especially in small children and immunocompromised individuals, such as those who are HIV-positive (Sponseller et al. 2014, Khan et al. 2018). The study of the biology of this pathogen has recently increased thanks to the establishment of

new molecular tools for genetic modification and propagation in mice (Vinayak et al. 2015).

The most widely studied Apicomplexa parasites are *Plasmodium* spp. and *Toxoplasma* spp., which are regarded as model organisms for Apicomplexa parasites and human pathogens. *Plasmodium* are the most lethal Apicomplexa parasites for humans, transmitted by female Anopheles mosquito bites (Alkema et al. 2021). Five *Plasmodium* species are reported to cause human malaria, among which *P. falciparum* and *P. vivax* are the most life-threatening. According to the World Malaria Report 2020 released by the World Health Organization (WHO), an estimated 229 million new malaria cases occurred and over 400,000 people died in 2019 (https://www.who.int/teams/global-malaria-programme/reports/world-malaria-report-2020).

The *Toxoplasma* genus consists of only one species, *Toxoplasma gondii*. Unlike other Apicomplexa parasites, it can infect virtually any nucleated cell derived from warm-blooded animals. *T. gondii* belongs to the cyst-forming Coccidia and was first identified in a hamster-like rodent, *Ctenodactylus gundi*, in 1908 (Nicolle et al. 1908). Toxoplasmosis affects approximately one third of the world's population, causing widespread concern. People who are immunocompetent and positive for this pathogen usually are asymptomatic or have flu-like symptoms. However, primary infection in pregnant women may pose a threat to foetuses since this protozoan parasite can penetrate the placenta, infect the foetus and result in multiple symptoms, including hydrocephalus, organ damage and

abortion. In most cases, there are no obvious symptoms at birth or complications later in life if the infection occurs before pregnancy except for infection close to conception (Rorman et al. 2006, Chaudhry et al. 2014, Caldas et al. 2018). Notably, ocular toxoplasmosis resulting from both congenital and acquired infection is nonnegligible in immunocompetent individuals since it is the leading cause of infectious posterior uveitis (Saadatnia et al. 2012). *T. gondii* infection is also risky for immunocompromised patients because reactivation of latent infection can result in life-threatening toxoplasmic encephalitis (TE).

In addition to humans, *T. gondii* causes a production impact on domestic animals such as sheep, pigs and cattle. The flesh of infected animals might also be a cause of infection for people (Dubey 2009, Stelzer et al. 2019, Dubey et al. 2020). Even though *T. gondii* has been known for over a century and has a significant public health impact, no human vaccinations are currently available, and drugs allowed for the treatment of toxoplasmosis such as pyrimethamine and sulfadiazine have limitations in use because of their side effects and parasite drug resistance. Moreover, no current drug can clear *T. gondii* cysts (Kur et al. 2009, Konstantinovic et al. 2019).

2. The life cycle of *T. gondii*

T. gondii, unlike *Cryptosporidium* and other apicomplexan parasites, has a dixenous life cycle, requiring distinct hosts to complete: asexual stages in intermediate species (virtually any warm-blooded animal) and sexual stages that only occur in felids (definitive host; Figure I-1;

Hunter et al. 2012, Robert-Gangneux et al. 2012). Notably, *T. gondii* transmission is not restricted to intermediate hosts and definitive hosts; it may also occur between intermediate hosts without the need for the sexual cycle to be completed (Robert-Gangneux et al. 2012).

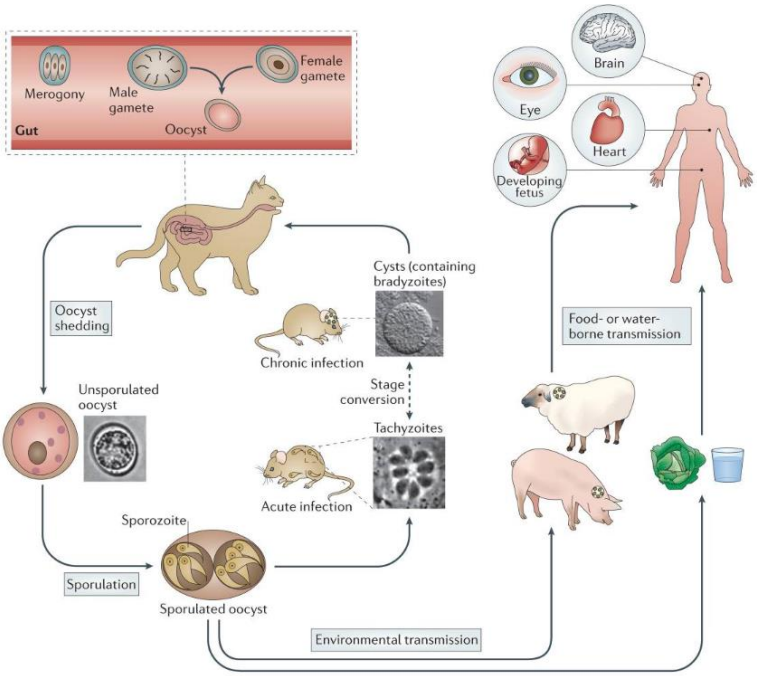

Figure I-1. The life cycle of *T. gondii*.

A diagram depicting the life cycle of *T. gondii* in its various hosts and the transmission routes. *T. gondii* infections in definitive hosts result in the development of oocysts via the processes of merogony and fertilisation. Oocysts undergo sporogony after being expelled into the environment and contaminate food and water. Ingestion of sporulated oocysts by intermediate hosts initiates the infection, where sporozoites transform into tachyzoites that multiply rapidly by a special replication process called endodyogeny (see section 2.2.2) and cause acute infection. Shortly after, tachyzoites convert into bradyzoite-consisting cysts causing chronic infection. The ingestion of tissue cysts by definitive hosts initiates a new life cycle. Images copied from (Hunter et al. 2012) with licence number 5387730194535.

2.1 *T. gondii* development in hosts

Feline hosts, such as domestic and feral cats, are the definitive hosts of *T. gondii*; they become infected by eating cyst-carrying meat, such as infected mice. Following digestion in the stomach and intestines, the cysts rupture, and parasites replicate within the gut enterocyte via merogony, resulting in the formation of male and female gametes. These are further fertilised into diploid oocysts that are discharged into the environment by faeces (Figure I-1; Hunter et al. 2012, Frénal et al. 2017). Oocyst shedding in cats typically lasts for one to two weeks and then ceases. A cat may discharge millions of unsporulated oocysts in its faeces, resulting in environmental pollution (Hill et al. 2002, Robert-Gangneux et al. 2012).

Oocysts might live for months to years under the protection of the oocyst wall, a multi-layered structure, if the environment is non-aggressive, i.e. in a moist environment (such as wet soil and fresh and marine waters) with a range of temperatures (-20 to +37 °C). Although the oocyst is resilient to chemical agents such as detergents and disinfectants, it is not resistant to high temperatures over 45 °C. The oocyst's high survivability in external conditions allows it to infect a variety of hosts (Hill et al. 2002, Robert-Gangneux et al. 2012, Freppel et al. 2019). Once the oocysts are exposed to the environment, they sporulate (sporogony) and develop sporozoites inside the oocyst, a process that typically takes several days (Figure I-1). The oocysts contaminate vegetables, water and other materials that may be consumed by intermediate hosts, which include mammals and birds. The haploid sporozoites are one of the invasive forms of *T. gondii*.

After ingestion of the oocyst, the sporozoites are released and infect the host's intestines, transforming into tachyzoites, which are the fast-replication form of *T. gondii*. This stage often results in acute and potentially severe infection in hosts, although it could be asymptomatic. The parasites multiply fast, exit the infected cell and infect neighbouring cells for several cycles. This cycle, also known as the lytic cycle, is discussed in length in section 2.2. Under the stress of the host immune system, tachyzoites transform into bradyzoites, a slow-dividing yet infectious stage, and develop cysts in the brain, muscles and other organs, where persistent infection occurs (Figure I-1; Robert-Gangneux et al. 2012, Blader et al. 2015). Of relevance, myb-like transcription factor (BFD1) is a newly found key factor involved in tachyzoite-to-bradyzoite differentiation by binding to promoters of many stage-specific genes and regulating their expression, acting as a master regulator of differentiation in *T. gondii* (Waldman et al. 2020). When the host's immune system is compromised, bradyzoites may redifferentiate into tachyzoites, causing harm to the infected organ and often encephalitis.

2.2 Lytic cycle of *T. gondii*

Before invading a host cell for multiplication, *T. gondii* searches for a suitable host cell to invade. Active orientation and penetration of the host cell facilitate the process of host cell invasion. Following the invasion, the parasite multiplies inside the parasitophorous vacuole (PV) for 6–8 rounds (64–256 parasites per PV), culminating in the lysis of the host cell. Once

extracellular, they glide and infect adjacent cells to initiate a new lytic cycle (Figure I-2).

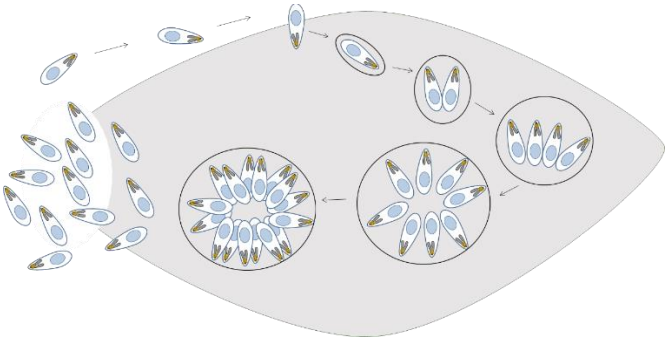

Figure I-2. The lytic cycle of *T. gondii*.

After successfully invading host cells, the parasites form a parasitophorous vacuole and divide inside through endodyogeny. Eventually, they leave the host cell and infect new adjacent cells, employing gliding motility.

2.2.1 Invasion

As an obligatory intracellular parasite, effective invasion is necessary for parasite survival; this involves the successive and sequential secretion of proteins: micronemes and rhoptries. Invasion is an active and orchestrated process that takes place within minutes. The parasites initially attach to the host cell surface via GPI-anchored surface antigens (SAGs), orientate themselves for entry into the host cells and sequentially secrete proteins (Carruthers et al. 2007). Penetration of the parasite occurs via a tight or moving junction (MJ) formed by different proteins from the parasite and host cell (Figure I-3). Microneme proteins such as apical membrane antigen 1 (AMA1), which are secreted on the plasma membrane as adhesins, are a component of the MJ alongside rhoptry proteins such as RON2, a

short extracellular domain of which is inserted into the plasma membrane of the host cell, and the cytosol part of which forms a complex with RON4/RON5/RON8 (RON complex) in the host cell cytosol and binds to AMA1 (Figure I-3; Alexander et al. 2005, Straub et al. 2009, Frénal et al. 2017, Lentini et al. 2021). Some host cell proteins are recruited to the MJ and probably interact with host cell actin and actin-binding proteins (Figure I-3; Guérin et al. 2017). In conjunction with parasites' glideosome (see section 4.4.1), the MJ translocates from the apical to the basal pole during parasite penetration into host cells. After the parasites are completely internalised into the host cell, a non-fusogenic PV is produced from the invagination of the host plasma membrane and decorated with rhoptry proteins to surround the parasites and offer a safe environment for parasite growth inside the cell (Figure I-3; Sweeney et al. 2010, Portes et al. 2020).

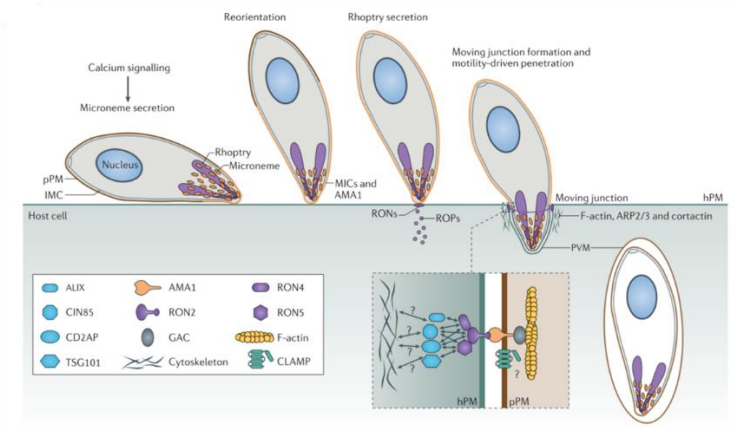

Figure I-3. Invasion process of *T. gondii*.

Microneme and rhoptry proteins are secreted in sequence after attachment to the host cell, and the MJ, which is composed of the RON complex and AMA1, is produced afterwards. The RON complex actively recruits some host cell proteins, including TSG101, CD2AP, CIN85 and ALIX to the MJ for efficient host cell invasion. Host cell actin, ARP2/3 and cortactin might interact with CD2AP, CIN85 and ALIX to stabilise the MJ. Claudin-like apicomplexan microneme protein (CLAMP) is involved in invasion, but its exact role is uncertain. Parasite penetration into host cells is aided by the parasites' gliding movement. The PV is generated once the parasite has fully penetrated the cells. The interactions between the glideosome and the MJ and the interactions between the MJ and host proteins are highlighted in the enlarged picture (inset). Abbreviations: ALIX: apoptosis-linked gene 2-interacting protein X; ARP2/3: actin-related protein 2/3 complex; CD2AP: CD2-associated protein; CIN85: CBL-interacting protein of 85 kDa; CLAMP: claudin-like apicomplexan microneme protein; GAC: glideosome-associated connector; IMC: inner membrane complex; pPM: parasite plasma membrane; PVM: parasitophorous vacuole; RONs: rhoptry neck proteins; RoPs: rhoptry bulb proteins; TSG101: tumour susceptibility gene 101 protein. Image copied from (Frénal et al. 2017) with licence number 5387730474718.

2.2.2 Replication

T. gondii replicates via endodyogeny, in which a single cycle of DNA replication is soon followed by nuclear division and two daughter cells emerge from within a mother cell rather than fission of the mother cell (Figure I-4; Francia et al. 2014). After mitosis, mammalian cells undergo cytokinesis, which results in the generation of daughter offspring. In contrast, *T. gondii* cytokinesis occurs before the completion of mitosis (Francia et al. 2014). The course of the cell cycle is highly regulated and sequential. Each replication takes six to seven hours to complete (Anderson-White et al. 2012).

During replication, centrosomes and the Golgi complex are the first organelles that duplicate, followed by division while the apicoplast elongates (Hartmann et al. 2006, Nishi et al. 2008, Anderson-White et al. 2012). Daughter conoids are formed, and IMC assembly begins. Eventually, certain daughter cell IMCs, including IMC1, reach from the apical to the basal end (Hu et al. 2002, Anderson-White et al. 2012). The extension of the daughter cell IMCs is contemporaneous with the

separation, migration and division of organelles such as the apicoplast, nucleus, and endoplasmic reticulum (ER) into the developing daughter cells (Figure I-4B; Nishi et al. 2008). Notably, during nucleus mitosis, unlike human cell division, the nuclear envelope of *T. gondii* parasites stays intact and chromosomes do not condense. This characteristic is conserved across apicomplexan parasites (Francia et al. 2014). Micronemes and rhoptry proteins are mostly synthesised *de novo* (Nishi et al. 2008). Once the daughter cell IMC development is complete, mitochondria enter the cell. In the last stage, mature daughter cells develop from mother cells, and the plasma membranes of the mother cells and freshly generated plasma membranes are incorporated into the daughter cells (Figure I-4C; Anderson-White et al. 2012, Gubbels et al. 2020). At the end of the budding process, the remnant of the mother cell transforms into the residual body (RB) connecting the newly formed cells (Frénal et al. 2017, Periz et al. 2017).

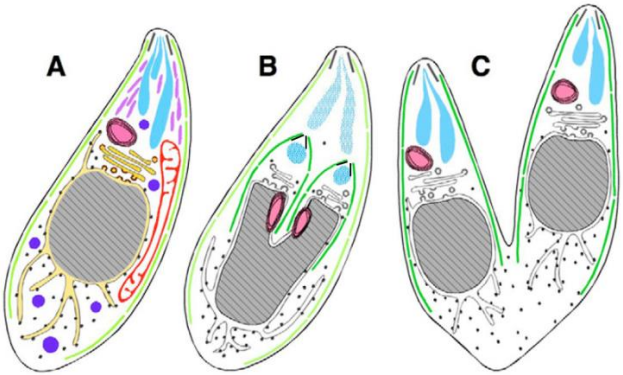

Figure I-4. Endodyogeny of *T. gondii* tachyzoites.

A) Interphase parasites that have not yet begun to bud. The centrosomes, the Golgi complex, and the apicoplast are tightly associated with the nucleus. The various organelles are shown in different colours: conoids (black lines), IMCs (light green lines), rhoptries (turquoise), micronemes (lavender), dense granules (blue), apicoplasts (pink), mitochondria (red), the Golgi complex (gold), nuclei (grey) and ER (yellow). B) The daughter IMC scaffold (dark green) and daughter conoids (black) are formed, with divided Golgi complexes and the apicoplast, and a lobbed nucleus. The degradation of maternal rhoptries is shown by hatching in turquoise. C) Daughter cells soon arise and acquire plasma membrane from the mother cell. Note: in B) and C), other organelles are not coloured or shown. Images copied from (Nishi et al. 2008) with the licence number 1268625-1.

2.2.3 Egress

Egress is regarded as the last step of the lytic cycle, which is critical for parasite survival and pathogenicity. Microneme secretion, parasite motility and egress are all intertwined. Parasite egress requires the activation of microneme secretion and gliding, but the exact signalling mechanisms governing those processes are yet unknown. Commonly used compounds and chemicals that act on this signalling pathway are summarised in Table I-1.

Table I-1. List of inducers and inhibitors commonly used in the *T. gondii* signalling cascade of microneme secretion and egress.

Description	Chemical Name	Molecular Formula	Mechanism of Action	Reference
BIPPO	5-Benzyl-3-isopropyl-1h-pyrazolo[4,3-d]pyrimidin-7(6h)-one	$C_{15}H_{16}N_4O$	Inhibitors of phosphodiesterase	(Bisio et al. 2019)
Calcium ionophore A23187	5-(methylamino)-2-[[(2S,3R,5R,8S,9S)-3,5,9-trimethyl-2-[1-oxo-1-(1H-pyrrol-2-yl)propan-2-yl]-1,7-dioxaspiro[5.5]undecan-8-yl]methyl]-1,3-benzoxazole-4-carboxylic acid	$C_{29}H_{37}N_3O_6$	Leading to an increase in cytosolic Ca^{2+}	(Endo et al. 1982)
Propranolol	1-naphthalen-1-yloxy-3-(propan-2-ylamino)propan-2-ol	$C_{16}H_{21}NO_2$	Inhibitor of phosphatidic acid phosphatase	(Bisio et al. 2019)

Nigericin	(2R)-2-[(2R,3S,6R)-6-[[(2S,4R,5R,6R,7R,9R)-2-[(2R,5S)-5-[(2R,3S,5R)-5-[(2S,3S,5R,6R)-6-hydroxy-6-(hydroxymethyl)-3,5-dimethyloxan-2-yl]-3-methyloxolan-2-yl]-5-methyloxolan-2-yl]-7-methoxy-2,4,6-trimethyl-1,10-dioxaspiro[4.5]decan-9-yl]methyl]-3-methyloxan-2-yl]propanoic acid	$C_{40}H_{68}O_{11}$	Causing an efflux of K^+ from host cell	(Fruth et al. 2007)
Thapsigargin	[(3S,3aR,4S,6S,6aR,7S,8S,9bS)-6-acetyloxy-4-butanoyloxy-3,3a-dihydroxy-3,6,9-trimethyl-8-[(Z)-2-methylbut-2-enoyl]oxy-2-oxo-4,5,6a,7,8,9b-hexahydroazuleno[4,5-b]furan-7-yl] octanoate	$C_{34}H_{50}O_{12}$	Inhibitor of the sarcoplasmic-endoplasmic reticulum calcium ATPase (SERCA), resulting in elevated calcium	(Nagamune et al. 2007)
Zaprinast	2-(2-Propyloxyphenyl)-8-azapurin-6-one	$C_{13}H_{13}N_5O_2$	Inhibitors of phosphodiesterase	(Sidik et al. 2016)
Dithiothreitol (DTT)	(2S,3S)-1,4-Dimercaptobutane-2,3-diol	$C_4H_{10}O_2S_2$	Inducing Ca^{2+} flux	(Stommel et al. 1997)
Ethanol		C_2H_6O	Leading to an increase in intracellular Ca^{2+}	(Donahue et al. 2000, Arrizabalaga et al. 2004)
Compound 1	Tri-substituted pyrrole 4-[2-(4-fluorophenyl)-5-(1-methylpiperidine4-yl)-1H-pyrrol-3-yl]pyridine	$C_{21}H_{22}FN_3$	Inhibitor of PKG	(Donald et al. 2002)
3-MB-PP1	1-(1,1-dimethylethyl)-3-[(3-methylphenyl)methyl]-1H-pyrazolo[3,4-d]pyrimidin-4-amine	$C_{17}H_{21}N_5$	Inhibition of CDPK1 by blocking the ATP binding site	(Lourido et al. 2010)
BAPTA-AM	1,2-Bis(2-aminophenoxy)ethane-N,N,N‘,N’-tetraacetic acid tetrakis(acetoxymethyl ester)	$C_{34}H_{40}N_2O_{18}$	Intracellular Ca^{2+} chelator	(Heaslip et al. 2011)
U73122	1-[6-[[(17β)-3-Methoxyestra-1,3,5(10)-trien-17-yl]amino]hexyl]-1H-pyrrole-2,5-dione	$C_{29}H_{40}N_2O_3$	Inhibitor of phospholipase C	(Moudy et al. 2001)

Parasites could escape at any stage of replication in response to extrinsic or intrinsic cues and remain invasive after egress, stimulating the invasion of other cells to ensure their survival (Hoff et al. 2002, Bisio et al. 2019). A low PH and K^+ induce parasite egress. The exact mechanisms of parasites sensing the K^+ and H^+ levels are still not clear, although guanylate cyclase (GC) is implicated in the process (Bisio et al. 2019, Günay-Esiyok et al. 2019). In early research, the plant hormone abscisic acid (ABA) was seen as an endogenous cue (quorum sensing) that prompts natural egress via the release of Ca^{2+} from the internal reserves (Nagamune et al. 2008). Nonetheless, the receptor platform for ABA detection and transduction remains unknown. More recently, it has been suggested that phosphatidic acid (PA) produced by diacylglycerol kinase 2 (DGK2) regulates the natural egress of *T. gondii* through the GC signalling complex, as opposed to the mammalian G-protein coupled receptors for signal detection, which are absent in apicomplexan parasites (Figure I-5; Bisio et al. 2019).

The GC signalling complex contains GC, unique GC organizer (UGO) and cell division control 50.1 (CDC50.1). It is distributed in the apical pole and RB of the parasite. The perception of signals by parasites initiates the signalling cascade in the parasite plasma membrane apex (Figure I-5). Two secondary messengers, cGMP and Ca^{2+}, are essential for signalling pathway activation. The activation of PKG not only leads to the increased level of parasite Ca^{2+} but also results in the formation of PA, which activates calcium-dependent protein kinases (CDPKs) and pleckstrin homology domain–containing protein (AHP) and finally mediates microneme secretion (Figure I-5; Bullen et al.

2016, Dubois et al. 2019; for recent reviews see Bisio et al. 2019, Carruthers 2019). In the process of egress, F-actin is disassembled (see section 4.4.2), PVM and PM of the host cell are permeabilised, and motility is initiated (see section 4.4.1), resulting in parasite exit from the host cell.

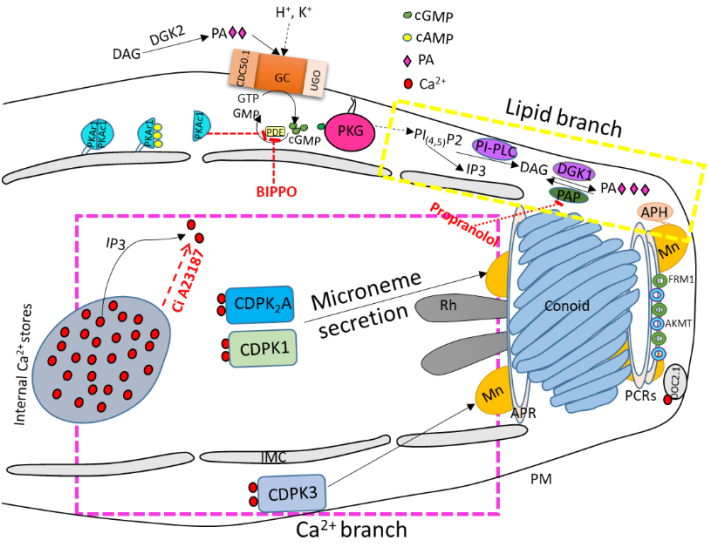

Figure I-5. Signalling cascade for egress of *T. gondii*.

After parasites detect signals based on the GC/CDC50.1/UGO complex, a signalling cascade involving the activation of PKG is initiated. The activation of PKG leads to the activation of downstream effectors and results in the generation of PA, which is sensed by APH and thus triggers microneme secretion (here referred to as lipid branch, shown in the yellow box). How PKG is connected to $PI(_{4,5})P2$ is unclear. When $PI(_{4,5})P2$ is hydrolysed by PI-PLC, it produces DAG and IP3. DAG forms PA through the activity of DGK1, and the production of PA accumulates at the PM and is sensed by APH, which is critical to microneme secretion (Bullen et al. 2016). IP3 likely raises the parasitic cytoplasm Ca^{2+} concentration by releasing Ca^{2+} from internal stores such as mitochondria, acidocalcisomes and ER, which activates CDPKs (CDPK3, CDPK1 and $CDPK_2A$) and further leads to microneme secretion and initiation of motility (here referred to as Ca^{2+} branch, shown in the magenta box; McCoy et al. 2012, Gaji et al. 2015, Bullen et al. 2016, Shortt et al. 2022). In this secretion, DOC2.1 protein may have a role in microneme exocytosis by facilitating membrane fusion via Ca^{2+}-dependent recruitment of membrane fusion machinery to the parasites' apical end (Farrell et al.

2012). The activation of PKAc1 negatively regulates egress since its activation results in phosphorylation and activation of PDEs (Jia et al. 2017, Uboldi et al. 2021). Abbreviations: AKMT, apical complex lysine (K) methyltransferase; APH, acylated pleckstrin homology domain–containing protein; APR, apical polar ring; cAMP, cyclic adenosine monophosphate; CDC50.1, cell division control protein 50.1; CDPKs, calcium-dependent protein kinases; cGMP, cyclic guanosine monophosphate; DAG, diacylglycerol; DGK1, diacylglycerol kinase 1; DGK2, diacylglycerol kinase 2; DOC2.1, double C2 domain–containing protein 1; FRM1, formin1; GC, guanylate cyclase; IMC, inner membrane complex; IP3, inositol triphosphate; PA, phosphatidic acid; PAP, phosphatidic acid phosphatase; PCRs, preconoidal rings; PDE, phosphodiesterase; $PI_{(4,5)}P2$, phosphatidylinositol 4,5-bisphosphate; PI-PLC, phosphoinositide phospholipase C; PKAc1, protein kinase A catalytic 1 domain; PKAr1, PKA regulatory subunit; PKG, protein kinase G; PM, plasma membrane; Mn, microneme; Rh, rhoptry; UGO, unique guanylate cyclase organizer.

3. The morphology of *T. gondii* tachyzoites

3.1 An overview of *T. gondii* tachyzoites' ultrastructure

The tachyzoites are crescentic in form, with a more pointed apical end and a more rounded basal pole (Figure I-6). The tachyzoites of *T. gondii* are approximately 2 µm in width and 6 µm in length. In 1954, Gustafson et al. described the ultrastructure of *T. gondii* revealed by electron microscopy (EM) for the first time (Gustafson et al. 1954). Like other eukaryotes, tachyzoites have a nucleus, an ER network associated with the nucleus, a Golgi complex, and a single mitochondrion, mostly in a lasso or open lasso shape, as well as an acidocalcisome inside their cytosol and a plasma membrane (PM) enclosing the entire parasite (Nishi et al. 2008, Mallo et al. 2021). Other organelles or structures include the IMC, a double membrane structure composed of flattened alveolar sacs (also known as alveoli), which is placed just beneath the plasma membrane. Specialised secretory organelles such as micronemes and rhoptries are situated in the apical region, forming an apical complex that includes intraconoidal microtubules and the conoid (see section 3.3). The apicoplast is positioned above the nucleus, and numerous apicoplast

enzyme proteins are involved in parasite metabolic activity. Its biosynthesis of fatty acids, heme and isoprenoid is crucial to the parasite's survival (Mazumdar et al. 2006, Nair et al. 2011, McFadden et al. 2017). A plant-like vacuole (PLV) or vacuolar compartment (VAC) controls proteolysis (McDonald et al. 2020). Another unique secretory organelle, the dense granule, accumulates proteins important for the maintenance of the infection within the host cell (Figure I-6; Griffith et al. 2022).

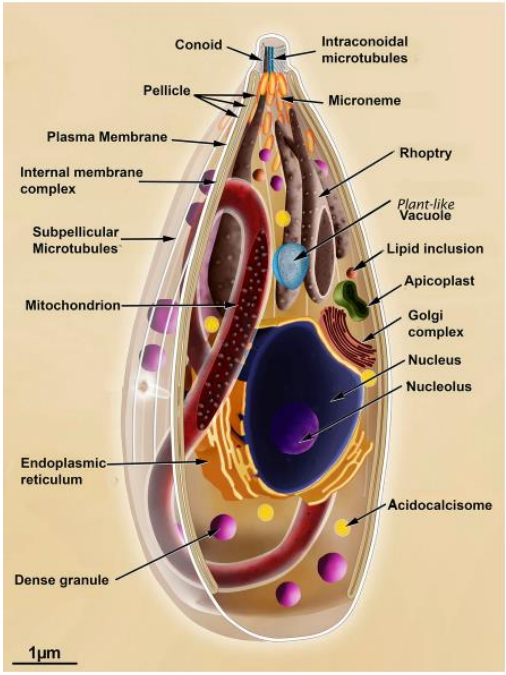

Figure I-6. Ultrastructure of *T. gondii* tachyzoites in longitudinal section view.

The basic components and organelles of the tachyzoite form of *T. gondii* are shown in this longitudinal section view. The endoplasmic reticulum surrounds the nucleus. The

Golgi complex and the apicoplast are visible above the nucleus. The cytosol distributes the solitary mitochondrion, dense granules and acidocalcisome. The cylindrical conoid, intraconoidal microtubules, micronemes and rhoptries are located in the apical region. Three membranes and 22 subpellicular microtubules surround the cell. Figure copied from (Attias et al. 2020).

3.2 The pellicle of *T. gondii* tachyzoites

The pellicle of tachyzoites has three layered membrane structures, the PM and the IMC, which are found in all alveolates (Figure I-7A). The distance between the IMC and PM is crucial for the function of gliding machinery. Underlying the IMC is an alveolin network made up of 10-nm intermediate filament-like proteins. This network connects the IMC with subpellicular microtubules and spans from the apical polar ring to the basal complex **(**Figure I-7A; Frénal et al. 2017, Dos Santos Pacheco et al. 2020). The IMC is classified into three compartments: apical cap, central and basal (Figure I-7B). The function of the IMC is not only to maintain the parasite's shape and stability but also to participate in its intracellular replication, motility and invasion (Egarter et al. 2014, Harding et al. 2016).

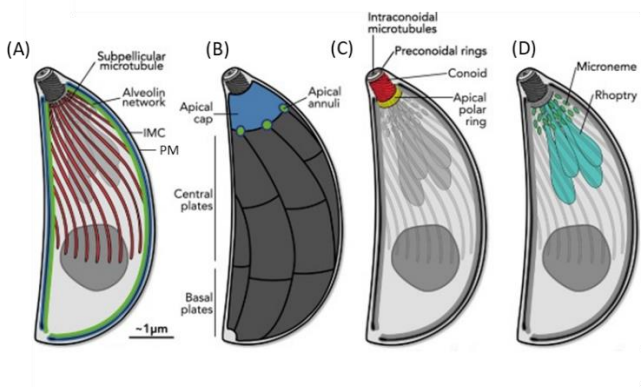

Figure I-7. The pellicle and apical complex of *T. gondii*.

(A) Diagram depicts the pellicle of the parasites. (B–D) The apical complex is comprised of the apical cap within IMC plates (B), the conoid complex (C) and the secretory organelles (D). Images copied from (Dos Santos Pacheco et al. 2020) with licence number 5387751290693.

3.3 The apical complex of *T. gondii*

The phylum Apicomplexa has the apical complex, which is one of the defining structures of apicomplexan parasites. The apical complex is in the apical area of the parasite and plays a significant role in host cell recognition, interaction and injection of proteins into host cells, making it vital for host cell attachment, gliding motility, invasion and egress. Understanding the apical complex can thus aid in understanding the biological process and help find a solution for controlling toxoplasmosis (Dos Santos Pacheco et al. 2020).

The apical complex is made up of the apical cap, the conoid complex and secretory organelles (rhoptries and micronemes; Figure I-7B-D). More than 250 proteins have been identified as belonging to the apical complex in a previous proteome-based study, and the recent localisation of organelle protein data also designates some proteins as belonging to the apical complex, but most lack validation of their localisations (Hu et al. 2006, Long et al. 2017, Long et al. 2017, Barylyuk et al. 2020). A recent study employing BioID techniques examined several apical proteins, and some were analysed further using super-resolution microscopy (Koreny et al. 2021). Although many proteins have been identified and localised to the apical complex, the biological function of many of them remains unclear. In the following overview, the identified, individual components of the apical complex are briefly described (for more information see a recent review: Dos Santos Pacheco et al. 2020).

3.3.1 Apical cap

The apical cap is a single cone-shaped IMC plate that is located at the most apical region of the IMC (Figure I-7B). The location of Centrin 2 at the annuli marks its border with the central IMC compartment (Leung et al. 2019). Several apical cap proteins have been identified and are important for the stability of the apical complex and parasite pathogenicity (Engelberg et al. 2020, Tosetti et al. 2020).

3.3.2 The conoid complex

The conoid is a barrel-like structure formed by tubulin-rich fibres that is associated with preconoidal rings (PCRs) and apical polar rings (APRs). Two intraconoidal microtubules are located inside the conoid. All of them constitute the conoid complex (Figure I-7C).

The conoid is a motile organelle that reacts to Ca^{2+} signalling inside the cell. As the Ca^{2+} concentration of tachyzoites increases, the conoid of parasites protrudes, emerging from within the APR (Figure I-8). Many conoid proteins have been identified and contribute to parasite fitness. For instance, the spindle assembly abnormal 6-like (SAS6L) protein localises to the conoid body; once depleted, parasites were less fit (de Leon et al. 2013, Koreny et al. 2021). Myosin H (MyoH), localising at the conoid body, is involved in parasite invasion, motility and egress (Graindorge et al. 2016).

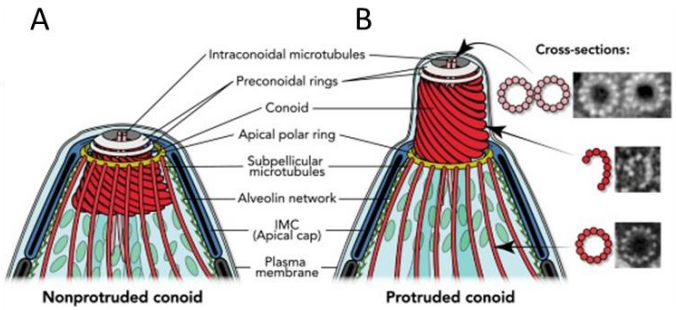

Figure I-8. The conoid in *T. gondii*.

(A) The retracted conoid in *T. gondii*. (B) The protruded conoid in *T. gondii*. In non-protruded cells (A), the conoid is surrounded by APR, whereas it is above the APR in protruded cells (B). As in other organisms, the two intraconoidal microtubules and subpellicular microtubules are composed of 13 protofilaments, whereas the tubulin fibres of the conoid are composed of nine protofilaments arranged in a characteristic 'comma' cross-section. Images copied from (Dos Santos Pacheco et al. 2020) with the licence number 5387751290693.

T. gondii has two APRs surrounding the non-protruded conoid. They are too close to be distinguished by normal light microscopy but can only be observed by electron microscopy. APR1 is associated with the apical margin of the IMC, whereas APR2 is regarded as the microtubule organisation centre (MTOC), from which 22 subpellicular microtubules (SPMTs) emit and the subpellicular microtubules extend in a helical fashion to around two thirds of the parasite length. These SPMTs, together with the IMC and plasma membrane, confer the rigidity and structure of the tachyzoites (Leung et al. 2017, Koreny et al. 2021).

Regarding the proteins found in these APRs, only a few are so far known to be localised to these structures (Koreny et al. 2021, Dos Santos Pacheco et al. 2022). Among them, RNG2 emerges in the early

stages of daughter generation (Katris et al. 2014). RNG2-lacking parasites showed impaired rhoptry and microneme secretion, as well as poor motility and invasion without noticeable changes in APRs, conoid structure or SPMTs (Katris et al. 2014).

The preconoidal rings are comprised of two rings. Some proteins localising at this structure are crucial for parasite survival. For instance, AKMT, glideosome-associated connector (GAC) and formin1 (FRM1) are involved in parasite motility (see section 4.4.1), invasion and egress (Heaslip et al. 2011, Jacot et al. 2016, Tosetti et al. 2019, Dos Santos Pacheco et al. 2022). Recently, some novel preconoidal proteins (Pcr1-7) have been described. Among them, Pcr2 regulates the parasite's persistent movement with so far unravelled mechanisms (Lopez et al. 2022). Pcr4–Pcr6 are involved in the assembly of PCRs, which serve as an anchor for protein resident at preconoidal rings and thus are important for parasite gliding motility, invasion and egress. Pcr1 and Pcr7 are dispensable during the lytic cycle, with Pcr7 exclusively distributed in the PCRs in the nascent daughter cells (Dos Santos Pacheco et al. 2022).

3.3.3 Apical secretory organelles: micronemes and rhoptries

Parasite survival, dissemination and pathogenesis require highly specialised apical organelles: micronemes and rhoptries. A tachyzoite possesses 50–100 micronemes (Venugopal et al. 2018). Recent research indicates that microneme proteins (MICs) in each tachyzoite both come from de novo synthesis and are recycled from the maternal cell (Venugopal et al. 2018, Periz et al. 2019). Micronemes are tiny rod-shaped organelles (40 x 100 nm) clustered at the apical pole of

tachyzoites that play essential roles in host attachment, invasion, egress and gliding motility via the exocytosis of adhesins and perforins such as MIC2 (host cell attachment, invasion and gliding), AMA1 (tight junction), PLP1 (perforin-like protein 1, egress) and MIC8 (rhoptry secretion; Carruthers et al. 1999, Alexander et al. 2005, Kessler et al. 2008, Kafsack et al. 2009, Gras et al. 2017, Whitelaw et al. 2017). The shedding of transmembrane microneme adhesins from the surface of tachyzoites, such as MIC2, requires the activity of rhomboid proteases (Shen et al. 2014). The microneme secretion signalling cascade is not completely understood (for a recent review, see Dubois et al. 2019). The suggested microneme secretion signalling route converges with the egress signalling pathway (see section 2.2.3).

Rhoptries are club-shaped organelles. Each rhoptry is between 2 and 3 µm in length (Boothroyd et al. 2008). They are composed of a rhoptry neck, closer to the conoid, and a rhoptry bulb, the basal section of the rhoptry. The proteins that reside in these two compartments are referred to as rhoptry neck (RON) and rhoptry bulb (ROP) proteins, respectively. A tachyzoite has eight to twelve rhoptries, but only one or two rhoptries are located in the conoid's internal region; their necks are apically docked for secretion (Suarez et al. 2019).

Rhoptry exocytosis plays an important role in subverting host cell immune responses such as ROP16 and host invasion such as the RON2/RON4/RON5/RON8 complex (see section 2.2.1; Boothroyd et al. 2008, Hakimi et al. 2017). However, the signalling mechanism for rhoptry discharge and molecules involved in rhoptry docking and fusion remain mostly unclear, despite recent discoveries that have

found certain players in rhoptry secretion and unravelled probable rhoptry exocytic routes (Coleman et al. 2018, Suarez et al. 2019, Aquilini et al. 2021; for more information, see a recent review: Cova et al. 2022). Importantly, a recent study has suggested that the rhoptry is not directly fused to the plasma membrane during secretion, but rather, its tip is closely associated with the apical vesicles beneath the apical rosette, which is embedded in the plasma membrane. This might be a plausible rhoptry secretion mechanism for Apicomplexa parasites. Non-discharge (ND) proteins ND6 and ND9 are implicated in the rosette assembly and rhoptry exocytosis (Aquilini et al. 2021).

4. Intravacuolar network

During parasite division within the host cell, an extensive filamentous network is generated between parasites via RB, linking parasites within a vacuole and controlling parasite egress. This network is essential for cell communication and material exchange and regulates parasite egress (Frénal et al. 2017, Periz et al. 2017). Filamentous actin (F-actin) is required for the formation and maintenance of this network (Figure I-9; Periz et al. 2017).

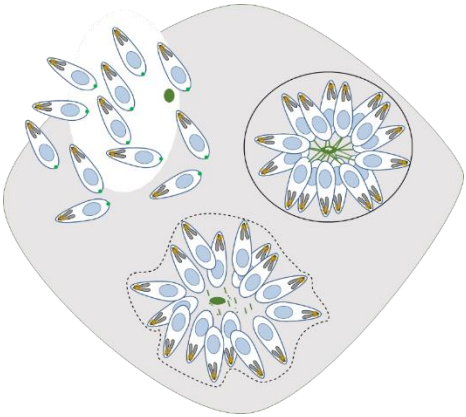

Figure I-9. The F-actin network during the lytic cycle.

An intensive F-actin network (green) is formed during intracellular replication. In the process of egress, this network breaks down before parasite movement. Posterior F-actin is seen in the gliding parasites.

4.1 *T. gondii* F-actin

T. gondii has a single actin-encoding gene, *Tgactin1* (*Tgact1*). TgACT1 is distinct from other eukaryotic actin but shares 80% of its amino acid sequence with mammalians. It is conserved in apicomplexan parasites and shows 93.1% amino acid sequence similarity with PfACT1 (Dobrowolski et al. 1997, Das et al. 2021).

According to previous *in vivo* and *in vitro* investigations, F-actin in *T. gondii* parasites is unusually short even after Jasplakinolide treatment, which could reach 200 nm on average but was still not comparable to rabbit actin (Sahoo et al. 2006). A previous investigation based on the solubility differences between G-actin (globular actin; soluble) and F-actin (insoluble) suggested that the predominant form of TgACT1 is G-actin rather than F-actin (Dobrowolski et al. 1997). Recently, the

adaptation of chromobody revealed the mystery of F-actin in *T. gondii* and gave insight into the function of actin throughout the lytic cycle (Periz et al. 2017).

4.2 Actin nucleating and regulating proteins

Similar to eukaryotes, *T. gondii* has two forms of actin: G-actin and F-actin. G-actin polymerisation results in the formation of F-actin, whereas depolymerisation of F-actin releases G-actin. All of these processes require actin nucleators and actin-binding proteins (ABPs), which regulate polymerisation and depolymerisation and serve distinct functional roles. In contrast to other eukaryotes in which many ABPs have been discovered, *T. gondii* lacks many, including the canonical actin nucleator: Arp2/3 complex. Only a few actin nucleators and actin-binding proteins have been found to date (Das et al. 2021).

The only actin nucleators found in *T. gondii* thus far are three formins (FRMs), with FRM1 nucleating actin at the apical tip, FRM2 nucleating actin at the Golgi complex and apicoplast area, and FRM3 responsible for nucleating actin at the parasite basal end and residual body (Tosetti et al. 2019). FRM1 and FRM2 are well-conserved in apicomplexans, but FRM3 is unique to Coccidians (Daher et al. 2012, Tosetti et al. 2019). All FRMs include the formin homology (FH) domain, which is required for actin assembly. In the process of filament elongation, the proline-rich FH1 domain binds to the profilin-actin complex and promotes rapid assembly. The FH2 domain initiates actin filament assembly by associating with the barbed filament terminal. FH1 and FH2 domains feature FRM1 and FRM2, with the

FH1 domain immediately upstream of FH2 domains at C-term. FRM3 contains the FH2 domain, which is very divergent from the classic FH2 domain (Daher et al. 2010, Daher et al. 2012).

Regarding ABPs, profilin and actin depolymerising factor (ADF), also termed cofilin, sequester G-actin and inhibit actin polymerisation (Allen et al. 1997, Mehta et al. 2010, Frénal et al. 2017). ADF is also indicated as playing a role in disassembling short actin oligomers (Mehta et al. 2010). Notably, although conserved in eukaryotes, profilin's function in higher eukaryotes of regulating actin polymerisation by binding to actin polymers and delivering G-actin to nascent filaments or augmenting FRM activity is different to its function in *T. gondii* (Frénal et al. 2017). Cyclase-associated protein (CAP) was recently identified as a new actin regulator in *T. gondii*. However, whether it regulates actin via sequestering G-actin and/or exchange of nucleotides as in other apicomplexan parasites is unknown (Hunt et al. 2019). Coronin is an ABP that promotes actin polymerisation by binding to F-actin, increasing the rate of actin polymerisation, stabilising newly formed filaments and cross-linking F-actin (Salamun et al. 2014).

4.3 F-actin network

Interestingly, with the current use of Cb for *T. gondii*, a vast F-actin network linking parasites inside the PV has been identified. This Cb binds exclusively to F-actin, allowing actin filaments to be visualised by fusing to other fluorophores such as EmeraldFP without affecting parasite viability (Periz et al. 2017). The successful application of Cb in *T. gondii* revealed F-actin's distribution in the apical pole (FRM1-

mediated), Golgi complex and apicoplast region (FRM2 involved), basal pole (FRM3 involved), parasite periphery (FRM2 related) and RB (FRM3 involved), which forms an F-actin network connecting each parasite (Periz et al. 2017, Del Rosario et al. 2019, Stortz et al. 2019, Tosetti et al. 2019). Due to the existence of an actin flux, the F-actin network is dynamic rather than static.

In intracellular parasites, F-actin flow in the cytosol and periphery is bidirectional, with actin flowing either from the basal end to the apical end (retrograde) or vice versa (anterograde; for more information about actin flow, see a recent review: Das et al. 2021). F-actin in the Golgi complex and apicoplast area is very dynamic and interacts with the periphery actin. It is suggested that FRM2 is the primary regulator of intracellular F-actin flow and dynamics because the absence of FRM2 causes not only a loss of the actin polymerisation centre at the Golgi complex and apicoplast region but also a reduction of peripheral actin while apical and basal actin remain present and measurable (Stortz et al. 2019). Similarly, dynamic F-actin is found in extracellular parasites, likewise in a bidirectional way, with the flow occurring mostly in the cytosol and some F-actin flow at the periphery. Furthermore, fluxes from the cytosol towards the periphery have been observed. Actin flow in the cytosol and the periphery together contributes to the dynamic F-actin network within parasites (Del Rosario et al. 2019). When parasites are invading or gliding, actin flow results in the accumulation of actin in the posterior pole of the parasite, which is FRM1- and CDPK1-dependent and controlled by calcium signalling (Tosetti et al. 2019).

4.4 Multiple functions of F-actin

F-actin has been associated with several *T. gondii* processes (for more information, see a recent review: Das et al. 2021). Apicoplast inheritance, dense granule transport, intracellular growth, gliding motility and invasion are a few examples (Egarter et al. 2014, Periz et al. 2017, Whitelaw et al. 2017, Del Rosario et al. 2019). ACT1-depleted mutants suffer abnormalities in apicoplast inheritance, as evidenced by an erroneous apicoplast–parasite ratio in ACT1-negative vacuoles. Furthermore, directed dense granule movements are inhibited (Whitelaw et al. 2017). In addition, the absence of RB causes the usual rosette organisation of parasites inside the PV to disappear, and parasite division becomes asynchronous (Periz et al. 2017). It has been suggested that actin plays a role in the formation of attachment sites for the onset of parasite gliding motility (Whitelaw et al. 2017). During the invasion process, F-actin has been seen to surround parasite nuclei in place to enable parasite entrance into the host through the F-actin meshwork (Del Rosario et al. 2019). Recent research has shown an additional function of F-actin in the recycling of mother organelles into daughter cells (Periz et al. 2019).

4.4.1 F-actin involvement in gliding motility

Host cell invasion and egress are dependent on the ability of *T. gondii* to find the next cell by employing a type of motility known as gliding motility (Hoff et al. 2002, Frénal et al. 2017). *T. gondii* has three forms of gliding motility in a 2D environment: twirling, circular movement and helical movement, with the latter two being productive (Tosetti et al. 2019). However, in a 3D environment, parasites display motility in a corkscrew-like fashion (Leung et al. 2014).

T. gondii has a specialised gliding apparatus that relies primarily on an F-actin- and myosin-based actomyosin motor complex and regulatory components (Figure I-10; Gaskins et al. 2004, Egarter et al. 2014, Frénal et al. 2017). According to the current linear model, parasite motility is linked with F-actin translocation, which needs MyoH and MyoA for the generation of central movement power (Figure I-10; (Meissner et al. 2002, Graindorge et al. 2016). First, F-actin polymerises at PCRs, then MyoH translocates F-actin towards and anchored to APRs, followed by the conoid protrusion. Eventually, F-actin is translocated first by MyoH at the conoid level and then by MyoA at the pellicle to initiate motility (Figure I-10; Frénal et al. 2010, Graindorge et al. 2016, Tardieux et al. 2016, Frénal et al. 2017, Dos Santos Pacheco et al. 2022). Additionally, in the present model, GAC connects F-actin to transmembrane adhesins (micronemal proteins) and impacts the F-actin translocation towards the back of the parasite, causing the parasites to move (Figure I-10; Jacot et al. 2016, Tosetti et al. 2019). Although the linear model has been widely accepted, it cannot account for some findings (see a recent review: Das et al. 2021). For instance, MyoA/MLC1/GAP45/ACT1 KO mutants are still invasive and motile, although inefficiently (Egarter et al. 2014). Other models that work in concert with the current linear gliding model have been proposed, such as retrograde membrane flow, which relies on parasite secretion and endocytosis (Gras et al. 2019). The exact mechanisms involved in gliding motility are still a matter of debate.

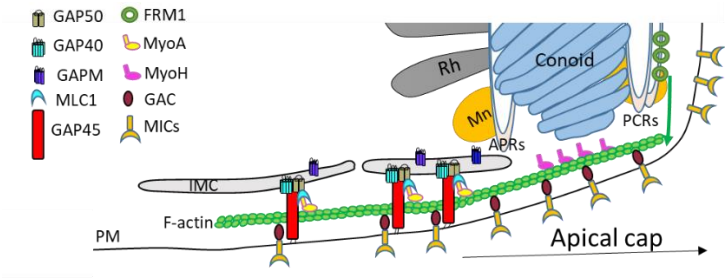

Figure I-10. Current linear model for gliding motility.

MyoA glides along F-actin polymerised by FRM1 at the PCRs, causing parasites to glide ahead. Abbreviations: APRs, apical polar rings; FRM1: formin1; GAC: glideosome-associated connector; GAPM: glideosome-associated protein with multiple-membrane spans; GAP40: gliding-associated protein 40; GAP50: gliding-associated protein 50; IMC, inner membrane complex; MICs: microneme proteins; MLC1: myosin light chain 1; Mn, microneme; MyoA: myosin A; MyoH: myosin H; PCRs, preconoidal rings; PM: plasma membrane; Rh, rhoptry.

4.4.2 F-actin regulation in egress

In addition to these roles, actin is involved in egress. Upon induction of egress by calcium ionophores (Ci) A23187, this network is rapidly destroyed before the start of parasite movement and egress from the host cell, leaving behind RB containing F-actin. After egressing, the F-actin signal is observed at the basal end (Figure I-9; Periz et al. 2017). Consistent with this, upon BIPPO treatment, the F-actin network is also rapidly disassembled, and posterior F-actin has been observed even before parasite egress (Tosetti et al. 2019). When ACT1 is knocked out, parasite egress is inhibited, with just 2% of mutants able to egress when stimulated by Ci A23187 (Egarter et al. 2014). Interestingly, parasites could induce lysis of the PVM and host cell membrane despite remaining confined to the host cell (Whitelaw et al. 2017). This indicates that actin is important for movement initiation but not for microneme secretion.

Depletion of actin regulators has also an effect on parasite egress. ADF-deficient parasites had a partial egress phenotype following the induction of egress, with some parasites successfully exiting the host cell while others stayed linked by filamentous actin, remaining inside the host cell (Li et al. 2022). CAP-depleted parasites exhibited a delay in egress relative to wildtype parasites. This may be due to the presence of prominent and striking actin filaments in CAP-depleted parasites (Hunt et al. 2019). Therefore, F-actin plays a critical role during parasite egress.

5. Molecular genetic tools for analysis of specific genes in *T. gondii*

The establishment of molecular tools has been of great importance in studying the biology of different organisms. So far, several genetic tools have been developed and made accessible in *T. gondii*, making it a paradigm for apicomplexan biology research.

The generation of direct knockouts by replacing the gene with a resistance cassette could be easily achieved for non-essential genes (Shen et al. 2014). Several inducible techniques have been successfully used in *T. gondii*, making possible the study of essential genes. Among them are the tetracycline-inducible (TET) system regulating at the transcription level, the U1 small nuclear ribonucleic particle (U1snRNP)-mediated gene-silencing system (U1 silencing system) regulating at the translational level, the dd (destabilisation domain) FKBP system, the auxin-inducible degron (AID) system regulating at the protein level, the clustered regularly interspaced short palindromic repeats and CRISPR-associated protein 9 (CRISPR Cas9),

the split Cas9 (sCas9) and the dimerisable recombinase (DiCre) system regulating at the genetic level (Wang et al. 2016, Li et al. 2022). These techniques finally accomplish the depletion of the protein of interest (POI) in various ways, each with its own benefits and limitations (Table I-2). Within this study, the DiCre and sCas9-systems were used for the generation of conditional mutants and are described in more detail. All these systems, except Cas9, are only compatible with parasites lacking non-homologous end joining (NHEJ) repair machinery. Since Ku80 is a core subunit of the NHEJ machinery (Vartak et al. 2018), a *Δku80* parasite strain was established to edit genes of interest (Huynh et al. 2009).

Table I-2. Overview of conditional systems in *T. gondii*.

AID: auxin degron domain; ATc: anhydrotetracycline; GOI: gene of interest; IAA: 3-indoleacetic acid; Indels: insertions and deletions; TATi: trans-activator trap identified; ORF: open reading frame. POI: protein of interest; Shld1: Shield-1.

System	Description	Advantages	Disadvantages	Reference
TET system	Regulates the transcription of GOI by replacing the endogenous promoter with a tetracycline-responsive one. The addition of ATc inhibits transcription via interacting with a particular transactivator: TATi	Regulable and reversible	POI expression level might be affected; background expression	(Meissner et al. 2002)
U1 silencing system	Inhibits the translation of GOI by introducing U1 recognition sequences proximal to the termination codon to control mRNA degradation			(Pieperhoff et al. 2015)
dd FKBP system	POI is fused to a destabilisation domain: ddFKBP; the absence of Shld1 results in the degradation of POI, while the presence of Shld1 stabilises the POI	Fast-regulated and reversible	May not be suitable for some proteins	(Herm-Götz et al. 2007)
AID system	Proteins tagged with AID in the presence of auxin, also known as (IAA), are ubiquitinated and further degraded by the cytoplasmic distributed proteasome			(Brown et al. 2018)
DiCre system	DiCre activity is controlled by rapamycin; the addition of rapamycin results in removal of GOI to generate conditional null mutants	No background level; tight control	Slow regulation kinetics and irreversible	(Andenmatten et al. 2013)
CRISPR Cas9 system	The ORF is disrupted because of indels in the sequence achieving functional KO	Suit for every gene and strain; less time-consuming; no background expression	Cas9 toxicity; irreversible; potential off-target	(Sidik et al. 2014)

sCas9 system	Cas9 is tightly controlled by rapamycin, and the addition of rapamycin results in disruption of GOI	Tight control; suit for every gene and strain; less time-consuming; no background expression	Non-specific genotype; irreversible; potential off-target	(Li et al. 2022)

5.1 DiCre in *T. gondii*

Bacteriophage P1-derived Cre recombinase is a member of the integrase family of site-specific recombinases. This protein promotes the effective recombination of two loxP sequences. This sequence is a 34 bp (base pair) consensus motif composed of two 13 bp recognition sequences at each end and a central 8 bp spacer region. The Cre/loxP technique can in principle be used in any organism. Given these characteristics, this technique is designed and widely used in many species to complete the excision, inversion and translocation of genes flanked by loxP sequences (also termed floxed genes; Nagy 2000, Jullien et al. 2003, Van Duyne 2015). The establishment of the DiCre system has overcome the lack of temporal control of the Cre activity via splitting this recombinase into two subunits and fusing each to the rapamycin binding domains FRB and FKBP (Jullien et al. 2003). The addition of rapamycin results in the excision of the floxed gene. This inducible system has been adapted successfully in *T. gondii* (Figure I-11) and *P. falciparum* (Andenmatten et al. 2013, Collins et al. 2013).

For the establishment of inducible KO strains, DiCreΔ*ku80* parasites were generated. By supplying exogenous DNA containing homologous regions and selection markers, the floxed GOI parasites could be obtained (Andenmatten et al. 2013). Recently, the

combination of transiently expressed Cas9 to generate double-strand breaks (DSB) to force integration of exogenous DNA with shorter overhangs in DiCreΔ*ku80* parasites increased the effectiveness of the generation of inducible cKO parasites without the need for selection cassettes and time-consuming cloning of KO-vectors (Stortz et al. 2019; for details, see Figure III-6).

The establishment of the DiCre system in *T. gondii* has significantly facilitated the study of essential genes. However, although the floxed gene can be effectively removed in a short amount of time (one hour), it takes time for the mRNA pool and encoded proteins to degrade. Thus, one of the disadvantages is the slow regulation kinetics, compared to techniques directly regulating protein degradation.

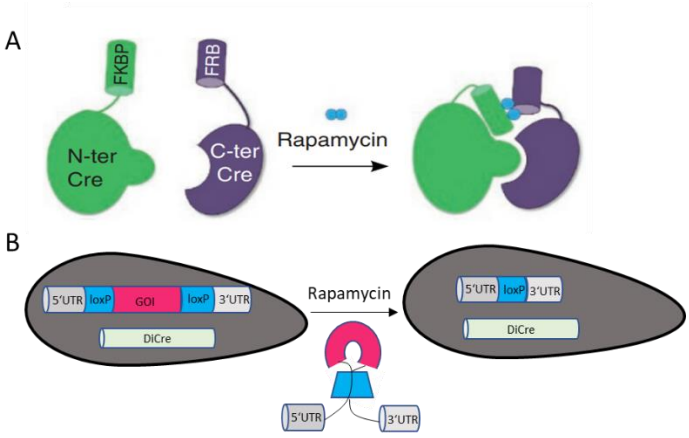

Figure I-11. Adaptation of the DiCre system in *T. gondii*.

A) Cre recombinase is split into two fragments, Cre1-59 (Green) and Cre 60-343 (purple), and fused to the FKBP and FRB domains. The addition of rapamycin

reconstitutes Cre activity. Image from (Andenmatten et al. 2013). B) Upon addition of rapamycin, the floxed gene is excised in DiCre-expressing parasites. Image adapted from (Andenmatten et al. 2013) with the licence number 5387760462632.

5.2 sCas9 in *T. gondii*

CRISPR-Cas is an adaptive immune system identified in archaea and bacteria that protects these organisms against invading nucleic acids (Chylinski et al. 2014, Sander et al. 2014). The CRISPR-Cas9 system is derived from the *Streptococcus pyogenes* type II CRISPR-Cas system. Cas9 is an endonuclease directed by a single guide RNA (sgRNA) that is a chimeric RNA containing 20 nucleotides targeting GOI and a Cas9-binding RNA scaffold. Cas9 produces a DSB in the targeted gene after the complex screens the whole genome. This DSB might be repaired by NHEJ or homologous recombination (HR), which are present in almost all cell types and species, including *T. gondii* (Sander et al. 2014). NHEJ is the preferred repair mechanism for *T. gondii*, although it often results in insertion and deletion mutations (indels), hence causing a frameshift and disruption of the open reading frame and, consequently, no protein production or expression of a truncated protein (Sander et al. 2014, Sidik et al. 2014). However, the constitutive expression of Cas9 in *T. gondii* is shown to be toxic. Different strategies to avoid Cas9 toxicity have been established previously, such as the employment of a decoy sgRNA (Sidik et al. 2016) or the regulation of Cas9 expression using ddCas9 where Cas9 is fused to ddFKBP (Serpeloni et al. 2016). This last strategy allowed temporal control of Cas9 activity, although long incubation (over 4 hours) with Shld resulted in aberrant parasites due to over-stabilisation of ddCas9 (Serpeloni et al. 2016).

The sCas9 system, with precise temporal control, has been successfully adapted from the system in mammalian cells, overcoming these shortcomings (Zetsche et al. 2015, Li et al. 2022). Similar to the DiCre system, the Cas9 nuclease was split into two fragments and fused to rapamycin-sensitive dimerisation domains: FKBP for the C-terminus (Cas9(C)-FKBP) and FRB for the N-terminus (Cas9(N)-FRB). The Cas9(C)-FKBP subunit contains two nuclear localisation sequences (NLSs) and is actively imported into the nucleus, whereas the Cas9(N)-FRB fragment contains a nuclear export sequence (NES) and is kept in the cytosol. Thus, Cas9 subunits are spatially separate. Only the addition of rapamycin restores Cas9 function, allowing for the achievement of functional KO (Figure I-12). This technique enables the effective generation of conditional mutants and has potential use in a wide variety of applications, such as genome-wide dropout screens and phenotypic screens that can detect a variety of phenotypes.

Notably, Cas9 causes a non-specific phenotype in a parasite subpopulation (around 40%) in which parasite morphology and nuclear shape are aberrant. This is due to insufficient repair following DSB in the parasite subpopulation. As a result, if the targets of the screen are defects in replication and/or nuclear morphology, further analyses for confirmation of the phenotype are necessary. Alternatively, the readout of phenotypes should allow the exclusion of non-specific phenotypes (Li et al. 2022).

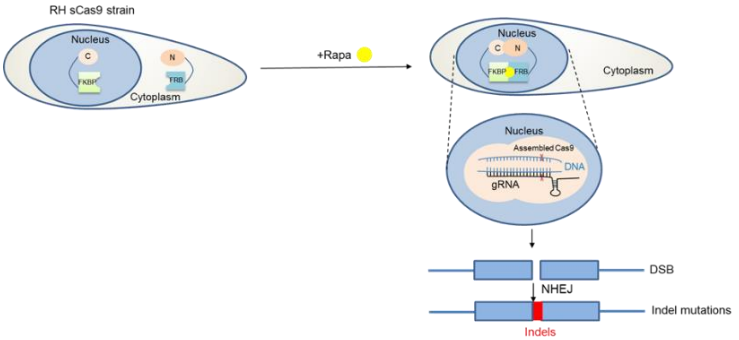

Figure I-12. Adaptation of the sCas9 system in *T. gondii*.

Transgenic parasites express both sCas9 subunits, with the C-term Cas9 fused to FKBP and the N-term Cas9 fused to FRB. Two Cas9 fragments are separated in distinct compartments after expression in *T. gondii*. Rapamycin causes Cas9 dimerisation, which restores Cas9 activity and thereby disrupts the targeted gene in the presence of sgRNA.

6. Aim of study

T. gondii, a model organism for apicomplexan parasites, is capable of infecting and causing toxoplasmosis in almost all warm-blooded mammals. Egress, one of the key processes in its lytic cycle, plays a crucial role in the dissemination of parasites, but it is poorly understood despite the identification of some players.

During replication, parasites construct an intravacuolar F-actin network that links individual parasites and is essential for synchronous replication and material exchange between parasites. Before parasite egress, this network disintegrates rapidly (Periz et al. 2017). Many signalling platform components necessary for natural and induced egress are localised to this network (Bisio et al. 2019). Importantly, stabilising this network, for example after ADF depletion, leads to delayed or blocked egress, showing a tight control of F-actin

breakdown and activation of the motility machinery for egress (Li et al. 2022).

High-throughput screens enable us to study the fitness of *T. gondii* genes on a large scale. Recently, a genome-wide CRISPR screen has scored each gene's contribution to parasite fitness, referred to as phenotypic scores, which enables the rapid and efficient generation of genome-wide mutant libraries. However, the function of each gene remains unclear and requires the time-consuming generation of mutants using these conditional systems to obtain additional information regarding their function (Sidik et al. 2016). A high-throughput CRSPR-mediated tagging method combing with an auxin-inducible degron and fluorophore was developed, allowing for the direct localisation and rapid regulation of POI. However, some proteins might be difficult to tag and regulate by this system and therefore potentially miss some promising candidates (Smith et al. 2022). The successful adaption of sCas9 in *T. gondii* by Johannes Stortz, a former PhD student in the Meissner lab, allows in principle phenotypic screens at a large scale. Therefore, one aim of this study was the application of the spitCas9 technology to screen for genes crucially required for parasite egress. The DiCre technique was further used to validate and investigate the gene functions of interesting candidates in depth (Andenmatten et al. 2013, Li et al. 2022). The overall aims of this study were:

1) Identification of genes involved in egress by sCas9 phenotypic screen

2) Characterisation of those specific egress-related genes

2.1) Identification of potential interactors of those specifically related genes

3) Investigation of the dynamics and modulation of F-actin during parasite egress involving the specific egress-related genes.

II. MATERIALS AND METHODS

1. Materials

1.1 Laboratory equipment

Table II-1. Equipment used in this study.

Equipment	Manufacturer
DMi8 wide-field microscope	Leica
3D STED microscope	Abberior
Axiovert A1 fluorescence microscope	Zeiss
ACSAria™ III Cell Sorter	BD bioscience
4D-Nucleofactor™ electroporation units	Lonza
PCR Cycler, thermomixer C, pipette, thermomixer	Eppendorf
ErgoOne® single & multi-channel pipettes, Vortex	Starlab
Pipette	A. Hartenstein, Eppendorf
FastGene® Blue/Green LED Transilluminator	Nippon genetics
Centrifuge	Roth, Thermoscientific, Eppendorf, Hettich
NanoDrop 1000 Spectrophotometer	ThermoFisher scientific
Printer	Mitsubishi
Odyssey CLX-1849	LI-COR Biosciences
-80 °C freezer	Haier biomedical
Microwave	Sharp
Vortex-Genie 2	Scientific industries
ThermoMixer™ C	Eppendorf
Fridge	Siemens, Bosch
Agarose gel electrophoreses equipment	BioRad, Avantor
SDS-PAGE system, Blotting apparatus	BioRad
Incubator	Memmert
Safety cabinets	Thermofisher scientific
Incubator shaker	New brunswick scientific
Shaker/mixer	Heidolph, Sarstedt, Flow Laboratory
CO_2-incubator for tissue culture	Thermo scientific
Scale	KERN
Water Bath	PHOENIX Instrument
Analytical balances	Sartorius
Vacuum pump	A. Hartenstein
PH meter	Wagner&Munz

1.2 Computer software

Table II-2. Computer software used in this study.

Program	Source
InkscapeTM: Open Source Scalable Vector Graphics Editor	Inkscape Project
Windows 10, Microsoft Office 2019	Microsoft Corporation
Basic Local Alignment search tool (BLAST), Primer-BLAST	National Institute for Biotechnology Information (NCBI)

Icy image processing software 1.8.6.0	Institut Pasteur
ToxoDB	National Institute of Allergy and Infectious Diseases (NIAID)
Fiji (ImageJ) software v.2.1.0	National Institutes of Health (NIH)
NEB tools™: Double Digest Finder, Tm Calculator	New England Biolabs (NEB)
ApE Plasmid Editor	University of Utah (by M. Wayne Davis, v.2.0.53c)
Eukaryotic Pathogen gRNA Design Tool (EuPaGDT)	University of Georgia
LasX software (v. 3.4.2.183668)	Leica
LI-COR Image Studio software	LI-COR Biosciences
Huygens Essential v.18.04.	Scientific Volume Imaging
Graphpad Prism 8.2.1.	GraphPad
EndNote X9	Clarivate
DOG (Domain Graph, version 2.0)	(Ren et al. 2009)
Clustal Omega	European Bioinformatics Institute
Perseus 1.6.15.0	(Tyanova et al. 2016)
Imspector 16.3.14274	Abberior instruments

1.3 Consumables, biological and chemical reagents

Table II-3. Consumables.

Consumables	**Company**
Magnets, waste rack, test tube rack for glass, parafilm, cell scratcher, bacteria cell spreaders, tweezers, filter nylon 0,2 µm, waste bags, DMSO	Roth
Gloves, TPP cell culture flask, TPP centrifuge tubes, TPP cell culture dishes, TPP cryo tubes, TPP cell culture test plates (6 well, 96 well), TPP syringe filter, TPP vacuum filtration system, TPP cell scrapers, aluminium foil	Faust Lab Science
Eppis, tips	Eppendorf
Plastic box	Bueroshop24
µ-Dish 35 mm high, µ-Slide 8 Well, µ-Plate 96 well black	Ibidi
Mouth mask	Häberle
Aspiration pipette	Greiner Bio-One
Sterican blint needles	Droh GmbH
Weighting rings, cover slips, cellscraper	A. Hartenstein
Cryo box yellow 9x9, slide box, PCR storage box	NeoLab
Corning™ Falcon™ round bottom polystyrene tube	Fisher scientific
Tips, filters, rack	Star lab
Lens Tissues	Thorlabs
Lab coat	CaptainWorkwear
Storage cabinet	Certeo
Membrane filter 3 µm, flasks	Merck
Serological Pipettes, falcons	Sarstedt

Waste box for sharp items, gloves	SMS medipool
Filters, cover glasses, PCR 8-strips with individual cover, gloves, PCR tubes, petridish	Avantor
Counting chamber	Assistent

Table II-4. Biological and chemical reagents used in this study.

Reagents	**Company**
HEPES	Avantor
GABA	Tocris
Trypsin/EDTA, ultra pure water	Biochrom
Odyssey Blocking Buffer (TBS), ChameleonTM Duo Li-Cor marker	LI-COR Biosciences
4–20% precast polyacrylamide gel	BioRad
GelRed® Nucleic Acid Gel Stain, 10,000X	Biotrend
Biozym LE GeneticPure Agarose	Biozym
Dry ice, CO_2	Linde
Paraformaldehyde 20%, Immersion oil type 37	Electron microscopy science
Type F Immersion liquid, Carl Zeiss™ immersion oil	Fisher scientific
Incuwater-clean, trypton, agar bacteriology grade, tryptone, yeast extract	A. Hartenstein
Midori Green Advance	Nippon genetics
Hoechst 20 mM	life technologies
T4 DNA ligase, restriction enzymes, DNA ladder 1kb (plus), Q5 HF DNA Polymerase, dNTP Mix, SOC Outgrowth Medium,	New England Biolabs
SDS, sodium acetate, DMSO, ethanol, TAE Buffer 50x, NaCl, glycerine, glycine, methanol, Ponceau S, acetic acid	Roth
DNA Ladder 250bp, MES hydrate, Calcium Ionophore A23187, rapamycin, gabapentin, FBS, PBS, propranolol hydrochloride, DMEM, L-glutamine, pyrimethamine, rapamycin, BSA, KCl, EGTA, sodium deoxycholate, EDTA, Triton TX-100, Orange G, Tween-20, $MgSO_4$, sucrose, Tris base, Tris-HCl, glucose, $MgCl_2$, MES, KCl, Hemacolor® Rapid staining of blood smear Solution 2, Hemacolor® Rapid staining of blood smear Solution 3, sodium acetate, dithiothreitol	Merck
HBSS, PBS, ProLong™ gold antifade mountant, FluoroBrite Gibco, Proteinase K, Dynabeads™ MyOne™ Streptavidin T1, Pierce™ protease inhibitor mini tablets, K_2SO4	ThermoFisher scientific
BIPPO	Thompson laB
20% PFA solution	Science Service
Skimmed milk powder	Heirler cenovis
GelRed® Nucleic Acid Gel Stain	Biotrend

1.4 Kits

Table II-5. Kits used in this study.

Company	**Kits**
Blirt	ExtractMe DNA Clean-Up&Gel-Out Kit, ExtractMe genomic DNA Kit, ExtractMe plasmid Mini Kit
Lonza	P3 Primery cell 4D Nucleofector® X Kit L

1.5 Buffers

Table II-6. Buffers for bacteria, HFFs, and *T. gondii* culture.

Buffer	Components	Purpose
LB medium	10 g/l tryptone, 5 g/l yeast extract, 10 g/l NaCl	Bacteria culture
LB agar	1.5% (w/v) agar in LB medium	Bacteria culture
Ampicillin (1000X)	100 mg/ml in H_2O	Bacteria culture
50% glycerol	50 % glycerol (v/v), 50 % ultrapure water (v/v)	Bacteria freezing
$DMEM_{complete}$	500 ml DMEM, 10 % FCS (v/v), 4 mM L-glutamine, 20 µg/ml gentamicin	*T. gondii* and HFFs cell culture
2 x Freezing solution	50 % FBS (v/v), 20 % DMSO (v/v) in $DMEM_{complete}$	*T. gondii*/HFFs freezing

Table II-7. Buffers for DNA.

Buffer	Components
Annealing Buffer	10 mM Tris, pH 7.5–8.0, 50 mM NaCl, 1 mM EDTA

Table II-8. Buffers for WB.

Buffer	Components
Orange Protein Loading Buffer (4x)	125 mM Tris-HCl pH 6.5, 50% (v/v) glycerol, 4% (w/v) SDS, 0.2% (w/v) Orange G
Running buffer (10x)	250 mM Tris base, 1.92 M glycine, 1% (w/v) SDS
Transfer buffer (10x)	480 mM Tris base, 390 mM glycine, 10-20% methanol (vol/vol)
Tris-Buffered saline (TBS) (10x)	152 mM Tris-HCl, 46 mM Tris base, 1.5 M NaCl
TBST	1×TBS, 0.2% Tween-20
Ponceau S Stain	0.1% (w/v) Ponceau S, 5% (v/v) acetic acid
$RIPA\ buffer_{complete}$	50mM Tris-HCl (PH=8), 0.5% sodium deoxycholate, 150 mM NaCl, 1 mM EDTA, 0.1% SDS, 1% Triton TX-100

Table II-9. Reagents for phenotypic assays.

Reagents	Components	Purpose
$DMEM\ FluoroBrite_{incomplete}$	500 ml DMEM, 4 mM L-glutamine, 20 µg/ml gentamicin	Time-lapsed video for egress
$DMEM_{incomplete}$	500 ml DMEM, 4 mM L-glutamine, 20 µg/ml gentamicin	Egress assay

Ci A23187 (1000X)	2 mM in DMSO	Egress assay and microneme secretion assay
BIPPO (1000X)	50 mM in DMSO	Egress assay
Propranolol hydrochloride (2000X)	250 mM in DMSO	Egress assay
BIPPO (1000X)	5 mM in DMSO	Microneme secretion assay
GABA (stock solution)	100 mM in ddH_2O	Plaque assay
Gabapentin (stock solution)	50 mM in ddH_2O	Plaque assay
Pyrimethamine (1000X)	1 mM in Ethanol	Drug selection for *T. gondii*
Rapamycin (1000X)	50 µM in DMSO	Inducing KO for *T. gondii*
Endo buffer	44.7 mM K_2SO_4, 10 mM $MgSO_4$, 100 mM sucrose, 5 mM glucose, 20 mM Tris, 0.35% w/v BSA, pH 8.2	Gliding assay
Gliding Buffer	1 mM EGTA and 100 mM HEPES in HBSS solution	Gliding assay
Intracellular buffer	5 mM NaCl, 142 mM KCl, 1 mM $MgCl_2$, 2 mM EGTA, 5.6 mM glucose, 25 mM HEPES, pH 7.2	Microneme secretion assay
Tris-HCl	50 mM Tris-HCl, PH=8	BioID
RIPA $buffer_{complete}$	50 mM Tris-HCl (PH=8), 0.5% sodium deoxycholate, 150 mM NaCl, 1 mM EDTA, 0.1% SDS, 1% Triton TX-100	BioID
RIPA $buffer_{incomplete}$	50mM Tris-HCl (PH=8), 0.5% sodium deoxycholate, 150 mM NaCl, 1mM EDTA, 0.1% SDS	BioID
4% PFA	20% PFA in PBS	Fixation
Cytoskeleton buffer: CB1	MES 10 mM pH 6.1, KCl 138 mM, $MgCl_2$ 3 mM, EGTA 2 mM, 5% PFA	Fixation
Cytoskeleton buffer: CB2	MES 10 mM pH 6.1, KCl 163.53 mM, $MgCl_2$ 3.555 mM, EGTA 2.37 mM, sucrose 292 mM	Fixation

1.6 Antibodies and dyes

Table II-10. Antibodies used in this study for IFA.

	Name	**Dilution**	**Origin / cat. Number**
Primary Antibodies	Mouse α-SAG1	1/1000	Lourido's Lab
	Rabbit α-GAP45	1/5000	Soldati's Lab
	Mouse α-IMC1	1/500	Ward's Lab
	Rabbit α-*T. gondii*	1/1000	Abcam, ab138698
	Mouse α-GFP	1/500	Roche, 11841460001
	Rat α-HA	1/500	Roche, 1187431001
	Camelid sdAb α-GFP-ATTO 488	1/500	Nano Tag Biotechnologies, N0304-At488-L
	Rabbit α-RFP	1/250	Rockland, 600-401-379
	Mouse α-ISP1	1/1000	Bradley's Lab

	Mouse α-MIC2	1/500	Carruthers' lab
	Rabbit α-CPN60	1/2000	Sheiner's Lab
	Mouse α-ROP1	1/200	
	Mouse α-ROP2,4	1/500	
	Rabbit α-MIC6	1/3000	Soldati's Lab
	Rabbit α-MIC8	1/500	
	Mouse α-AMA1	1/500	Ward's Lab
	Rabbit α-GFP	1/1000	Abcam, ab290
Secondary antibodies	Goat anti-Mouse IgG (H+L) Alexa Fluor 350	1/1000	Thermo Fisher Scientific, A11045
	Goat anti-Rabbit IgG (H+L) Alexa Fluor 350	1/1000	Thermo Fisher Scientific, A11046
	Goat anti-Mouse IgG (H+L) Alexa Fluor 488	1/1000	Thermo Fisher Scientific, A11001
	Goat anti-Rat IgG (H+L) Alexa Fluor 488	1/1000	Thermo Fisher Scientific, A11006
	Goat anti-Rabbit IgG (H+L) Alexa Fluor 488	1/1001	Thermo Fisher Scientific, A32731
	Abberior STAR 580, goat anti-mouse IgG	1/1000	Abberior ST580-1001-500UG
	Abberior STAR 580, goat anti-rabbit IgG	1/1000	Abberior ST580-1002-500UG
	Abberior STAR 635P, goat anti-mouse IgG	1/1000	Abberior ST635P-1001-500UG
	Abberior STAR 635P, goat anti-rabbit IgG	1/1000	Abberior ST635P-1002-500UG
	Abberior STAR 635P, goat anti-rat IgG	1/1000	Abberior ST635P-1007-500UG

Table II-11. Antibodies used in this study for WB.

	Name	**Dilution**	**Origin / cat. Number**
Primary Antibodies	Mouse α-GRA1	1/3000	BIOTEM, Clone TG 17.43, Ref # BIO.018.4
	Mouse α-MIC2	1/2000	Carruthers' lab
	Rabbit α-aldolase	1/5000	Sibley's Lab
Secondary antibodies	IRDye680RD Donkey anti-Rabbit IgG	1/10000	LI-COR Biosciences, 925-68073
	IRDye800CW Donkey anti-Mouse IgG	1/15000	LI-COR Biosciences, 925-32212
	IRDye 800CW Streptavidin	1/20000	LI-COR Biosciences, 926-32230

Table II-12. Dyes used in this study.

Name	Concentration	Origin/ cat. Number
Janelia Fluor HaloTag ligand 646	20 nM	Promega, GA112A
HaloTag Oregon Green	0.2 µM	Promega, G280B
HaloTag TMR	5 µM	Promega, G229A
Janelia Fluor HaloTag ligand 549	200 nM	Promega, GA111A
SNAP-Cell 647-SiR	1 µM	Biolabs, S9102S

1.7 Oligonucleotides

Table II-13. gRNAs for generation of parasites in DiCreΔ*ku*80 strain.

gRNA name	Target Gene	gRNA sequence (5´- 3´)	Usage	Reference
slf-sgRNA1	*sodium:neurotransmitter symporter family protein (TGGT1_208420)*	GCCTCCAAGTCTTAACTCACG	Tagging	This study
cgp-sgRNA1	*hypothetical protein TGGT1_240380*	GAGCGGTGGAGGGTGGATTTC	Tagging	This study
slf-sgRNA2	*sodium:neurotransmitter symporter family protein (TGGT1_208420)*	GTTCTAGAAAAGAGTCAAAG	Introduce 5' loxp	This study
cpg-sgRNA2	*hypothetical protein TGGT1_240380*	GTGTCGACGCAGAGAAGTGGA	Introduce 5' loxp	This study
gc-sgRNA	*guanylate cyclase (TGGT1-254370)*	GTCTGGAGCAACGCAGAACCT	Tagging	This study
cdc50.1-sgRNA	*cdc50.1 (TGGT1_230820)*	GAATCATGCTGTACCCAATG	Tagging	This study
ugo-sgRNA	*ugo (TGGT1_238390)*	GAGAGCTTGTCAGCATGGAGT	Tagging	This study
gc-sgRNA	*guanylate cyclase (TGGT1-254370)*	GTTCGTCGTATTCGATAGCTC	Introduce 5' loxP	This study
cdc50.1	*cdc50.1 (TGGT1_230820)*	GATGCAGAGGCTAATCGACAC	Introduce 5' loxP	This study
ugo-sgRNA	*ugo (TGGT1_238390)*	GCGTATCCTCGGTCTCTCCAC	Introduce 5' loxP	This study

sas6l-sgRNA	*sas6l-Like (TGGT1_301420)*	GAGAAATAGAAAAGTCTGGA	Tagging	Ross Waller lab
mg2-sgRNA	*rng2 (TGGT1_244470)*	GCATCAACAAACTAAAAAAA	Tagging	Ross Waller lab
gac-sgRNA	*gac (TGGT1_312630)*	GTAAGGGCAGTCTCTGGAGTC	Tagging	Designed by Julia von Knoerzer-Suckow
frm1-sgRNA	*frm1 (TGGT1_462965)*	GAAATGAGTCTGAGACTTTC	Tagging	Designed by Mirko Singer
frm1-sgRNA	*frm1 (TGGT1_462965)*	GAAAGCGTATCAGACATGGT	Introduce 5' loxP	Designed by Mirko Singer
myoh -sgRNA	*myoh (TGGT1_243250)*	GTCCCAGTTCGGATTCACCGA	Tagging	This study
centrin1 -sgRNA	*centrin1 (TGGT1_ 247230)*	GAGGTTATCTCTGCGTGCGT	Tagging	Designed by Mirjam Wagner
TGGT1_212780-sgRNA	*hypothetical protein (TGGT1_212780)*	gCGGGGAATGAAAGCCCCACA	Tagging	This study
aamt-sgRNA	*aamt (TGGT1_310070)*	gCGACGAACTGAACCGGTGTG	Tagging	This study
TGGT1_263070-sgRNA	*CMGC kinase, CK2 family (TGGT1_263070)*	gAAGTCCATGAAAAAGGTCTC	Tagging	This study
TGGT1_284620-sgRNA	*hypothetical protein (TGGT1_284620)*	GAGATGCCTTAACTGTCGAA	Tagging	This study
icap16-sgRNA	*icap16 (TGGT1_202120)*	GACATTGAATAAAACAGTGG	Tagging	This study

TGGT1_231160-sgRNA	*hypothetical protein (TGGT1_231160)*	g ATTCTGCTGCTAAgtgcaaa	Tagging	Designed by Peipei Qin
TGGT1_238170-sgRNA	*hypothetical protein (TGGT1_238170)*	g TAAgcgaagagtcgaacctc	Tagging	Designed by Peipei Qin
TGGT1_253440-sgRNA	*putative cell-cycle-associated protein kinase SRPK (TGGT1_253440)*	gcatacacgtgTCACTGTTGC	Tagging	Designed by Peipei Qin
TGGT1_293480-sgRNA	*MoeA N-terminal region (domain I and II) domain–containing protein (TGGT1_293480)*	g TGAtctgcctcgcgagctct	Tagging	Designed by Peipei Qin
akmt-sgRNA	*akmt (TGGT1_216080)*	GGCCAGTTGAggaacaattg	Tagging	Designed by Elena Jimenez-Ruiz
TGGT1_284620-sgRNA	*hypothetical protein (TGGT1_284620)*	gTTCTTTGGTGGACGTGGAGA	Introduce 5' loxP	This study
akmt-sgRNA	*akmt (TGGT1_216080)*	gtgatgttgatggagagtcg	Introduce 5' loxP	Designed by Elena Jimenez-Ruiz
pckmt-sgRNA	*pckmt (TGGT1_292170)*	GAAGTAGcaaggatcaaagc	Tagging	Designed by Elena Jimenez-Ruiz
uprt-sgRNA	*uprt (TGGT1_312480)*	GCCAGGAAGAAAGCATTCTCC	Introducing CbEm	Designed by Janessa Grech

Table II-14. Oligonucleotides used in this study.

[#]: oligos designed by Julia von Knoerzer-Suckow. [##]: oligos designed by Mirko Singer. [###]: oligos designed by Mirjam Wagner; [§]: oligos designed by Peipei Qin. [§§]: oligos designed by Elena Jimenez-Ruiz. [§§§]: oligos designed by Janessa Grech.

Oligo name	Sequence 5' - 3'	Purpose
pU6-gRNA-sequencing-fw[§§]	CTTGCGCAGCATACACTCGAAGC	Sequencing primers
TGGT1_240380 3' tagging homology primer fwd	AAGAGGATGACCTAGCATGGAGACTAGCGGTGGAGGGTGGtTTcCTcGCTGCTAAAATTGGAAGTGGAGG	PCR amplification of tags for C-terminal tagging
TGGT1_240380 3' tagging homology primer rvs	CGCCAGCCTGTCTATTATGAAAATGCAAAGTGTCTGATGAGGAAACCAGTATAACTTCGTATAATGTATGCTATACG	PCR amplification of tags for C-terminal tagging
TGGT1_240380 3' tagging analytical primer fwd	TCGCTTCAGAAGTTTGGTGG	Genotyping primers for C-terminal tagging
TGGT1_240380 3' tagging analytical primer rvs	CATACAGTGGTTGTGGCACT	Genotyping primers for C-terminal tagging
TGGT1_240380 5' loxp insertion homology	TTTCTGAAGGACCTCTTGTCGACGCAGAGAAGTATAACTTCGTATAGCATACATTATACGAAGTTATGGAAGGAAGATGGAAGGAGAGGATAAGAGAGAG	Repair templates for insertion of 5' loxp
TGGT1_240380 5' loxp insertion analytical primer fwd	GCATACATTATACGAAGTTATGGAAGG	Integration primers for insertion of 5' loxp
TGGT1_240380 5' loxp insertion analytical primer rvs	CTCTCCTGTTCTTCTGTGGT	Integration/genotyping primers for insertion of 5' loxp
TGGT1_240380 5' loxp insertion analytical primer fwd	ATCTCTCTCGCCACTTTGAC	Genotyping primers for insertion of 5' loxp
TGGT1_208420 3' tagging homology primer fwd	CACTGGTGTTCCCTTCTTGTTATGTTTTCTCTGTCGCAGCCTCCAAGTCTGCTAAAATTGGAAGTGGAGG	PCR amplification of tags for C-terminal tagging
TGGT1_208420 3' tagging homology primer rvs	TTTCGAGATGCGTCTGGAGAGAGTCATGTGGCGAATCCAGCCGACCTCGTATAACTTCGTATAATGTATGCTATACG	PCR amplification of tags for C-terminal tagging
TGGT1_208420 3' tagging analytical primer fwd	ATCACGGATTACGGAGACAG	Genotyping primers for C-terminal tagging
TGGT1_208420 3' tagging analytical primer rvs	CCAAACCACAATCGAAGCTC	Genotyping primers for C-terminal tagging

TGGT1_208420 5' loxp insertion homology	CATCCATCTGCTCTCACACTTCTAGCGCCACTTATAACTTCGTATAGCATACATTATAC GAAGTTATTGACTCTTTTCTAGAACGGCGCCTCCCCCCCCC	Repair templates for insertion of 5' loxp
TGGT1_208420 5' loxp insertion analytical primer fwd	GCATACATTATACGAAGTTATTGACTCTT	Integration primers for insertion of 5' loxp
TGGT1_208420 5' loxp insertion analytical primer rvs	CACAGGACAAACAACTCTGG	Integration/genotyping primers for insertion of 5' loxp
TGGT1_208420 5' loxp insertion analytical primer fwd	TCATTTCCGCGTCTCTACTC	Genotyping primers for insertion of 5' loxp
TGGT1_254370 3' tagging homology primer fwd	ACGCGTCGCCTTCGGATATAGGGTCGACACCTGGCTCTGCACTCGGGTCGGCTAAAAT TGGAAGTGGAGG	PCR amplification of tags for C-terminal tagging
TGGT1_254370 3' tagging homology primer rvs	CGACTGCCCGAAGCGGCAGGACACAGACCCGCCTCTGGAGCAACGCAGAAATAACTT CGTATAATGTATGCTATACG	PCR amplification of tags for C-terminal tagging
TGGT1_254370 3' tagging analytical primer fwd	TGGGATTCCGAGAGATATTGG	Genotyping primers for C-terminal tagging
TGGT1_254370 3' tagging analytical primer rvs	CCTTTCCTCTTCTGGTTCCT	Genotyping primers for C-terminal tagging
TGGT1_254370 5' loxp insertion homology	CTCTTCGTTTCCCCTCTGTCTTCTATTCCGGAGATAACTTCGTATAGCATACATTATACG AAGTTATCTATCGAATACGACGAAAATGAAGAAGACGCGA	Repair templates for insertion of 5' loxp
TGGT1_254370 5' loxp insertion analytical primer fwd	GCATACATTATACGAAGTTATCTATCGAA	Integration primers for insertion of 5' loxp
TGGT1_254370 5' loxp insertion analytical primer rvs	CAACGAATGAGCGAAAGTGC	Integration/genotyping primers for insertion of 5' loxp
TGGT1_254370 5' loxp insertion analytical primer fwd	CTTGTCTCTGTCTTGAGGACTTG	Genotyping primers for insertion of 5' loxp
TGGT1_230820 3' tagging homology primer fwd	TTCGAGATCTTCGGTGGCAGACGAAGACTCGTGGAAGCAAAAAAACGAAAGCTAAAA TTGGAAGTGGAGG	PCR amplification of tags for C-terminal tagging
TGGT1_230820 3' tagging homology primer rvs	TGACAGCTACTGCCTGGAGACGAGGGTGCACAGTATGCAGAACACCACATATAACTTC GTATAATGTATGCTATACG	PCR amplification of tags for C-terminal tagging
TGGT1_230820 3' tagging analytical primer fwd	TCGGTTGCCTATTGACCATG	Genotyping primers for C-terminal tagging
TGGT1_230820 3' tagging analytical primer rvs	GCAAGTCCTGTCCTACTGTT	Genotyping primers for C-terminal tagging

TGGT1_230820 5' loxp insertion homology	CGTCAGCAGTCATATGTTACGTTTCGTCCTGTGATAACTTCGTATAGCATACATTATAC GAAGTTATTCGATTAGCCTCTGCATCTTTTTTTCATGGGTG	Repair templates for insertion of 5' loxp
TGGT1_230820 5' loxp insertion analytical primer fwd	GCATACATTATACGAAGTTATTCGATTAGC	Integration primers for insertion of 5' loxp
TGGT1_230820 5' loxp insertion analytical primer rvs	GAGCGGAAGAGATAGAGCAC	Integration/genotyping primers for insertion of 5' loxp
TGGT1_230820 5' loxp insertion analytical primer fwd	CCCGTCTTTATCCACTGAGAG	Genotyping primers for insertion of 5' loxp
TGGT1_238390 3' tagging homology primer fwd	AGGATGAGGTGTCTATGGGCTCTGGCCACCTTGTCGGCGATCGTAGCGCGGCTAAAAT TGGAAGTGGAGG	PCR amplification of tags for C-terminal tagging
TGGT1_238390 3' tagging homology primer rvs	ATATGTTTGGCTGTATATTCACAAATCCGTTTTGTCTATCCGTCCGACTATAACTTCGT ATAATGTATGCTATACG	PCR amplification of tags for C-terminal tagging
TGGT1_238390 3' tagging analytical primer fwd	GACGGTTGTTCTGCAAGTAC	Genotyping primers for C-terminal tagging
TGGT1_238390 3' tagging analytical primer rvs	CTGTTTCTCTTTCCACTCTCCC	Genotyping primers for C-terminal tagging
TGGT1_238390 5' loxp insertion homology	CAGTGCGCGGGAGTTTCGTATCCTCGGTCTCTCATAACTTCGTATAGCATACATTATAC GAAGTTATCACGGGTCGGTCAAGATGCGGATGCAGTGGTTT	Repair templates for insertion of 5' loxp
TGGT1_238390 5' loxp insertion analytical primer fwd	GCATACATTATACGAAGTTATCACGG	integration primers for insertion of 5' loxp
TGGT1_238390 5' loxp insertion analytical primer rvs	CAACACCGGCATGATGTACG	Integration/genotyping primers for insertion of 5' loxp
TGGT1_238390 5' loxp insertion analytical primer fwd	GTATTTGTCCTGTTCCGACTTC	Genotyping primers for insertion of 5' loxp
TGGT1_243250 3' tagging homology primer fwd	CGCGAGGCGCTGCTGCTGCTCCCTCTGCAATCCGCACCCGTCCGTCGGTaAACCCaAAtT GGGAcCCgATGGCgTAtAAt GCTAAAATTGGAAGTGGAGG	PCR amplification of tags for C-terminal tagging
TGGT1_243250 3' tagging homology primer rvs	AAGAAAGGCCTTTTTTCAACACTCACCAGCGGGCAGCCGCCAAAAAGATC ATAACTTCGTATAATGTATGCTATACG	PCR amplification of tags for C-terminal tagging
TGGT1_243250 3' tagging analytical primer fwd	CGCCGTGTACCAATACATTC	Genotyping primers for C-terminal tagging
TGGT1_243250 3' tagging analytical primer rvs	GAGAACAACTGACGCAAGAC	Genotyping primers for C-terminal tagging

TGGT1_208420 3' tagging gRNA fwd	AAGTT gCCTCCAAGTCTTAACTCACG G	gRNA for C-terminal tagging
TGGT1_208420 3' tagging gRNA rvs	AAAAC CGTGAGTTAAGACTTGGAGGc A	gRNA for C-terminal tagging
TGGT1_208420 5' upstream loxP gRNA fwd	AAGTT GTTCTAGAAAAGAGTCAAAG G	gRNA for 5' loxP insertion
TGGT1_208420 5' upstream loxP gRNA rvs	AAAAC CTTTGACTCTTTTCTAGAAC A	gRNA for 5' loxP insertion
TGGT1_240380 3' tagging gRNA fwd	AAGTTgAGCGGTGGAGGGTGGATTTCG	gRNA for C-terminal tagging
TGGT1_240380 3' tagging gRNA rvs	AAAACGAAATCCACCCTCCACCGCTcA	gRNA for C-terminal tagging
TGGT1_240380 5' upstream loxP gRNA fwd	AAGTT gTGTCGACGCAGAGAAGTGGA G	gRNA for 5' loxP insertion
TGGT1_240380 5' upstream loxP gRNA rvs	AAAAC TCCACTTCTCTGCGTCGACAc A	gRNA for 5' loxP insertion
TGGT1-254370 3' tagging gRNA fwd	AAGTTgTCTGGAGCAACGCAGAACCTG	gRNA for C-terminal tagging
TGGT1-254370 3' tagging gRNA rvs	AAAACAGGTTCTGCGTTGCTCCAGAcA	gRNA for C-terminal tagging
TGGT1-254370 5' upstream loxP gRNA fwd	AAGTTgTTCGTCGTATTCGATAGCTCG	gRNA for 5' loxP insertion
TGGT1-254370 5' upstream loxP gRNA rvs	AAAACGAGCTATCGAATACGACGAAcA	gRNA for 5' loxP insertion
TGGT1_230820 3' tagging gRNA fwd	AAGTTGAATCATGCTGTACCCAATGG	gRNA for C-terminal tagging
TGGT1_230820 3' tagging gRNA rvs	AAAACCATTGGGTACAGCATGATTCA	gRNA for C-terminal tagging
TGGT1_230820 5' upstream loxP gRNA fwd	AAGTTgATGCAGAGGCTAATCGACACG	gRNA for 5' loxP insertion
TGGT1_230820 5' upstream loxP gRNA rvs	AAAACGTGTCGATTAGCCTCTGCATcA	gRNA for 5' loxP insertion
TGGT1_238390 3' tagging gRNA fwd	AAGTTgAGAGCTTGTCAGCATGGAGTG	gRNA for C-terminal tagging
TGGT1_238390 3' tagging gRNA rvs	AAAACACTCCATGCTGACAAGCTCTcA	gRNA for C-terminal tagging
TGGT1_238390 5' upstream loxP gRNA fwd	AAGTTgCGTATCCTCGGTCTCTCCACG	gRNA for 5' loxP insertion
TGGT1_238390 5' upstream loxP gRNA rvs	AAAACGTGGAGAGACCGAGGATACGcA	gRNA for 5' loxP insertion
UPRT 1st exon gRNA fwd[§§§]	AAGTTGCCAGGAAGAAAGCATTCTCCG	gRNA for replacing UPRT locus with chromobody-emerald construct
UPRT 1st exon gRNA rvs[§§§]	AAAACGGAGAATGCTTTCTTCCTGGCA	gRNA for replacing UPRT locus with chromobody-emerald construct

CbEmerald construct amplification + homologies for insertion into UPRT locus fwd[§§§]	CAGGTCCCAGCGAGCGGAAAGCTCCTTGTCGATCCCCGATATTCGACAAACGACCAGG AAGAAAGCATTCCCCCCTCGAGGTCGACG	Chromobody-emerald construct amplification with homologies
CbEmerald construct amplification + homologies for insertion into UPRT locus rvs[§§§]	GTTTATCCTCTTGAGGCGTGCTTTTTCCAGTCCGCGATTCCGTCAGCGGTCTGTCAAAA AAACTAGAGACGTGTCACTGTAGCCTGCCA	Chromobody-emerald construct amplification with homologies
CbEmerald construct insertion into UPRT locus genotyping fwd[§§§]	TTTCTCGGCTCCACCTCATTCC	Chromobody-emerald genotyping primer
CbEmerald construct insertion into UPRT locus integration rvs[§§§]	CCCGATTTTCCCAAAAATGGCG	Chromobody-emerald integration primer
CbEmerald construct insertion into UPRT locus genotyping rvs[§§§]	CCGTTACAGGTGTACGGGACTC	Chromobody-emerald genotyping primer
frm1 3' tagging gRNA fwd[##]	AAGTTGAAATGAGTCTGAGACTTTCG	gRNA for C-terminal tagging
frm1 3' tagging gRNA rvs[##]	AAAACGAAAGTCTCAGACTCATTTCA	gRNA for C-terminal tagging
frm1 3' tagging homology primer fwd[##]	caactcccgtggcgctgcttgtgtgtgtgttcaataacagGGATGAAAGCTAAAATTGGAAGTGGAGGA	PCR amplification of tags for C-terminal tagging
frm1 3' tagging homology primer rvs[##]	GTCGACCAACAGTCGCTCCTTCAGCACCTGACCACTGAGCGCTTCCGGAAATAACTTC GTATAATGTATGCTATACG	PCR amplification of tags for C-terminal tagging
frm1 3' tagging analytical primer fwd[##]	GACTCAAGTCGACTGCAGTC	Genotyping primers for C-terminal tagging
frm1 3' tagging analytical primer rvs[##]	TGGCATTGCCTAAATGATTG	genotyping primers for C-terminal tagging
frm1 5' upstream loxP gRNA fwd[##]	AAGTTGAAAGCGTATCAGACATGGTG	gRNA for 5' loxP insertion
frm1 5' upstream loxP gRNA rvs[##]	AAAACACCATGTCTGATACGCTTTCA	gRNA for 5' loxP insertion
frm1 5' loxp insertion homology[##]	CCCAAGCACCGATTTGGAGTCTCTAGTCCCACCATAACTTCGTATAGCATACATTATAC GAAGTTATATGTCTGATACGCTTTCGGAATCAATTGAACTC	Repair templates for insertion of 5' loxp
frm1 5' loxp insertion analytical primer fwd[##]	TCTAGTCCCACCATAACTTCG	Integration primers for insertion of 5' loxp
frm1 5' loxp insertion analytical primer rvs[##]	AGACTACCAGCACGTGTG	Integration/genotyping primers for insertion of 5' loxp
frm1 5' loxp insertion analytical primer fwd[##]	CTCTGTCTGGGAAGTTTCTTACC	Genotyping primers for insertion of 5' loxp
gac 3' tagging gRNA fwd[#]	AAGTTGTAAGGGCAGTCTCTGGAGTCG	gRNA for C-terminal tagging

gac 3' tagging gRNA rvs[#]	AAAACGACTCCAGAGACTGCCCTTACA	gRNA for C-terminal tagging
gac 3' tagging homology primer fwd[#]	CATTTGTCGAGATGATGGTGCAGTGGCGTGACGCTGCAACGTACAATTTTGCTAAAATT GGAAGTGGAGG	PCR amplification of tags for C-terminal tagging
gac 3' tagging homology primer rvs[#]	CGGCGTTGACTAGCGTCCGGTCGCGTCCTCAGGCGCAGCGGCCGCCGGACATAACTTC GTATAATGTATGCTATACG	PCR amplification of tags for C-terminal tagging
gac 3' tagging analytical primer fwd[#]	CATGGTCGCGAAGAGTCAG	Genotyping primers for C-terminal tagging
gac 3' tagging analytical primer rvs[#]	ACTTGCCGAACTCCAAGG	Genotyping primers for C-terminal tagging
myoh 3' tagging gRNA fwd	AAGTTgTCCCAGTTCGGATTCACCGAG	gRNA for C-terminal tagging
myoh 3' tagging gRNA rvs	AAAACTCGGTGAATCCGAACTGGGAcA	gRNA for C-terminal tagging
myoh 3' tagging homology primer fwd	CGCGAGGCGCTGCTGCTGCTCCCTCTGCAATCCGCACCCGTCCGTCGGTaAACCCaAAtT GGGAcCCgATGGCgTAtAAt GCTAAAATTGGAAGTGGAGG	PCR amplification of tags for C-terminal tagging
myoh 3' tagging homology primer rvs	AAGAAAGGCCTTTTTTCAACACTCACCAGCGGGCAGCCGCCAAAAAGATC ATAACTTCGTATAATGTATGCTATACG	PCR amplification of tags for C-terminal tagging
myoh 3' tagging analytical primer fwd	CGCCGTGTACCAATACATTC	Genotyping primers for C-terminal tagging
myoh 3' tagging analytical primer rvs	GAGAACAACTGACGCAAGAC	Genotyping primers for C-terminal tagging
centrin1 3' tagging gRNA fwd[###]	AAGTTGAGGTTATCTCTGCGTGCGTG	gRNA for C-terminal tagging
centrin1 3' tagging gRNA rvs[###]	AAAACACGCACGCAGAGATAACCTCA	gRNA for C-terminal tagging
centrin1 3' tagging homology primer fwd[###]	AAATCAATGAAGAGGAGTTCATTCGTATCATGAGAAAGACGAATCTGTTCGCTAAAAT TGGAAGTGGAGG	PCR amplification of tags for C-terminal tagging
centrin1 3' tagging homology primer rvs[###]	GCGGAACCGGGACCGGTCCTGGAATCCCCGGGTTCGTTGCTTTCCCCACGATAACTTCG TATAATGTATGCTATACG	PCR amplification of tags for C-terminal tagging
centrin1 3' tagging analytical primer fwd[###]	GGAACCGCAGAATTTGAAGC	Genotyping primers for C-terminal tagging
centrin1 3' tagging analytical primer rvs[###]	CACACATTCTTGCTGGTCCG	Genotyping primers for C-terminal tagging
TGGT1_212780 3' tagging gRNA fwd	AAGTT gCGGGGAATGAAAGCCCCACA G	gRNA for C-terminal tagging

TGGT1_212780 3' tagging gRNA rvs	AAAAC TGTGGGGCTTTCATTCCCCGc A	gRNA for C-terminal tagging
TGGT1_212780 3' tagging homology primer fwd	AGAAAGTACAGGAACTCCGGAGACAACTGAGGGAACATGGGGTGCTATCTGCTAAAA TTGGAAGTGGAGG	PCR amplification of tags for C-terminal tagging
TGGT1_212780 3' tagging homology primer rvs	CAGGAACTGTGGCCTGTGAATCTGCCGTCTGTGCGGGGAATGAAAGCCCCATAACTTC GTATAATGTATGCTATACG	PCR amplification of tags for C-terminal tagging
TGGT1_212780 3' tagging analytical primer fwd	CAGTTCAGGTGACTTTGTGCAG	Genotyping primers for C-terminal tagging
TGGT1_212780 3' tagging analytical primer rvs	CGTTTCACTTGCGATTCTGG	Genotyping primers for C-terminal tagging
aamt 3' tagging gRNA fwd	AAGTT g CGACGAACTGAACCGGTGTG G	gRNA for C-terminal tagging
aamt 3' tagging gRNA rvs	AAAAC CACACCGGTTCAGTTCGTCGc A	gRNA for C-terminal tagging
aamt 3' tagging homology primer fwd	AAGCCCCTGCACAGGTGTCCTCGGATGCCGCCAAAGGTGCCCCGACGAACGCTAAAAT TGGAAGTGGAGG	PCR amplification of tags for C-terminal tagging
aamt 3' tagging homology primer rvs	TATGTGTTGCTTTCGGCTTATATGCGGCCCACTTTCCCCAGTCTCCACACATAACTTCGT ATAATGTATGCTATACG	PCR amplification of tags for C-terminal tagging
aamt 3' tagging analytical primer fwd	cacatcgtgtgggtagatcg	Genotyping primers for C-terminal tagging
aamt 3' tagging analytical primer rvs	GCAGAACAGAGTCGAAGTCTAC	Genotyping primers for C-terminal tagging
TGGT1_263070 3' tagging gRNA fwd	AAGTT gAAGTCCATGAAAAAGGTCTC G	gRNA for C-terminal tagging
TGGT1_263070 3' tagging gRNA rvs	AAAAC GAGACCTTTTTCATGGACTTc A	gRNA for C-terminal tagging
TGGT1_263070 3' tagging homology primer fwd	AAGAAGAGCAACAGAAGGCAGCGAACCTTTCGGCGTCGAGCGTGAAAGCCGCTAAAA TTGGAAGTGGAGG	PCR amplification of tags for C-terminal tagging
TGGT1_263070 3' tagging homology primer rvs	AGCAAAAAGTCCCCTCCGGTCGATCATAAAAAAAAGTCCATGAAAAAGGT ATAACTTCGTATAATGTATGCTATACG	PCR amplification of tags for C-terminal tagging
TGGT1_263070 3' tagging analytical primer fwd	tttcagtgttgagtggcgac	Genotyping primers for C-terminal tagging
TGGT1_263070 3' tagging analytical primer rvs	CACCTACAGCATCTCTGCACTC	Genotyping primers for C-terminal tagging
TGGT1_284620 3' tagging gRNA fwd	AAGTT GAGATGCCTTAACTGTCGAA G	gRNA for C-terminal tagging

TGGT1_284620 3' tagging gRNA rvs	AAAAC TTCGACAGTTAAGGCATCTCA	gRNA for C-terminal tagging
TGGT1_284620 3' tagging homology primer fwd	GTGAAGGCTCTAAAAACAATAGCGATGCTGAAAGGTCCGAAAAGAGCGAC GCTAAAATTGGAAGTGGAGG	PCR amplification of tags for C-terminal tagging
TGGT1_284620 3' tagging homology primer rvs	AAGAGATACCAGCTGCATGCACAAAAATAGATGCTTCATCCTCACCATTC ATAACTTCGTATAATGTATGCTATACG	PCR amplification of tags for C-terminal tagging
TGGT1_284620 3' tagging analytical primer fwd	CAAAGCAGAACAGGATGCAGG	Genotyping primers for C-terminal tagging
TGGT1_284620 3' tagging analytical primer rvs	GATATAAGCACAACTCTCTCGCG	Genotyping primers for C-terminal tagging
icap16 3' tagging gRNA fwd	AAGTT GACATTGAATAAAACAGTGG G	gRNA for C-terminal tagging
icap16 3' tagging gRNA rvs	AAAAC CCACTGTTTTATTCAATGTC A	gRNA for C-terminal tagging
icap16 3' tagging homology primer fwd	AAGATGACGCTCAGGATCTTTCTTCGCGGTCCTCTACCAGCGGCAGCGGT GCTAAAATTGGAAGTGGAGG	PCR amplification of tags for C-terminal tagging
icap16 3' tagging homology primer rvs	GCGCACTTCTCGCCGAAGGCAGTCAGTCCAATCTTTGATTTACTCCTCCA ATAACTTCGTATAATGTATGCTATACG	PCR amplification of tags for C-terminal tagging
icap16 3' tagging analytical primer fwd	GGACGGCGTGTACTTTAATC	Genotyping primers for C-terminal tagging
icap16 3' tagging analytical primer rvs	CTCATTCTGTAAGCCGTTGC	Genotyping primers for C-terminal tagging
TGGT1_231160 3' tagging gRNA fwd§	AAGTTg ATTCTGCTGCTAAgtgcaaa G	gRNA for C-terminal tagging
TGGT1_231160 3' tagging gRNA rvs§	AAAAC tttgcacTTAGCAGCAGAAT c A	gRNA for C-terminal tagging
TGGT1_231160 3' tagging homology primer fwd§	CGGCTGCCAAGAAGATCTCCAAGAGCTCCAAGTCACGGGGATTCTGCTGCGCTAAAAT TGGAAGTGGAGG	PCR amplification of tags for C-terminal tagging
TGGT1_231160 3' tagging homology primer rvs§	agcacgtcgaaggaactgggaagag cag cggcgtcg cacg catg ccctttt ATAACTTCGTATAATGTATGCTATACG	PCR amplification of tags for C-terminal tagging
TGGT1_231160 3' tagging analytical primer fwd§	cgtgcagagagtgggggagaca	Genotyping primers for C-terminal tagging
TGGT1_231160 3' tagging analytical primer rvs§	agcagccagagcgagggagaaa	Genotyping primers for C-terminal tagging
TGGT1_238170 3' tagging gRNA fwd§	AAGTT g TAAgcgaagagtcgaacctc G	gRNA for C-terminal tagging

TGGT1_238170 3' tagging gRNA rvs§	AAAAC gaggttcgactcttcgcTTA c A	gRNA for C-terminal tagging
TGGT1_238170 3' tagging homology primer fwd§	TCGCCATCGCCACGAAATCGCGTCTCTTCTCGCTCTTACACGACCTTCTT GCTAAAATTGGAAGTGGAGG	PCR amplification of tags for C-terminal tagging
TGGT1_238170 3' tagging homology primer rvs§	gtatacgtatgagaacgtatttgagtgtttgtaagcatgtttatcccgagATAACTTCGTATAATGTATGCTATACG	PCR amplification of tags for C-terminal tagging
TGGT1_238170 3' tagging analytical primer fwd§	TCTCCTCTCGCTCGTCAACGCA	Genotyping primers for C-terminal tagging
TGGT1_238170 3' tagging analytical primer rvs§	cgtagactgctgccagctctgc	Genotyping primers for C-terminal tagging
TGGT1_253440 3' tagging gRNA fwd§	AAGTT gcatacacgtgTCACTGTTGC G	gRNA for C-terminal tagging
TGGT1_253440 3' tagging gRNA rvs§	AAAAC GCAACAGTGAcacgtgtatg c A	gRNA for C-terminal tagging
TGGT1_253440 3' tagging homology primer fwd§	TCGGAAAGGCACAACAACAATTTCAACAACAGCAACAGCTCCAGCAACAG GCTAAAATTGGAAGTGGAGG	PCR amplification of tags for C-terminal tagging
TGGT1_253440 3' tagging homology primer rvs§	gctttgccgcatcacgcaaactgtgcattcccagcgcacgcatacacgtgATAACTTCGTATAATGTATGCTATACG	PCR amplification of tags for C-terminal tagging
TGGT1_253440 3' tagging analytical primer fwd§	TACCAGGCGCGTCACCAACAAC	Genotyping primers for C-terminal tagging
TGGT1_253440 3' tagging analytical primer rvs§	tgcgcgaaaaagggagatgcgt	Genotyping primers for C-terminal tagging
TGGT1_293480 3' tagging gRNA fwd§	AAGTT g TGAtctgcctcgcgagctct G	gRNA for C-terminal tagging
TGGT1_293480 3' tagging gRNA rvs§	AAAACagagctcgcgaggcagaTCA c A	gRNA for C-terminal tagging
TGGT1_293480 3' tagging homology primer fwd§	CCCTGTTGCCGGTTTTACCCCACGCGTTGGAAGTTGTCACTTCGGGGGCGGCTAAAATT GGAAGTGGAGG	PCR amplification of tags for C-terminal tagging
TGGT1_293480 3' tagging homology primer rvs§	ggaacggacactgcggcatatatttagccatcaagtagaagtcgcctaga ATAACTTCGTATAATGTATGCTATACG	PCR amplification of tags for C-terminal tagging
TGGT1_293480 3' tagging analytical primer fwd§	TTCGGTGCGAGACGTCACTCCT	Genotyping primers for C-terminal tagging
TGGT1_293480 3' tagging analytical primer rvs§	ggcgactgacttccccaaacgg	Genotyping primers for C-terminal tagging
akmt 3' tagging gRNA fwd§§	AAGTT GGCCAGTTGAggaacaattg G	gRNA for C-terminal tagging

akmt 3' tagging gRNA rvs§§	AAAAC caattgttccTCAACTGGCC A	gRNA for C-terminal tagging
akmt 3' tagging homology primer fwd§§	TCGCTGCCGGAACCAAAAAAACTGCATGCGAGGAACGCCTACCGGCCAGT GCTAAAATTGGAAGTGGAGG	PCR amplification of tags for C-terminal tagging
akmt 3' tagging homology primer rvs§§	agccctttacccctttgcgaacacgagaagtcctccgccagtctcccacaa ATAACTTCGTATAATGTATGCTATACG	PCR amplification of tags for C-terminal tagging
akmt 3' tagging analytical primer fwd§§	CGGCCCACAAGCTGAACGTGAT	genotyping primers for C-terminal tagging
akmt 3' tagging analytical primer rvs§§	tttcgacagagtgcacacggcc	Genotyping primers for C-terminal tagging
akmt 5' upstream loxP gRNA fwd§§	AAGTT gtgatgttgatggagagtcg G	gRNA for 5' loxP insertion
akmt 5' upstream loxP gRNA rvs§§	AAAAC cgactctccatcaacatcac A	gRNA for 5' loxP insertion
akmt 5' loxp insertion homology§§	gagccgtgcccctggtgaccacagtaccctcgaATAACTTCGTATAGCATACATTATACGAAGTTATctctcca tcaacatcacgtcttaatctaacaga	Repair templates for insertion of 5' loxp
akmt 5' loxp insertion analytical primer fwd§§	GCATACATTATACGAAGTTATctctccatc	Integration primers for insertion of 5' loxp
akmt 5' loxp insertion analytical primer rvs§§	TTCCCCGTAGTCGTCACCGCTT	Integration/genotyping primers for insertion of 5' loxp
akmt 5' loxp insertion analytical primer fwd§§	acgtgtggaatgccttgcctcg	Genotyping primers for insertion of 5' loxp
TGGT1_284620 5' upstream loxP gRNA fwd	AAGTT gTTCTTTGGTGGACGTGGAGA G	gRNA for 5' loxP insertion
TGGT1_284620 5' upstream loxP gRNA rvs	AAAAC TCTCCACGTCCACCAAAGAAc A	gRNA for 5' loxP insertion
TGGT1_284620 5' loxp insertion homology	CCGAATCTTCAGGCTTTTTCGATTCTTCCCTCTATAACTTCGTATAGCATACATTATACG AAGTTATCCACGTCCACCAAAGAAAGATGAGCCGCCGCGT	Repair templates for insertion of 5' loxp
TGGT1_284620 5' loxp insertion analytical primer fwd	GCATACATTATACGAAGTTATCCACG	Integration primers for insertion of 5' loxp
TGGT1_284620 5' loxp insertion analytical primer rvs	CTCAACATCGACATCCAAATCACC	Integration/genotyping primers for insertion of 5' loxp
TGGT1_284620 5' loxp insertion analytical primer fwd	CTCTAATTGCCTCACCAGTC	Genotyping primers for insertion of 5' loxp
Pckmt 3' tagging gRNA fwd§§	AAGTTGAAGTAGcaaggatcaaagcG	gRNA for C-terminal tagging

pckmt 3' tagging gRNA rvs§§	AAAACcccgctttgatccttgCTACTTCA	gRNA for C-terminal tagging
pckmt 3' tagging homology primer fwd§§	AGAAAGGTCCGCCTTTGCTTGGGAAGAAAGGTTTACCACCTCCAAAGAAGGCTAAAATTGGAAGTGGAGG	PCR amplification of tags for C-terminal tagging
pckmt 3' tagging homology primer rvs§§	caaaactgtcgaaaaccgggccatgaaatgcgagtgcccctttgcccgctATAACTTCGTATAATGTATGCTATACG	PCR amplification of tags for C-terminal tagging
pckmt 3' tagging analytical primer fwd§§	AAGAAAGCTCCACCGCCTCCAC	Genotyping primers for C-terminal tagging
pckmt 3' tagging analytical primer rvs§§	agcaaacgcggaattctgggca	Genotyping primers for C-terminal tagging

1.8 Plasmids

Table II-15. Plasmids used in this study.
1: PCR templates for generation of repair templates. 2: Generation of Cas9_sgRNA plasmid backbones. 3: Introduce DSB of a target gene. 4. PV marker.

Plasmid		Application	Source/Reference
HA plasmid	pUC19 3HA_LoxP_Amp	1	Meissner Lab
Halo plasmid	pUC19 Halo-LoxP_Amp	1	Meissner Lab
mCherry plasmid	pUC19 mcherry-LoxP_Amp	1	Meissner Lab
SYFP2 plasmid	pUC19 SYFP2-LoxP_Amp	1	Meissner Lab
TurboID plasmid	pGEM TurboID_ LoxP_Amp	1	Meissner Lab
SNAP plasmid	pGEM SNAP_ LoxP_Amp	1	Meissner Lab
CbEm plasmid	pDhfr_CbEm_Amp	1	(Periz et al. 2017)
Cas9_YFP plasmid	pTub_Cas9YFP/pU6_ccdB_tracrRNA_Amp	2	Meissner Lab
Cas9_YFP_sgRNA plasmid	pTub_Cas9YFP/pU6_sgRNA_Amp	3	This study
SAG1ΔGPI plasmid	pTub_SAGΔGPI_DsRed_CAT	4	Meissner lab

1.9 Cell strains

Table II-16. Bacteria and mammalian cell lines used in this study.

Strain/Cells	Source	Note
E. coli DH5α	New England BioLabs	Competence: chemically competent
Human foreskin fibroblasts (HFF)	ATCC® SCRC-1041™	Organism: Homo sapiens

Table II-17. *T. gondii* strains generated/used in this study.

Strains	Genotype	Reference
RHsCas9	RH sCas9/CbEm/FNR-RFP/Δhx	(Li et al. 2022)
RHsCas9-*act1*	RH sCas9/CbEm/FNR-RFP/Δhx/act1-gRNA	(Li et al. 2022)
RHsCas9-*sag1*	RH sCas9/CbEm/FNR-RFP/Δhx/sag1-gRNA	(Li et al. 2022)
DiCreΔ*ku80*	RH DiCre-T2A/Δku80/Δhx/CAT	(Andenmatten et al. 2013, Hunt et al. 2019)
cgp-Halo	RH DiCre-T2A/Δku80/Δhx/CAT/cgp-Halo-loxP	This study
slf-Halo	RH DiCre-T2A/Δku80/Δhx/CAT/slf-Halo-loxP	This study
slf-mCherry	RH DiCre-T2A/Δku80/Δhx/CAT/slf-mCherry-loxP	This study
loxP*slf*-Halo/CbEm	RH DiCre-T2A/Δku80/Δhx/CAT/loxp-slf-Halo-loxP/Δuprt/CbEm	This study
loxP*cgp*-Halo	RH DiCre-T2A/Δku80/Δhx/CAT/loxP-cgp-Halo-loxP	This study

loxP*slf*-mCherry	RH DiCre-T2A/Δku80/Δhx/CAT/loxP-slf-mCherry-loxP	This study
loxP*slf*-Halo	RH DiCre-T2A/Δku80/Δhx/CAT/loxP-slf-Halo-loxP	This study
loxP*cgp*-Halo/Centrin 1-3HA	RH DiCre-T2A/Δku80/Δhx/CAT/loxP-cgp-Halo-loxP/Centrin 1-3HA-loxP	This study
loxP*slf*-mCherry/*gc*-3HA	RH DiCre-T2A/Δku80/Δhx/CAT/loxP-slf-mCherry-loxP/gc-3HA-loxP	This study
loxP*slf*-mCherry/*ugo*-3HA	RH DiCre-T2A/Δku80/Δhx/CAT/loxP-slf-mCherry-loxP/ugo-3HA-loxP	This study
loxP*slf*-mCherry/*cdc50.1*-SYFP2	RH DiCre-T2A/Δku80/Δhx/CAT/loxP-slf-mCherry-loxP/cdc50.1-SYFP2-loxP	This study
loxP*slf*-mCherry/ugo-SYFP2	RH DiCre-T2A/Δku80/Δhx/CAT/loxP-slf-mCherry-loxP/ugo-SYFP2-loxP	This study
cdc50.1-SYFP2/*slf*-Halo	RH DiCre-T2A/Δku80/Δhx/CAT/cdc50.1-SYFP2-loxP/slf-Halo-loxP	This study
ugo-SYFP2/*slf*-Halo	RH DiCre-T2A/Δku80/Δhx/CAT/ugo-SYFP2-loxP/slf-Halo-loxP	This study
gc-SYFP2/*slf*-Halo	RH DiCre-T2A/Δku80/Δhx/CAT/gc-SYFP2-loxP/slf-Halo-loxP	This study
loxP*gc*-SYFP2/*slf*-Halo	RH DiCre-T2A/Δku80/Δhx/CAT/loxP-gc-SYFP2-loxP/slf-Halo-loxP	This study
loxP*ugo*-SYFP2/*slf*-Halo	RH DiCre-T2A/Δku80/Δhx/CAT/loxP-ugo-SYFP2-loxP/slf-Halo-loxP	This study
loxP*cdc50.1*-SYFP2/*slf*-Halo	RH DiCre-T2A/Δku80/Δhx/CAT/loxP-cdc50.1-SYFP2-loxP/slf-Halo-loxP	This study
loxP*cgp*-Halo/*rng2*-6HA	RH DiCre-T2A/Δku80/Δhx/CAT/loxP-cgp-Halo-loxP/rng2-6HA/dhfr	This study
loxP*cgp*-Halo/*sas6l*-eGFP	RH DiCre-T2A/Δku80/Δhx/CAT/loxP-cgp-Halo-loxP/sas6l-eGFP/dhfr	This study
loxP*cgp*-Halo/*myoh*-SYFP2	RH DiCre-T2A/Δku80/Δhx/CAT/loxP-cgp-Halo-loxP/myoh-SYFP2-loxP	This study
loxP*cgp*-Halo/*frm1*-SNAP	RH DiCre-T2A/Δku80/Δhx/CAT/loxP-cgp-Halo-loxP/*frm1*-SNAP-loxP	This study
loxP*frm1*-mCherry	RH DiCre-T2A/Δku80/Δhx/CAT/loxP-*frm1*-mCherry-loxP	Generated by Mirko Singer
loxP*frm1*-mCherry/*cgp*-Halo	RH DiCre-T2A/Δku80/Δhx/CAT/loxP-frm1-mCherry-loxP/*cgp*-Halo-loxP	This study
cgp-TurboID/*frm1*-3HA	RH DiCre-T2A/Δku80/Δhx/CAT/cgp-TurboID-loxP/frm1-3HA-loxP	This study
frm1-TurboID/loxP*cgp*-Halo	RH DiCre-T2A/Δku80/Δhx/CAT/loxP-cgp-Halo-loxP/frm1-TurboID-loxP	This study
253440-SYFP2	RH DiCre-T2A/Δku80/Δhx/CAT/loxP-cgp-Halo-loxP/253440-SYFP2-loxP	This study
231160-SYFP2	RH DiCre-T2A/Δku80/Δhx/CAT/loxP-cgp-Halo-loxP/231160-SYFP2	This study
263070-SYFP2	RH DiCre-T2A/Δku80/Δhx/CAT/loxP-cgp-Halo-loxP/263070-SYFP2-loxP	This study

212780-3HA	RH DiCre-T2A/Δku80/Δhx/CAT/loxP-cgp-Halo-loxP/212780-3HA-loxP	This study
238170-SYFP2	RH DiCre-T2A/Δku80/Δhx/CAT/loxP-cgp-Halo-loxP/238170-SYFP2-loxP	This study
293480-SYFP2	RH DiCre-T2A/Δku80/Δhx/CAT/loxP-frm1-Halo-loxP/293480-SYFP2-loxP	This study
loxP*cgp*-Halo/*akmt*-SYFP2	RH DiCre-T2A/Δku80/Δhx/CAT/loxP-cgp-Halo-loxP/akmt-SYFP2-loxP	This study
loxP*cgp*-Halo/*pckmt*-SYFP2	RH DiCre-T2A/Δku80/Δhx/CAT/loxP-cgp-Halo-loxP/pckmt-SYFP2-loxP	This study
loxP*cgp*-Halo/*icap16*-SYFP2	RH DiCre-T2A/Δku80/Δhx/CAT/loxP-cgp-Halo-loxP/icap16-SYFP2-loxP	This study
loxP*cgp*-Halo/*dap1*-SYFP2	RH DiCre-T2A/Δku80/Δhx/CAT/loxP-cgp-Halo-loxP/*dap1*-SYFP2-loxP	This study
loxP*cgp-Halo/gac-SYFP2*	RH DiCre-T2A/Δku80/Δhx/CAT/loxP-cgp-Halo-loxP/gac-SYFP2-loxP	This study
loxP*cgp-Halo/akmt-SYFP2*	RH DiCre-T2A/Δku80/Δhx/CAT/loxP-cgp-Halo-loxP/akmt-SYFP2-loxP	This study
loxP*cgp*-Halo/*aamt*-sYFP2	RH DiCre-T2A/Δku80/Δhx/CAT/loxP-cgp-Halo-loxP/*aamt*-sYFP2-loxP	This study
loxP*akmt*-SYFP2/*cgp*-Halo	RH DiCre-T2A/Δku80/Δhx/CAT/loxP-akmt-SYFP2-loxP/cgp-Halo-loxP	This study
loxP*frm1*-Halo	RH DiCre-T2A/Δku80/Δhx/CAT/loxP-frm1-Halo-loxP	This study
loxP*frm1*-Halo/*pckmt*-SYFP2	RH DiCre-T2A/Δku80/Δhx/CAT/loxP-frm1-Halo-loxP/pckmt-SYFP2-loxP	This study
loxP*frm1*-Halo/*dap1*-SYFP2	RH DiCre-T2A/Δku80/Δhx/CAT/loxP-frm1-Halo-loxP/dap1-SYFP2-loxP	This study
loxP*frm1*-Halo/*icap16*-SYFP2	RH DiCre-T2A/Δku80/Δhx/CAT/loxP-frm1-Halo-loxP/icap16-SYFP2-loxP	This study
loxP*frm1*-Halo/*akmt*-SYFP2	RH DiCre-T2A/Δku80/Δhx/CAT/loxP-frm1-Halo-loxP/akmt-SYFP2-loxP	This study
loxP*frm1*-Halo/*aamt*-SYFP2	RH DiCre-T2A/Δku80/Δhx/CAT/loxP-frm1-Halo-loxP/aamt-SYFP2-loxP	This study
loxP*frm1*-Halo/*gac*-SYFP2	RH DiCre-T2A/Δku80/Δhx/CAT/loxP-frm1-Halo-loxP/gac-SYFP2-loxP	This study
loxP*akmt*-SYFP2	RH DiCre-T2A/Δku80/Δhx/CAT/loxP-akmt-SYFP2-loxP	Generated by Elena Jimenez-Ruiz
loxP*akmt*-SYFP2/*frm1*-Halo	RH DiCre-T2A/Δku80/Δhx/CAT/loxP-akmt-SYFP2-loxP/frm1-Halo-loxP	This study
loxP*akmt*-SYFP2/*dap1*-Halo	RH DiCre-T2A/Δku80/Δhx/CAT/loxP-akmt-SYFP2-loxP/dap1-Halo-loxP	This study
loxP*dap1*-SYFP2	RH DiCre-T2A/Δku80/Δhx/CAT/loxP-dap1-SYFP2-loxP	This study
loxP*dap1*-SYFP2/*cgp*-Halo	RH DiCre-T2A/Δku80/Δhx/CAT/loxP-dap1-SYFP2-loxP/cgp-Halo-loxP	This study

loxP*dap1*-SYFP2/*frm1*-Halo	RH DiCre-T2A/Δku80/Δhx/CAT/loxP-dap1-SYFP2-loxP/frm1-Halo-loxP	This study
loxPdap1-SYFP2/icap16-Halo	RH DiCre-T2A/Δku80/Δhx/CAT/loxP-dap1-SYFP2-loxP/icap16-Halo-loxP	This study
loxPdap1-SYFP2/pckmt-Halo	RH DiCre-T2A/Δku80/Δhx/CAT/loxP-dap1-SYFP2-loxP/pckmt-Halo-loxP	This study
loxP*dap1*-SYFP2/*aamt*-Halo	RH DiCre-T2A/Δku80/Δhx/CAT/loxP-dap1-SYFP2-loxP/aamt-Halo-loxP	This study

2. Methods

2.1 Molecular biology methods

2.1.1 Restriction digest

Digestion setup was done following the manufacturer's instructions. Briefly, 5 µg of Cas9_YFP plasmid (Table II-15) was digested with 5 µL of BsaI-HFv2 and 5 µL of rCutSmart buffer (10x) and topped up with ultrapure water to a total volume of 50 µL. The mixture was incubated at 37 °C to digest for 2 hours and then subjected to agarose gel electrophoresis to obtain the backbones for generation of the Cas9_YFP_sgRNA plasmid, followed by DNA purification.

2.1.2 Agarose gel electrophoresis

Agarose gel electrophoresis was carried out to separate DNA fragments. For DNA loading, 0.8–1% agarose in 1x TAE buffer was prepared. The gel was loaded with a mixture of DNA, 6x purple loading dye (final concentration: 1x), GelRed nucleic acid stain (final concentration: 1/1200) and ultrapure water before being run at 80–120 V for varying lengths of time based on DNA fragment size and applied voltages. DNA ladders were used as markers for the size of DNA fragments. After electrophoresis, DNA was visualised by UV light. For DNA fragment recovery, GelRed nucleic acid stain was replaced

with Midori Green Advance 4 µL. Midori Green Advance was used for the staining of a 100-mL agarose gel.

2.1.3 DNA purification

An ExtractMe DNA Clean-Up&Gel-Out Kit (Table II-5) was used to purify DNA following the manufacturer's instructions. DNA was eluted in elution buffer for 5 minutes, followed by centrifugation for 1–2 minutes.

2.1.4 Annealing of oligonucleotides

The sgRNAs were ordered as oligonucleotides by Thermo Fisher Scientific Company. 2 µL of 10 pmol/µL forward primer and reverse primer were pipetted into a PCR tube and mixed with 16 µL of annealing buffer. The reactions were placed in a heat block at 95 °C for 5 minutes. It was then allowed to cool naturally to room temperature before being used for ligation.

2.1.5 Ligation

For the generation of the Cas9_YFP_sgRNA plasmid, annealed primers were ligated into Cas9_YFP_sgRNA plasmid backbones. Briefly, 25–50 ng of the purified Cas9_YFP_sgRNA plasmid backbone, 5 µL of bond primers, 1 µL of T4 DNA ligase and 1 µL of 10x T4 buffer were mixed and topped up with ultrapure water to a total volume of 10 µL. Ligation reactions were at room temperature for at least 2 hours before transforming into bacteria.

2.1.6 Plasmid extraction

An ExtractMe plasmid Mini Kit (Table II-5) was used for plasmid extraction from bacteria following the manufacturer's instructions. Before extraction, bacteria were pelleted. In the last step, DNA was

eluted in elution buffer for 5 minutes, followed by centrifugation for 1–2 minutes.

2.1.7 Genomic DNA extraction

Genomic DNA of *T. gondii* was extracted using the ExtractMe genomic DNA Kit (Table II-5) according to the manufacturer's instructions. Before extraction, parasites were pelleted by centrifugation at 1,500 g for 5 minutes.

2.1.8 Polymerase chain reaction (PCR)

In this study, PCR amplification was used to genotype parasites and generate repair templates. For genotyping, 25-µL reactions were used, and for making repair templates, 50-µL reactions were used. The reaction setup is shown in Table II-18. The thermocycling conditions set up are shown in Table II-19. The time depended on the PCR product size. In general, the longer products were, the longer the time required.

Table II-18. Reaction setup.

Component	25-µL reaction	50-µL reaction
5X Q5 reaction buffer	5 µL	10 µL
10 mM dNTPs	0.5 µL	1 µL
10 µM forward primer	1.25 µL	2.5 µL
10 µM reverse primer	1.25 µL	2.5 µL
Template DNA	1–2 µL	1–2 µL
Q5 high-fidelity DNA polymerase	0.25 µl	0.5 µL
Ultrapure water	to 25 µl	to 50 µL

Table II-19. Thermocycling conditions for PCR.

*Calculated by NEBTm Calculator.

Step	Temperature	Time
Initial denaturation	98 °C	30 s
35 cycles	98 °C	10 s

	*50–68 °C 72 °C	30 s 1–4 min
Final extension	72 °C	2–5 min
Hold	4 °C	

2.1.9 Ethanol precipitation of DNA

Repair templates made by PCR require purification and precipitation before transfection into *T. gondii*. The precipitation steps were as follows. First, DNA was mixed with 2.5–3 volumes of ice-cold 100% ethanol and 0.1 volume of sodium acetate (3M, PH=5). This mix was then incubated at -20 °C overnight or at -80 °C for 1 hour. The mixture was then centrifuged to pellet DNA for at least 1 hour at 0–4 °C, followed by two washes with 70% ethanol (centrifugation for at least 15 minutes at a maximum speed each time). After the final wash, the ethanol was removed under sterile conditions. Finally, the DNA pellet was dried and resuspended in Amaxa P3 buffer before transfection into parasites. If transfections could not be performed on the same day, then after drying the DNA pellet, the DNA was directly resolved in 5 µL of ultrapure water and stored at -20 °C until use.

2.1.10 DNA sequencing

PCR products and plasmids were sent for sequencing at Eurofins Genomics. PCR products were purified before being sent for sequencing.

2.2 Protein methods

2.2.1 Preparation of loading samples

Protein samples were mixed with orange protein loading dye buffer (working concentration: 1x; Table II-8) and dithiothreitol (working concentration: 100 µM) and boiled for 10 minutes at 95 °C. After boiling, the samples were pulse centrifuged before loading them on polyacrylamide gels.

2.2.2 SDS-polyacrylamide gel electrophoresis

Different molecular weights of proteins were separated using polyacrylamide gel electrophoresis (PAGE). Briefly, after loading samples into gel pockets, the machine was operated at 120–150 V with 1x running buffer (Table II-8) until the markers were sufficiently separated. Typically, the machine was stopped when the dye reached the bottom of the gel. 5-8 µL of Chameleon™ Duo Li-Cor marker was used to measure the molecular weight of proteins.

2.2.3 Western blot

After SDS-PAGE separation, proteins were transferred to nitrocellulose membranes using wet transfer and 400 mA for 60–70 minutes. Ponceau S staining (Table II-8) was then conducted to evaluate the transfer efficiency, followed by washing with 0.2% TBST (Table II-8) and ddH_2O. The membrane was blocked at room temperature for 1 hour, followed by labelling at room temperature or 4 °C overnight. The membrane was then washed three times for 5 minutes each time. The membrane was then incubated for 1 hour at room temperature with secondary antibodies. The blots were washed three times with 0.1% TBST, followed by a single wash with TBS (Table II-8). LI-COR Odyssey was used to scan the blots.

2.3 Microbiology methods

2.3.1 Bacteria transformation

For transformation, competent DH5α bacteria were used. The purpose of this step was to generate the Cas9_YFP-sgRNA plasmid. The bacteria were defrosted on ice, with 5 µL of ligated primers added to 30–50 µL of bacteria, and they were incubated on ice for 30 minutes. Next, the bacteria were heat-shocked for 30 seconds at 42 °C. The

bacteria were then placed on ice and allowed to incubate for 3 minutes before 250 µL of SOC medium was added. The bacteria were cultured at 37 °C for 1 hour while shaking. The bacteria were spread on LB agar plates supplemented with 100 g/mL of ampicillin and incubated at 37 °C for 14-17 hours.

2.3.2 Liquid cultures and cryopreservation stocks of *E. coli*

Single bacteria colonies or bacteria from cryopreservation stocks were transferred into a LB medium with 100 g/mL of ampicillin, and then bacteria were allowed to grow for 14–17 hours at 37 °C while shaking. To make cryopreservation stocks, freshly grown liquid cultures of *E. coli* were mixed with 50% glycerol (v/v; Table II-6) in a ratio of 2:1 and stored at -80°C.

2.4 Cell biology

2.4.1 Culturing of *T. gondii* and host cells

Human foreskin fibroblasts (HFFs) were cultured in $DMEM_{complete}$ media (Table II-6) at 37 °C and 5% CO_2. *T. gondii* tachyzoites were grown on a confluent HHF monolayer in $DMEM_{complete}$ medium (Table II-6) at 37 °C with 5% CO_2. Parasites were inoculated onto a new monolayer when the monolayer of host cells was completely lysed by parasites.

2.4.2 Trypsin/EDTA treatment of mammalian cell lines

HFFs were split 1:4 each week by our technician, Marzena Broniszewska. Confluent HFFs were washed with warmed PBS. Trypsin/EDTA was then added to the HFFs and incubated at 37 °C with 5% CO_2 for 10 minutes. After trypsination, warm $DMEM_{complete}$ media was added to the condition to stop the reaction, and the cell suspension was then transferred to new dishes or flasks.

2.4.3 Cryopreservation of *T. gondii* and thawing of stabilates

For the cryopreservation of *T. gondii*, parasites were allowed to grow on confluent HFFs to form late-stage vacuoles. After taking the media out, the cells were scratched and put in a mixture of $DMEM_{complete}$ media (Table II-6) and 2x freezing media (Table II-6) with a ratio of 1:1. The mixture was then transferred to cryotubes, frozen and stored at -80°C.

The parasites were thawed at 37 °C, and then transferred to the HFFs and kept at 37 °C with 5% CO_2. After several hours, the media was changed.

2.4.4 Generation of tagged and floxed lines

To tag or flox proteins in a parasite of the DiCre background, EuPaGDT (Peng et al. 2015) was used to design sgRNAs cutting upstream or downstream of the genes of interest. All gRNAs used in this study are listed in Table II-13. The sgRNAs were ligated into the Cas9_YFP_sgRNA plasmid backbone (Table II-15). To generate repair templates for C-terminal tagging, PCR was performed. The homology primers are shown in Table II-14. Plasmids with various tags were used as DNA templates to generate the repair templates displayed in Table II-15. For each transfection, 100-200 µL of PCR products were generated. The repair templates for C-term tagging contained 50 nt of homologous overhangs and the desired tag-LoxP sequence. Single-stranded DNA (ssDNA) oligos containing loxP sequences flanked by 33 nt of homology were ordered from Thermo Fisher as repair templates for the insertion of the upstream loxP sequence. 2.5-µL oligos (10 µM) were used for transfection; 10–12

µg of plasmids were cotransfected with repair templates per transfection.

Transfections were carried out using 0.5–1 mL of freshly lysed parasites from a 6-cm dish (total volume of 4 mL). Precipitated DNA was resuspended in 100 µL of P3 buffer (from a P3 Primary Cell 4D Nucleofector X Kit L; Table II-5) and then used to resuspend the parasite pellet, after which the mixture was transferred into cuvettes and immediately electrophored by an Amaxa© 4D-Nucleofactor using programme FI-158. After transfection, the parasites were resuspended in 1 mL of prewarmed $DMEM_{complete}$ media and transferred to confluent HFFs for 24–48 hours of growth before FACS.

To do FACS, parasites were released by 27 G needles and filtered through 3-µm filters to eliminate host debris. 5–10 YFP-positive parasites were sorted into 96 well plates covered with HFFs. Single plaques were screened and picked after 5–7 days of growth. The selected clones were then checked by microscopy and/or PCR.

For the insertion of CbEm into floxed lines, a sgRNA targeting the uracil phosphoribosyltransferase locus was designed and cloned into a Cas9_YFP_sgRNA vector (Table II-15). This step was done by my colleague, Janessa Grech. A CbEm cassette from the CbEm plasmid (Table II-15) was amplified by PCR and inserted into the UPRT locus.

For tagging RNG2 and SAS6L proteins, 1 µM pyrimethamine was added to the media 24 hours post transfection to select transfectants with the DHFR cassette (Barylyuk et al. 2020). After drug selection for around 5–7 days, pooled parasites were checked by PCR. Positive

clones were isolated via serial dilutions and confirmed by PCR and immunofluorescence assay (IFA).

2.4.5 Serial dilutions

Serial dilutions were used to isolate clonal parasites. 50 µL of lysed parasites were added to a 96-well plate covered with confluent HFFs with 150 µL of media, followed by serial dilution. After 5–7 days of growth, single plaques were screened and picked into a new dish for culture.

2.5 Phenotypic assays

2.5.1 Immunofluorescence assay

Parasites were fixed with 4% PFA at room temperature for 15–20 minutes. Samples were then blocked and permeabilised with 2% BSA containing 0.2% TX-100 in PBS solution for at least 20 minutes. Primary and secondary antibodies (Table II-10) were used to label proteins for 1 hour and 45 min, respectively. After each labelling, samples were washed three times with PBS. α-GFP-ATTO-488 antibody was directly used for 1 hour after permeabilization. For staining SAG1 protein in the intracellular parasites, 1.5 hours were required for the permeabilization. To prevent bleach fluorescence, all steps were performed in the dark. Parasites carrying Halo or SNAP tags were labelled with respective dyes for 1 hour and followed by washing steps. Afterwards, parasites were incubated with media for 1 hour before fixation, unless specifically indicated elsewhere (Table II-12).

2.5.2 Plaque assay

500–1,000 parasites per well were used to infect confluent HFFs in 6-well plates and grown for 6 days with or without 50 nM rapamycin. Wells were washed once with PBS and fixed with ice-cold MeOH for 20 minutes. HFFs were stained by using Hemacolor® Rapid staining of blood smear solution 2 staining for 30 seconds, followed by solution 3 staining for 2 minutes, and washed three times with PBS. The procedures are the same for GABA or gabapentin plaque assays, but variable concentrations of GABA or gabapentin are added. Images were obtained using the LASX Navigator software and a Leica DMi8 wide-field microscope with a 10x objective. By establishing focus maps and applying focusing settings, a 12 x 12 field area in the centre of the area was chosen and scanned. After acquiring the images, the 'mosaic merge' processing tool was applied to integrate them into one final image.

2.5.3 Egress assay

10^5 sCas9 parasites were used to infect HFFs and incubated with ±50 nM rapamycin for 4 hours. HFFs were washed three times with $DMEM_{complete}$ (Table II-9) medium to remove non-invaded parasites and rapamycin before allowing parasites to grow for 44 hours, followed by induction egress with 2 µM Ci A23187.

In the case of parasites in the DiCre background, they were pretreated with ±50 nM rapamycin for 24 hours before being manually released to invade HFFs for 1 hour (3×10^5 parasites per well). HFFs were also washed three times with $DMEM_{complete}$, and parasites were allowed to grow for 32 hours before inducing egress. 0.2 µM HaloTag Oregon

Green or 20 nM Janelia Fluor 646 was incubated with Halo-tagged parasites for 1 hour and washed three times with PBS before inducing egress. To induce egress, $DMEM_{complete}$ medium was exchanged with pre-warmed $DMEM_{incomplete}$ (Table II-9) with various inducers for different times (2 µM Ci A23187 for 5 minutes, 50 µM BIPPO for 5 minutes or 125 µM propranolol hydrochloride for 7 minutes).

After the stimulation of egress, parasites were fixed with 4% PFA for 15–20 minutes. Egressed and non-egressed vacuoles were counted. At least 100 vacuoles were counted in each condition. sCas9 parasites were visualised by CbEm expression. DiCre background parasites were stained with α-GAP45 or α-SAG1 antibody to visualise parasites, and α-RFP antibody was used to amplify the SLF-mCherry signal. For SAG1 antibody, parasites were fixed with 100% methanol instead of 4% PFA. For rapamycin-induced floxed parasites, only vacuoles that lost the signal of the respective protein were counted as cKO.

For egress time-lapsed videos, floxed loxP*cgp*-Halo/CbEm and loxP*slf*-Halo/CbEm parasites were pre-incubated ±rapamycin for 24 hours before release and subsequent infection of HFFs in glass-bottom live-cell dishes. Parasites were allowed to grow for a minimum of 32 hours before inducing egress. Janelia Fluor 646 (20 nM) was used to pre-label parasites for approximately 5 hours and then washed away by washing three times with PBS. Afterwards, parasites were incubated with normal media for at least 1 hour before egress induction.

Dishes were put in a preheated chamber of a Leica DMi8 microscope, and the medium was replaced with DMEM FluoroBrite$_{\text{incomplete}}$ (Table II-9) with respective egress inducers. Videos were taken with a ×63 oil objective at 0.33 frames per second (FPS). Videos were recorded in triplicate per condition as a minimum. Only vacuoles lacking the signals for SLF or CGP were considered as cKO.

To assess the CbEM fluorescence signal intensity following egress induction, regions of interest (ROI) were drawn around the apicoplast region, nuclear region (defined as the region between basal CbEm labelling and the apicoplast), the *T. gondii* cell and a background region outside the vacuole. The relative intensity of CbEm in the apicoplast area was calculated as:

$$relative\ intensity = \frac{(mean\ apicoplast - mean\ nuclear\ region) \times apicoplast\ area}{(mean\ total\ T.gondii - mean\ background) \times total\ T.gondii\ area}$$

The relative intensity of CbEm in the basal area was calculated as:

$$relative\ intensity = \frac{(mean\ basal\ part - mean\ nuclear\ region) \times basal\ part}{(mean\ total\ T.gondii - mean\ background) \times total\ T.gondii\ area}$$

where mean was defined as:

$$Mean = \frac{RawIntDen}{area}$$

To check PVM integrity, parasites (loxP*slf*-Halo/CbEm and loxP*cgp*-Halo/CbEm) were pre-incubated ±50 nM rapamycin for 24 hours and

then transfected with SAG1ΔGPI plasmid (Table II-15), followed by growing for 48 hours before inducing egress with 50 µM BIPPO. Egress was recorded as described but with 0.2 FPS for non-induced KO parasites and 0.1 PFS for cKO parasites. Over 10 egress events were recorded for each condition. Only vacuoles that lost the signal of the respective protein were counted as cKO.

To investigate the integrity of the F-actin intravacuolar network (IVN) after the stimulation of egress with Ci A23187 for 5 minutes, 2.5×10^5 loxP*slf*-Halo/CbEm parasites were used, and the egress assay was carried out as described. After triggering egress, parasites were fixed with CB buffers (CB1 and CB2 in a ratio of 4:1; Table II-9; Periz et al. 2019) for 25 minutes, and then treated with 50 mM NH_4Cl for 10 minutes, followed by washing three times with PBS. Anti-GFP-Atto-488 antibody and α-RFP antibodies were used to stain CbEm and SLF-mCherry, respectively, to amplify the signals for better visualisation. Only vacuoles lacking the signals for SLF were considered as cKO.

2.5.4 Invasion/replication assays

For sCas9 parasites, a 24-hour invasion and replication assay was carried out as previously described with some changes (Egarter et al. 2014). Parasites were pretreated with ±50 nM rapamycin for 48 hours. 5×10^6 freshly released parasites were inoculated on HFF monolayers in 24-well plates and placed on ice for 10 minutes before invasion for 20 minutes. The parasites then grew for 24 hours and were fixed with 4% PFA followed by IFA. Parasites were first labelled with α-SAG1 antibody without permeabilization, followed by permeabilization and labelling with α-GAP45 antibody. For invasion, the number of

vacuoles in 10 randomly chosen fields of view was counted. For replication, the number of parasites per vacuole was counted, and at least 100 vacuoles were analysed.

For floxed parasites, invasion assay and replication assay were done separately. loxP*cgp*-Halo parasites were used for invasion and replication assays. loxP*slf*-Halo was used for invasion assays, and loxP*slf*-mCherry was used for replication assays. In terms of the invasion assay, parasites were pretreated with ±50 nM rapamycin for 96 hours before being mechanically released, and 5×10^6 were used to infect HFFs. Parasites were allowed to settle on HFFs for 10 minutes on ice before invading HFFs for 1 hour. Afterwards, parasites were directly fixed by 4% PFA, and IFA was performed as sCas9 invasion assays, but α-IMC1 or α-GAP45 antibodies were used to visualise parasites. Before the invasion assay, LoxP*cgp*-Halo parasites were dyed with 0.2 µM HaloTag Oregon Green for 1 hour, and loxP*slf*-Halo parasites were labelled with 20 nM Halo Janelia 646 for 15 hours.

For replication, 4×10^6 parasites were used to infect HFFs. The parasites were handled similarly to the invasion assay, without pre-labelling Halo-tagged parasites with dyes and the 10-minute settling on ice. After 1 hour of invasion, extracellular parasites were washed away with $DMEM_{complete}$ (Table II-6) before growing for 24 hours and being fixed with 4% PFA. Parasites were labelled with α-GAP45 (loxP*cgp*-Halo) or IMC1 and α-RFP (loxP*slf*-mCherry). loxP*cgp*-Halo parasites were stained with 0.2 µM Halo Oregon Green for 0.5

to 1 hour before fixation. For replication, the number of parasites per vacuole was determined.

For floxed parasites, at least 100 (for replication assay) or 150 vacuoles (for invasion assay) were counted in each condition. Only parasites that lost the respective signal were considered as cKO in the count.

2.5.5 Trail deposition assay and live gliding assay

For trail deposition assays, parasites were pre-induced with ±50 nM rapamycin (loxP*cgp*-Halo: 72 hours and loxP*slf*-mCherry: 96 hours), rinsed, mechanically released and filtered through 3-µm filters. The parasites were spun at 1,000 g for 5 minutes at room temperature to obtain parasite pellets, which were then resuspended at a concentration of 2 x 10^6 parasites per mL in pre-warmed endo buffer (Table II-9). 1 ml of the mixture was added to an FCS-coated glass-bottom live-cell dish and allowed to settle for 15 minutes at room temperature. Afterwards, endo buffer was gently replaced with 1 mL of pre-warmed sterile gliding buffer (Table II-9). The parasites were then incubated for 20 minutes at 37 °C before being fixed with 4% PFA. α-*T. gondii* antibody was used to stain parasites without permeabilization. A total of 15 random fields of view were imaged, and the total number of trails was counted.

For live gliding experiments, time-lapse movies were captured with a 63x objective at 2 FPS under a Leica DMi8 microscope with differential interference contrast (DIC) to measure parasite gliding kinetics. After 20 minutes of recording each condition, a Z-stack picture of the fluorescence channel targeting the CGP or SLF was

captured to differentiate cKO parasites from non-induced parasites. Only cKOs were evaluated for rapamycin-induced parasite analysis. Before the live gliding experiments, Halo-tagged parasites were pre-incubated with 20 nM Janelia Fluor 646 dye or 500 nM HaloTag TMR for at least 2 hours. The manual tracking plugin of Icy was used to analyse the movement of parasites. Unless otherwise specified, all tests were performed in a Ca^{2+}-free gliding buffer.

For trail deposition and gliding experiments with 2 µM Ci A23187, chemicals were introduced to the gliding buffer as described.

2.5.6 Microneme secretion assay

The procedure for the microneme secretion assay was modified from (Bisio et al. 2019). Induced parasites (incubated with rapamycin for 72 hours) and non-induced parasites were mechanically released using 26-gauge needles. After being washed twice with cold intracellular buffer (Table II-9), the parasites were resuspended in pre-warmed intracellular buffer (Table II-9) that was supplemented with either 2 µM Ci A23187, 5 µM BIPPO or DMSO. Parasites were incubated at 37 °C for 30 minutes. The supernatant was then collected and subjected to further centrifugation before Western blot.

4–20% precast polyacrylamide gel was used to separate proteins. α-GRA1 and α-MIC2 antibodies (Table II-11) were used to label the membranes. After labelling with the respective secondary antibodies (Table II-11), membranes were imaged using Odyssey CLX-1849 (LI-COR). For quantification of microneme secretion, this experiment was done in triplicates and run on independent membranes. Measurements were done using ImageJ.

2.5.7 Purification of biotinylated proteins via BioID

The HFFs were heavily infected with parasites (*cgp*-TurboID/*frm1*-3HA, *frm*1-TurboID/loxP*cgp*-Halo and DiCre*Δku*80). After 24 hours post infection, the parasites were treated for 6 hours with ±150 µM biotin. They were then mechanically released, filtered through 3-µm filters, and washed three times with cold PBS. 6 x 10^7 biotin-pretreated parasites were pelleted to purify biotinylated proteins. 10^7 parasites treated with ± 150 µM biotin were collected for biotinylation analysis through Western blot. All harvesting steps were performed on ice or at 0–4 °C. Parasite pellets were kept at -80 °C before being used in subsequent steps.

To purify biotinylated proteins, 6 x 10^7 parasites were defrosted on ice and then lysed for 30 minutes in 950 mL of RIPA $buffer_{complete}$ buffer (Table II-9) with Pierce™ protease inhibitor (final concentration: 1 tablet in 10 mL of RIPA solution). The lysis was centrifuged for 4 minutes at maximum speed at 0 °C, and the supernatant was incubated with Dynabeads™ MyOne™ Streptavidin T1 at room temperature for 30 minutes while being gently rotated. The beads were then washed five times with 1 mL of RIPA $buffer_{incomplete}$ (Table II-9) that was supplemented with Pierce™ protease inhibitor (final concentration: 1 tablet in 50 mL) and three times with 50 mM Tris-HCl (pH=8). The beads were then resuspended in 200 µL of 50 mM Tris-HCl (pH=8) solution. The remainder of the beads were pelleted and stored at -80°C before being sent for mass spectrometry, and 20 µL was preserved for running Western blot.

Western blot was performed to check protein biotinylation. Parasite lysis preparation was the same as the preparation of lysate for incubation with beads. To elute biotinylated proteins from beads, 22 µM biotin was used. Li-COR blocking buffer TBS was used in the blocking process. α-Aldolase was used as a primary antibody and incubated for only one hour at room temperature. IRDye 800CW Streptavidin and IRDye680RD Donkey anti-Rabbit IgG were used as secondary antibodies (Table II-11).

2.5.8 Mass spectrometry

Beads were sent to Biomedical Center Munich in Ludwig Maximilian University to perform liquid chromatography with tandem mass spectrometry (LC-MS/MS; carried out by Ignasi Forné). The protocols were identical to (Singer et al. 2023). Briefly, the beads were treated with 10 ng/L of trypsin in 1 M urea and 50 mM NH_4HCO_3 for 30 minutes, then rinsed with 50 mM NH_4HCO_3. Afterwards, the supernatant was digested overnight with 1 mM DTT. Before LC-MS analysis, the peptides were alkylated and desalted after digestion. For LC-MS/MS, after desalting, the peptides were injected into an Ultimate 3000 RSLCnano system and separated in a 15-cm analytical column (75 m ID with ReproSil-Pur C18-AQ 2.4 m) over 50 minutes using a gradient of 4 to 40% acetonitrile in a 0.1% formic acid. The HPLC effluent was electrosprayed directly into a Qexactive HF instrument operating in data-dependent mode to automatically transition between full-scan mass spectrometry (MS) and MS/MS acquisition. Survey full-scan MS spectra (from m/z 375–1600) were acquired with resolution R=60,000 at m/z 400 (AGC target of 3x106). The 10 most intense peptide ions with charge states between 2 and 5

were sequentially isolated to a target value of 1x105 and fragmented at collision energy normalised to 27%.

MaxQuant 1.6.14.0 was used to identify and quantify proteins using iBAQ with the following parameters: UP000005641_*T. gondii*_20220321.fasta; MS tol: 10 ppm; MS/MS tol: 20 ppm Da; Peptide FDR: 0.1; Protein FDR: 0.01 min. peptide length: 7; Variable modifications: Oxidation (M); Fixed modifications: Carbamidomethyl (C); Peptides for protein quantitation: razor and unique; Min. peptides: 1; Min. ratio count: 2.

The identified proteins' MaxQuant iBAQ Z-score normalised values were plotted using Perseus, with missing values from the normal distribution replaced (width: 0.3 and downshift: 4), the false discovery rate (FDR) set to 0.05 and the S0 value set to 0.1. The *t*-test was used.

2.6 Microscopy

All microscopy images were captured with either a Leica DMi8 with a DFC9000 GTC camera or an Abberior 3D STED microscope. All confocal and STED images were performed on the Abberior 3D STED microscope.

2.7 Imaging processing

Leica LasX software and Imspector were used to acquire imaging data for parasites. LI-COR Image Studio software was used to acquire imaging data for WB pictures. Fiji (ImageJ) software and/or Icy image processing software were used to process all images and videos. All wide-field images were deconvolved using Huygens Essential, except images of parasites expressing CbEm and time-lapse videos.

2.8 Data analysis

Unless otherwise specified, all quantification data were presented as mean ± standard deviation (SD) and plotted by Graphpad Prism or Excel. P-values were calculated via Graphpad Prism and presented as follows: ns=non-significant; *p<0.05, **p< 0.01; ***p<0.001; ****p<0.0001.

III. RESULTS

Results presented in sections 1 and 2 (except Figure III-3, Figure III-4C, Figure III-5, Figure III-7D, Figure III-8 and Figure III-13) have been published in Wei Li, Janessa Grech, Johannes Felix Stortz, Matthew Gow, Javier Periz, Markus Meissner and Elena Jimenez-Ruiz (2022). "A splitCas9 phenotypic screen in *Toxoplasma gondii* identifies proteins involved in host cell egress and invasion." *Nat Microbiol* 7(6): 882–895. Results presented in section 3 (except Figure III-28A, B) are not yet published.

1. Identification of egress candidates from a sCas9 screen

1.1 sCas9 screen establishment

To identify the genes involved in egress, a sCas9 screen was established by my colleague Janessa Grech (thesis in preparation; Li et al., 2022). Briefly, a curated sgRNA library, consisting of 320 single guide RNAs, each targeting a different candidate gene, was selected from a list of sgRNAs in (Sidik et al. 2016). Those genes were annotated as having no signal peptide, being conserved in only apicomplexans, and with a phenotypic score <-1.5 indicating the contribution of a gene to parasite fitness (based on ToxoDB-30 release, www.toxoDB.org). Guide RNAs were synthesised as oligos, amplified by PCR and then cloned into the plasmid containing the TgU6 universal promotor for gRNA transcription and a dihydrofolate reductase (DHFR) cassette, which confers parasite pyrimethamine resistance (see also Materials and Methods 2.1; Figure III-1). This step was achieved by Gibson assembly, after which the products were

transformed into electrocompetent bacteria. The recovered bacteria after transformation were estimated to be 3×10^6 cfu, which was over the required number for maintenance of library heterogenicity, suggesting a good complexity of the vector library (Sidik et al. 2018). Moreover, sequencing of 35 randomly picked colonies identified 29 unique sgRNAs (83%), further confirming the complexity of the library. Plasmids were extracted and linearised before being transfected in the pool into the parental strain-RHsCas9 strain, expressing sCas9 (Figure I-12), chromobody-emeraldFP (CbEm) labelling F-actin (allowing visualisation of F-actin and detection of phenotypes involving actin dynamics) and FNR-RFP labelling apicoplast (allowing detection of phenotypes affecting the apicoplast; Figure III-1; Bednarek et al. 2003, Periz et al. 2017). Transfected parasites were then under pyrimethamine selection for 3 weeks before fluorescence-activated single cell sorting (FACS) into ten 96-well plates (Figure III-1). After a week, single plaques were isolated, resulting in a total of 608 clones that were maintained in culture. The obtained clones were treated with or without 50 nM rapamycin for 48 or 72 hours to induce disruption of targeted genes before fixation. Automated imaging was performed, and the images were analysed by two investigators independently for different phenotypes (F-actin, apicoplast, nuclear/replication and/or egress phenotypes; Figure III-1). The present thesis focuses on clones presenting egress phenotypes examined at 72 hours post induction (hpi), whereas other phenotypes discovered in the screen have been further analysed by my colleague (Janessa Grech, thesis in preparation; Li et al., 2022).

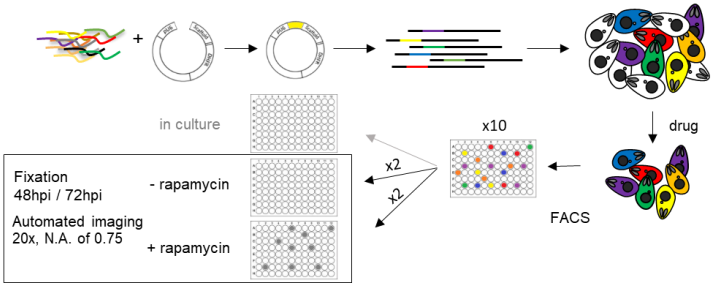

Figure III-1. Scheme of the workflow of the phenotypic screen.

320 sgRNAs were cloned into vector backbones containing the DHFR cassette. After transformation of the recombinant plasmids into bacteria, the plasmids were extracted, linearised and transfected into the RHsCas9 strain, resulting in a pool of parasites carrying different sgRNAs and non-transfected parasites. The application of pyrimethamine for 3 weeks killed the WT parasites, and parasites containing sgRNA(s) survived. Through FACS to sort single parasites into 10 plates, a final total of 608 clones was obtained, which were maintained in culture. Sister plates were incubated with or without 50 nM rapamycin for 48 or 72 hours before fixation with 4% PFA and stained with Hoechst to label nuclei, followed by automated imaging at 20x magnification. N.A.: numerical aperture.

Through imaging analysis at 72 hpi with 50 nM rapamycin, the majority of clones (92.2%) displayed normal egress, where the parasites lysed the host cells and reinvaded neighbouring ones, as evidenced by the dispersion of parasites within the cells and the formation of small vacuoles (Figure III-2A). Meanwhile, 48 clones (7.8%) showed suspected delay or blockage in host cell egress, with parasites still in relatively large vacuoles and failing to exit host cells, indicating a potential egress phenotype (Figure III-2A). Corresponding clones from the non-induced master plate were isolated and further analysed to identify the corresponding sgRNA and therefore gene of interest. Thirty-three unique sgRNAs were identified

by sequencing and were subjected to a second inspection due to their potential implication in parasite egress (Table III-1).

Table III-1. Candidate genes selected for characterisation.

Accession No.	Name	Natural egress in screen	Natural egress after second analysis	Induced egress
TGGT1_208420	sodium:neurotransmitter symporter family protein 1	✓	✓	✓
TGGT1_209100	PUB domain–containing protein	✓	✓	
TGGT1_209900	hypothetical protein	✓		
TGGT1_210230	hypothetical protein	✓		
TGGT1_210490	hypothetical protein	✓		
TGGT1_214560	hypothetical protein	✓		
TGGT1_214790	glycoprotein 1	✓	✓	
TGGT1_216000	alveolin domain-containing intermediate filament IMC3	✓	✓	
TGGT1_216040	putative 30S ribosomal protein S15	✓		
TGGT1_221600	hypothetical protein	✓		
TGGT1_229740	hypothetical protein	✓		
TGGT1_237010	hypothetical protein	✓		
TGGT1_240380	hypothetical protein 1	✓	✓	✓
TGGT1_240910	hypothetical protein	✓		
TGGT1_244430	putative pseudouridylate synthase	✓		
TGGT1_248640	regulator of chromosome condensation (RCC1) repeat-containing protein	✓	✓	✓
TGGT1_248660	hypothetical protein	✓		
TGGT1_249970	hypothetical protein	✓		
TGGT1_252465	radical SAM domain–containing protein	✓	✓	✓
TGGT1_253830	hypothetical protein	✓		
TGGT1_254600	ubiquitin family protein	✓		
TGGT1_259720	hypothetical protein	✓		
TGGT1_269330	hypothetical protein	✓		
TGGT1_269700	NLI interacting factor family phosphatase	✓		
TGGT1_273100	3'-5' exonuclease domain–containing protein 1	✓	✓	
TGGT1_294930	leucine-rich repeat-containing protein	✓	✓	
TGGT1_301410	hypothetical protein	✓		

TGGT1_305340	corepressor complex CRC230 1	✓	✓
TGGT1_306640	hypothetical protein	✓	
TGGT1_310430	HSP90 like protein	✓	
TGGT1_310500	hypothetical protein	✓	
TGGT1_310930	hypothetical protein	✓	
TGGT1_318420	30S ribosomal protein S16, putative	✓	

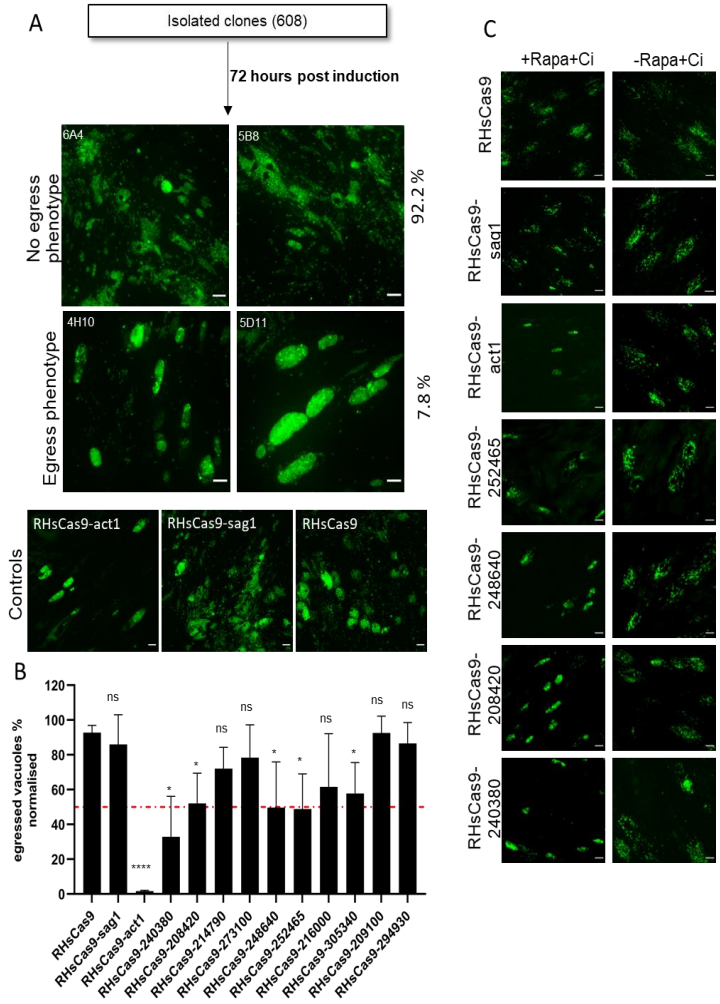

Figure III-2. Phenotypic screen for egress candidates.

(A) Representative images for clones in the screen and control parasites after 72 hours of incubation with 50 nM rapamycin. The upper panel shows clones with no obvious egress phenotype in the screen. The middle panel shows clones with egress phenotypes (potential delay or block in egress) in the screen. The bottom panel shows control parasites (RHsCas9-act1, RHsCas9-sag1 and RHsCas9) exhibiting egress or non-egress phenotypes. Clone numbers are indicated as the original plate number plus its position

in 96-well plates. For instance, 6A4 means clone isolated from plate 6 in well A4 in the 96-well plates. Scale bar, 30 µm. (B) Quantification of egressed vacuoles after stimulation with 2 µM Ci A23187. Parasites were inoculated on HFF cells treated with ±50 nM rapamycin for 4 hours and incubated a further 44 hours before induction of egress for 5 minutes. Results were standardised to the DMSO-treated control with Ci (-R+Ci). Three biological replicates were done. Red dashed line labels egress rates equal to 50%. Data are presented as mean + SD. (C) Representative images in (B) for control parasites and four candidate genes involved in egress. Scale bar, 30 µm. P-values were calculated by two-tailed unpaired Student's *t*-test compared to the RHsCas9 strain. ns: non-significant; *p<0.05; **p< 0.01; ***p<0.001; ****p<0.0001. Rapa: 50 nM rapamycin.

1.2 Validation of egress candidates

To verify the results obtained during the screen, those 33 isolated clones were treated with 50 nM rapamycin for 72 hours to check reproducibility and exclude clones displaying no obvious egress phenotype or showing a strong replication phenotype (indicated by parasites forming smaller or aberrant PVs). RHsCas9-act1 was used as a positive control since ACT1 is involved in egress, and RHsCas9-sag1 was used as a negative control since SAG1 is not involved in the regulation of parasite egress (Whitelaw et al. 2017). In addition, parental RHsCas9 parasites without cutting any genes in the genome were included. This step resulted in the selection of 10 clones with a strong egress phenotype for further investigation (Table III-1).

Next, Ci A23187 was used to induce parasite egress in selected clones. In most cases, regardless of the disruption of the gene, parasites were capable of exiting host cells, similar to RHsCas9-sag1 and RHsCas9 parasites (Figure III-2B). However, four genes showed a significant delay in egress upon induction of gene disruption, with egress rates around 50% (Figure III-2B and C). Thus, four candidate genes were prioritised for further characterisation.

Plaque assay is based on the parasite's capacity to generate plaques in a host cell monolayer. The parasites infect confluent HFFs and, after many rounds of lytic cycle completion, they lyse the cell and form visible plaques in the host cell. Therefore, plaque assays are commonly used to estimate gene essentiality. The analysis of plaque assays revealed that all four candidate genes were important for parasite growth given their impaired ability for plaque formation (Figure III-3). Those results were in accordance with their negative fitness score predicted in a recent genome-wide study (Sidik et al. 2016).

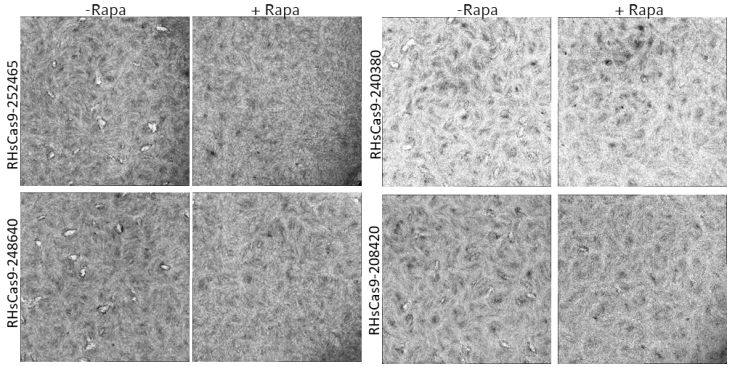

Figure III-3. Images of plaque assays on indicated parasites.

Parasites were grown on HFF cells for 6 days in the presence or absence of rapamycin (50 nM), before fixation and staining for the detection of plaques were performed.

Next, the role of candidate genes in replication and invasion was examined by carrying out 24-hour invasion replication assays (see Materials and Methods). Disruption of TGGT1_252465 resulted in significantly reduced replication rates, whereas parasite invasion was not significantly impaired. Thus, this candidate was dismissed from

further analysis (Figure III-4). With disruption of the remaining three candidate genes (TGGT1_248640, TGGT1_240380 and TGGT1_208420), parasite replication was not greatly affected, whereas parasite invasion was significantly impaired (Figure III-4). TGGT1_248640 was recently described as TgND6, which is involved in parasite invasion (Aquilini et al. 2021), and thus was omitted from further study.

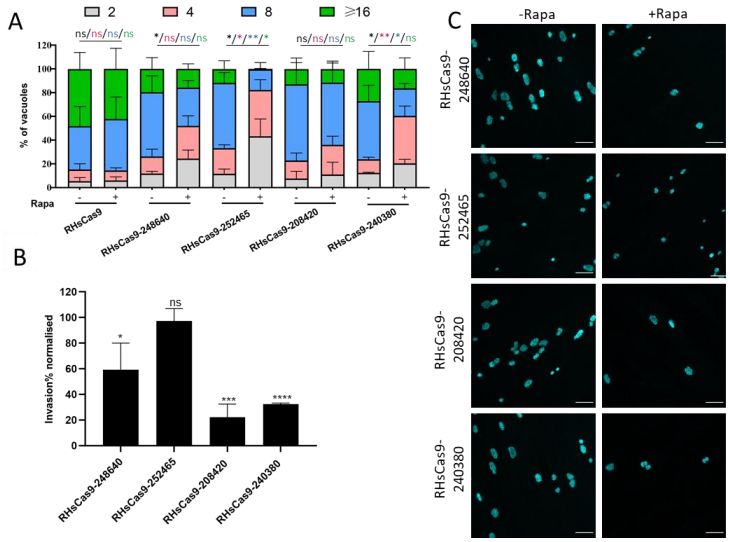

Figure III-4. 24-hour invasion replication assays on four candidates.

A) Quantification for parasite replication. The number of vacuoles containing 2, 4, 8, and 16 or more parasites was counted. B) Quantification for parasite invasion. The number of vacuoles was counted and normalised to the non-rapamycin-treated condition and then normalised to the RHsCas9 strain. C) Representative images in (A) and (B). Scale bar: 30 µm. The colour of the asterisk represents the conditions analysed in (A). P-values were compared to RHsCas9 strain in (B). Data were presented as mean + SD. P-values were calculated by two-tailed unpaired Student's *t*-test. ns: non-significant; *p<0.05; **p< 0.01; ***p<0.001; ****p<0.0001. Rapa: 50 nM rapamycin.

In summary, TGGT1_240380 and TGGT1_208420 were selected as candidates for further characterisation due to their roles in both egress and invasion. In the course of this project and based on the detected functions, they were named conoid gliding protein (*cgp*) and signalling linking factor (*slf*), respectively.

2. CGP and SLF are essential proteins involved in invasion and egress

2.1 Information on CGP and SLF

To obtain some initial information on SLF and CGP, bioinformatic data available on ToxoDB (www.toxoDB.org) were analysed (Table III-2). Apicomplexa-specific CGP is a huge protein, only found in the groups of Hematozoa and Coccidia. It is annotated as a hypothetical protein with a CLU-central domain and a tetratricopeptide (TPR)-like domain, a structural motif for mediating multiprotein complexes (Figure III-5; Zeytuni et al. 2012). A recent study provided a *T. gondii* proteome subcellular atlas via hyperLOPIT, which is based on protein density gradient profiles (Barylyuk et al. 2020). According to this, CGP is clustered with proteins localising at PM-peripheral 2 (probability: 1) via TAGM-MCMC analysis (Table III-2; Barylyuk et al. 2020).

SLF is a ~113-kDa protein with 12 transmembrane domains and a putative SNF-like domain, belonging to the sodium: neurotransmitter symporter superfamily (Figure III-5). This protein is highly conserved within the phylum Apicomplexa and is predicted to contribute to parasite fitness according to the phenotypic score (Sidik et al. 2016). However, a recent study indicated that SLF is dispensable, as

evidenced by plaque assay via the AID KD system, which is based on protein degradation (Table I-2; Bisio et al. 2019). GO term analysis predicts SLF is an integral component of membrane, having neurotransmitter: sodium symporter activity. The predicted cellular localisation by hyperLOPIT via TAGM-MCMC analysis was apical 1 (probability: 0.15), Golgi complex (probability: 0.5) and PM-peripheral 2 (probability: 0.33; Table III-2; Barylyuk et al. 2020). However, a recent publication revealed SLF localisation at the apical cap and RB (Bisio et al. 2019).

Table III-2. Information for CGP and SLF retrieved from ToxoDB.
* Data obtained from Sidik et al. (2016). # Data from Barylyuk et al. (2020) via TAGM-MCMC analysis.

Gene ID	Phenotypic score *	Molecular weight	Genomic sequence	Localisation hyperLOPIT#	Function prediction
TGGT1_240380	-3.85	544 kDa	25,738 bp	PM-peripheral 2	Protein binding
TGGT1_208420	-2.31	113 kDa	11,200 bp	Apical 1, Golgi complex, PM-peripheral 2	Neurotransmitter transport; integral component of membrane; neurotransmitter: sodium symporter activity

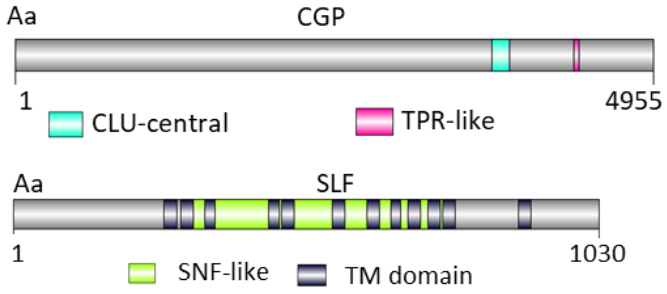

Figure III-5. Putative domains of CGP and SLF as predicted by toxodb.org.

Predicted domains are colour-coded, and their positions are shown in the scheme. Graphs made with DOG.2.0.1. Aa: amino acid.

2.2 Subcellular localisation of CGP and SLF

To analyse the subcellular localisation of CGP and SLF, both proteins were endogenously tagged at the C-terminus with different tags (Halo or mCherry) in the RH DiCreΔ*ku*80 parasite line (see Materials and Methods; Los et al. 2008). Parasites were transiently transfected with Cas9_YFP_sgRNA vectors, targeting the C-terminus region of the GOI, together with a repair template containing 50 bp of homologous overhangs and the desired tag-LoxP (Figure III-6A). The successfully tagged mutants were analysed by PCR to confirm the correct insertion of tags in the desired genomic location, and positive clones are hence referred to as *cgp*-Halo, *slf*-Halo or *slf*-mCherry (Figure III-6B).

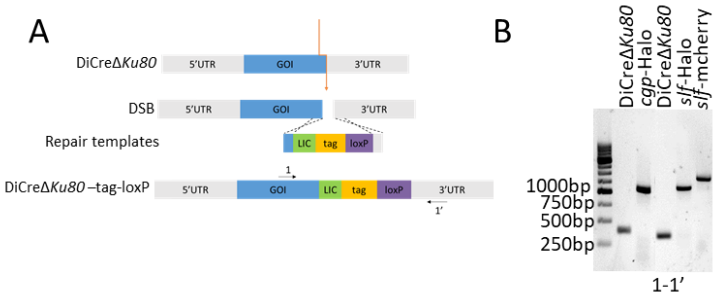

Figure III-6. Generation of endogenously tagged parasite lines.

A) Endogenous tagging scheme at C-terminus. The Cas9-targeted area is indicated by an orange arrow. 1 and 1' primers are indicated by black arrows to the areas outside of the homologous region employed for homologous recombination of the repair template. B) Genomic PCR results show the correct insertion of different tags (mCherry or Halo) at the C-terminus of the indicated parasite lines.

IFA staining of the intracellular parasites indicated that CGP most likely localised at the conoid of the parasite, as it locates apically to ISP1 and IMC1, which label the apical cap and the whole IMC, respectively (Figure III-7A; Mann et al. 2001, Beck et al. 2010). SLF showed dual localisation both apically and at the intravacuolar network at the residual body, as shown by the colocalisation of SLF with ISP1 and F-actin with CbEm (Figure III-7B and C). This basal localisation is lost in extracellular parasites as expected, meaning that the localisation of SLF is restricted to the intravacuolar network in intracellular parasites (Figure III-7D).

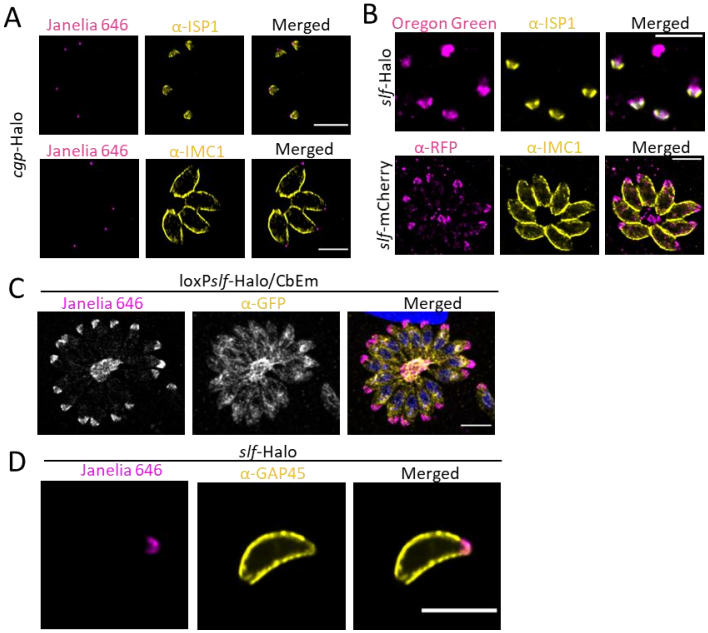

Figure III-7. Localisation of CGP and SLF.

A) Images depict the apical localisation of CGP and co-localisation with IMC1, a marker for parasite periphery, and ISP1, a marker for the apical end. B) Images of intracellular parasites depicting the localisation of SLF by using ISP1 and IMC1. C) STED images show SLF colocalised with F-actin in the intravacuolar network. α-GFP antibody was used to amplify the EmeraldFP signal of the CbEm. D) Images depicting SLF localisation in extracellular parasites. Scale bar: 5 µm.

To further investigate CGP or SLF during endodyogeny, their presence in different stages of the cell cycle was examined. The CGP signal appeared during early endodyogeny before the formation of the apical cap of the IMC in daughter cells, as shown when CGP is colocalised with ISP1 (Figure III-8A; Beck et al. 2010). Further analysis with Centrin 1, a centrosome marker commonly used to distinguish parasites in different phases during the cell cycle, showed that in the S phase, when Centrin 1 has been duplicated, CGP was not yet detectable. During early mitosis, CGP was seen and positioned above the nucleus but close to Centrin1. As the cell cycle progressed and forming daughter cells elongated, the distance between CGP and Centrin 1 increased (Figure III-8B). In contrast, SLF was not detected in the budding cells even after IMC1 was fully developed, suggesting that SLF was located at the plasma membrane (Figure III-8C). Indeed, a co-localisation study with the plasma membrane marker SAG1 suggests that SLF localises at the plasma membrane (Figure III-8D).

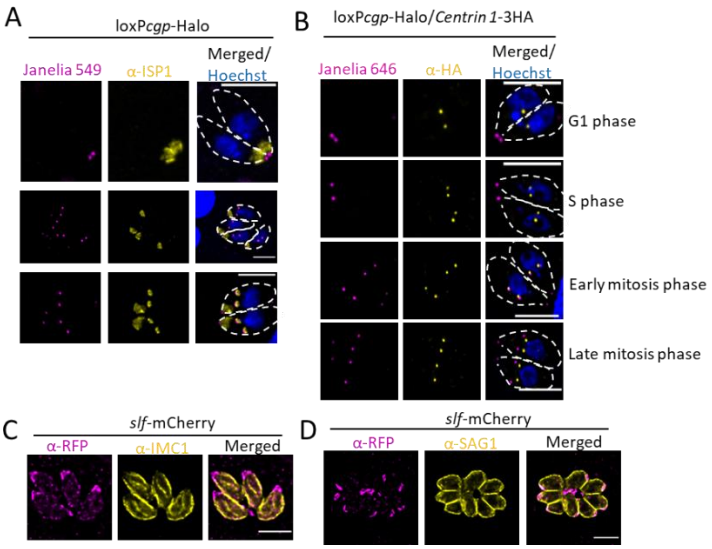

Figure III-8. CGP appeared very early during endodyogeny, whereas SLF was not detected in daughter cells.

A) Confocal images depict CGP in mature and budding cells. B) Halo-tagged CGP were stained with Halo Janelia 646 before fixation. IFA was done to stain Centrin 1 to indicate parasites in different phases during the cell cycle. C) IFA of intracellular parasites expressing *slf*-mCherry, which was labelled with α-RFP antibody. D) IFA illustrates SLF co-stained with SAG1 fixed by methanol. Scale bar: 5 µm.

2.3 Generation of conditional KO lines in DiCre background

Since non-specific phenotypes cannot be fully excluded by using the sCas9 system, it was decided to use an independent conditional system for their validation: the DiCre system, which allows the generation of conditional knockout (cKO) strains after the addition of rapamycin (Andenmatten et al. 2013). Similar to endogenous tagging, parasites were transiently transfected with the Cas9_YFP_sgRNA vector targeting the 5'UTR region close to the start codon of GOI and a

synthesised oligo as a repair template, which contains 33 bp of left homology to the targeted area followed by the loxP sequence and another 33 bp of right homology (Figure III-9A; see also Materials and Methods). Genomic gDNA was extracted and PCR was performed to confirm the correct insertion of the loxP sequence (Figure III-9B and C). Floxed cKO parasites are hence referred to as loxP*cgp*-Halo and loxP*slf*-mCherry or loxP*slf*-Halo.

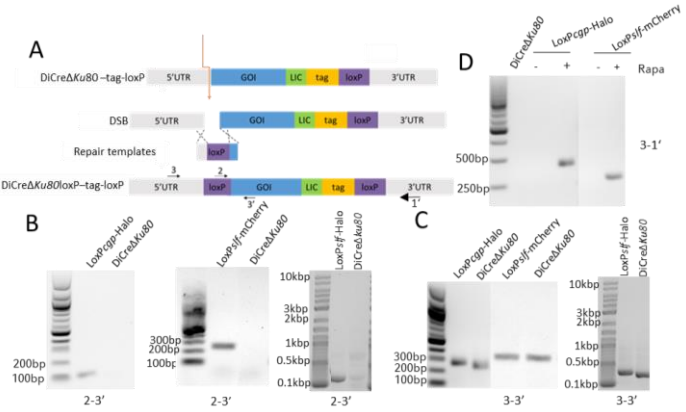

Figure III-9. Generation of cKO parasite lines (loxP*cgp*-Halo, loxP*slf*-mCherry and loxP*slf*-Halo).

A) Scheme for insertion of upstream loxP. The orange arrow indicates the targeting region for Cas9. Primer binding sequences are indicated by black arrows. Primers 3 and 3' bind outside of the homology region. Primer 2 binds to the loxP sequence. 1' binds to the area outside of the homologous region for C-term tagging. B–C) Integration PCR (2-3' primer set) results indicate the correct insertion of the loxP sequence at 5'UTR in indicated parasite lines. Analytical PCR products (3-3' primers) were purified and sent for sequencing to confirm the correct integration. D) Excision PCR (3-1' primer set) results for indicated parasites and conditions. Parasites were incubated ± 50 nM rapamycin for 48 hours and then gDNA was extracted for PCR. Rapa: 50 nM rapamycin.

Both *cgp* and *slf* genes could be efficiently excised after induction with 50 nM rapamycin (Figure III-9D). In good agreement with this result,

CGP and SLF were not detectable at the protein level indicated by IFA after KO induction with rapamycin (Figure III-10A and C). In the case of CGP, as early as 24 hours post induction, a lack of CGP signal was observed in a small percentage of vacuoles. At late time points (96 hours post induction), the majority of vacuoles (~70%) were depleted of CGP. However, a 100% KO efficiency was not achieved (Figure III-10B). In the case of SLF, the protein was not detectable at 48 hours post induction and reached a significantly higher KO efficiency at 72–96 hours post induction (Figure III-10D), with a lack of SLF signal in ~75% of vacuoles (Figure III-10D).

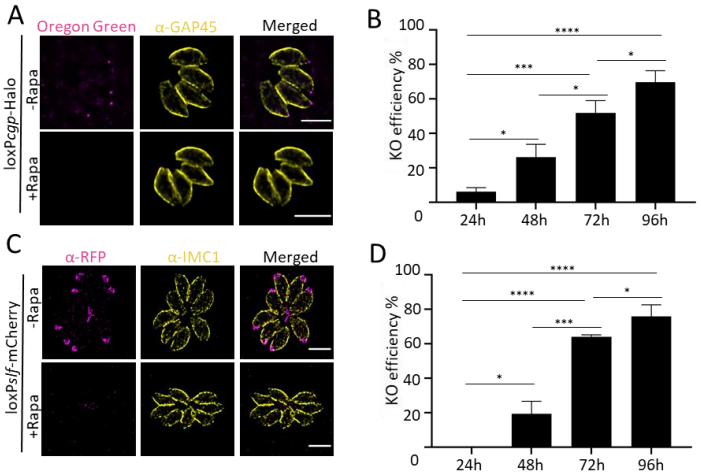

Figure III-10. Efficient depletion of CGP and SLF after induction with rapamycin.

A) Representative IFA pictures of the loxP*cgp*-Halo parasites treated with or without 50 nM rapamycin for 72 hours. GAP45 antibody was used to indicate parasite periphery. 0.2 mM Halo Oregon Green was used to label CGP. B) Quantification of vacuoles lacking CGP signal at different time points in (A). Parasites were inoculated onto confluent HFFs in the presence of 50 nM rapamycin and fixed at 24, 48, 72 and 96 hours

post infection. C) Representative IFA images of loxP*slf*-mCherry parasites treated with or without 50 nM rapamycin for 72 hours. IMC1 antibody was used to label the parasite periphery. α-RFP antibody was used to label SLF-mCherry. D) Quantification of vacuoles without SLF signal at different time points in (C). Scale bar: 5 µm. Data are presented as mean + SD. P-values were calculated by the two-tailed unpaired Student's *t*-test. ns: non-significant; *p<0.05; **p<0.01; ***p<0.001; ****p<0.0001. Rapa: 50 nM rapamycin.

2.4 CGP and SLF effect on lytic cycle

Since our experiment clearly showed the efficient regulation of both CGP and SLF cKO, we set out to investigate the function of both genes. To do this, the plaque assay was performed as the first step. Even though CGP and SLF remained in a small proportion of the population, differentiating whether the gene was essential was still thought possible. Both loxP*cgp*-Halo and loxP*slf*-mCherry parasite lines when induced with rapamycin had obvious defects in plaque formation: the former managed to form smaller plaques compared to the non-rapamycin treatment, and the latter barely formed any plaque (Figure III-11). This result suggests that both genes are essential, which is in good agreement with our observations during the sCas9 phenotypic screen and their negative phenotypic scores (Sidik et al. 2016). Accordingly, clonal CGP and SLF KO parasites could not be isolated.

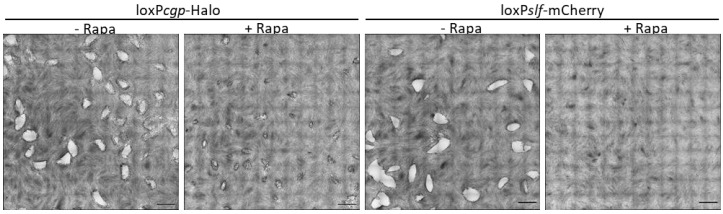

Figure III-11. CGP and SLF are essential for parasite growth.

Parasites were grown in different conditions (±50 nM rapamycin) and fixed after 6 days post infection. Scale bar: 1.5 mm. Rapa: 50 nM rapamycin.

From the sCas9 screen, both *cgp* and *slf* disrupted parasites were not greatly impaired in replication. To validate this, the parasite intracellular growth was examined (see Material and Methods). Both CGP- and SLF-depleted parasites were replicating at a similar speed to WT parasites and non-induced KO parasites, in good agreement with what was observed in the sCas9 screen (Figure III-12).

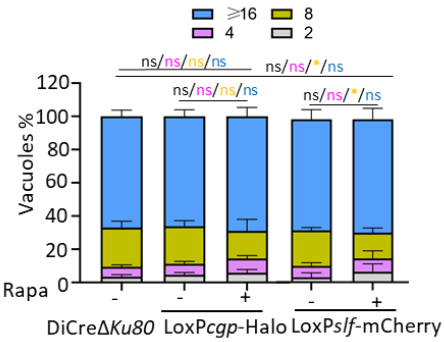

Figure III-12. CGP and SLF are not involved in parasite replication.

Parasites were pre-treated in the presence or absence of rapamycin for 96 hours before allowing invasion of confluent HFF cells for 1 hour and then growing for 24 hours. The percentages of vacuoles that contained 2, 4, 8 and ≥16 parasites were counted. Assays were done in three biological replicates. Data were presented as mean + SD. P-values were calculated by two-tailed unpaired Student's *t*-test. The colour of the asterisk represents the conditions analysed. ns: non-significant; *p<0.05; **p< 0.01; ***p<0.001; ****p<0.0001. Rapa: 50 nM rapamycin.

Notably, abnormal GAP45 staining was also observed in a small population (15.7%) of CGP cKO parasites (Figure III-13).

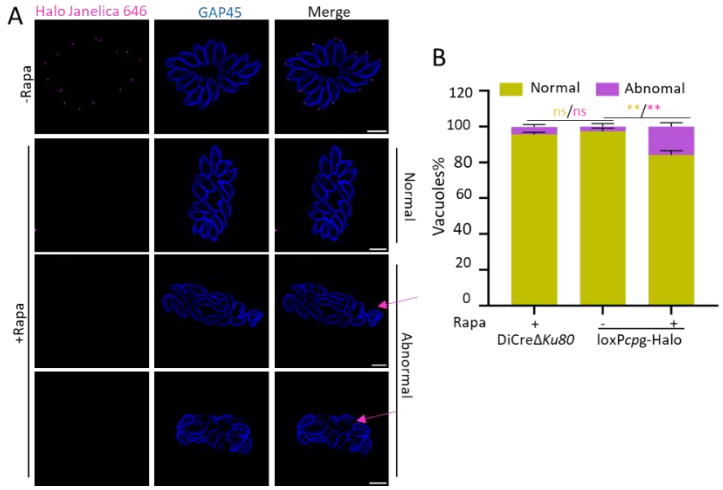

Figure III-13. The absence of CGP caused abnormal replication in a small subpopulation.

A) Representative images showing normal and abnormal GAP45 staining indicated by purple arrows in different conditions. B) Quantification in (A). Parasites were induced KO with ± 50 nM rapamycin for 72 hours and then allowed for invasion for 1 hour followed by growth for 24 hours before fixation. Scale bar: 5 µm. Data were presented as mean + SD. P-values were calculated by two-tailed unpaired Student's *t*-test. The colour of the asterisk represents the conditions analysed. ns: non-significant; *p<0.05; **p< 0.01; ***p<0.001; ****p<0.0001. Rapa: 50 nM rapamycin.

sCas9 clones targeting *slf* and *cgp* genes upon induction of rapamycin showed a defect in egress. To verify that the cKO presented this defect as well, egress assays were performed (see Materials and Methods). Moreover, knowing that SLF was identified in a pull-down assay with other members of a signalling platform (Bisio et al. 2019), egress was induced with different inducers (BIPPO, Ci A23187 and propranolol) that interfere at different steps of the signalling cascade, leading to egress (Table I-1, Figure I-5). Neither cKO parasite was able to egress at the level of the WT (over 90%) regardless of the inducer employed.

In the case of *cgp* cKO parasites, egress was strongly impaired, showing only 20.1% egress rates with BIPPO, 6.5% egress rates with Ci A23187 and 16.5% egress rates with propranolol (Figure III-14). The low egress efficiency (less than 20% regardless of inducers) indicates that CGP acts downstream of known signalling cascades (Figure III-14). Regarding *slf* cKO parasites, when BIPPO (7.1%) and propranolol (4.5%) were used for the induction of egress, parasites showed strong egress phenotypes where the majority of parasites failed to egress (over 90%). In contrast, when egress was induced with Ci A23187, the egress phenotype was significantly rescued, and only 31.5% of vacuoles failed to egress (Figure III-14). These results indicate that SLF acts upstream of calcium signalling.

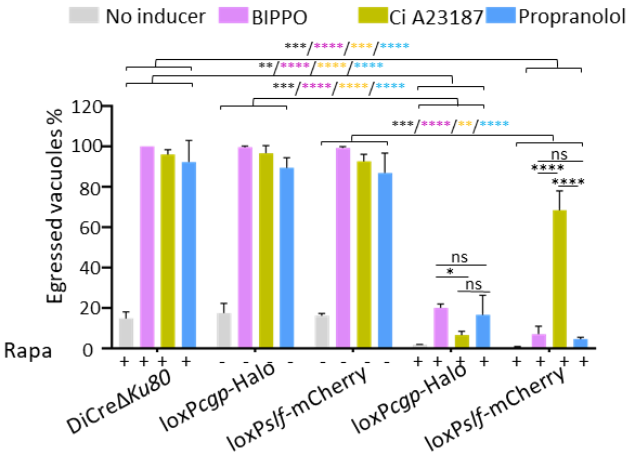

Figure III-14. CGP and SLF are involved in parasite egress.

The number of egressed and non-egressed vacuoles was counted after stimulation of egress with different inducers (50 µM BIPPO: 5 minutes; 2 µM Ci A23187: 5 minutes; 125 µM propranolol: 7 minutes). Data are presented as mean + SD. One-way analysis of variance (ANOVA) with Tukey's multiple comparison test was calculated. The

colour of the asterisk represents the conditions analysed. ns: non-significant; *p<0.05; **p< 0.01; ***p<0.001; ****p<0.0001. Rapa: 50 nM rapamycin.

In our sCas9 screen, both strains targeting *cgp* and *slf* showed an invasion defect once they were disrupted. To validate this, invasion assays were performed on loxP*cgp*-Halo and loxP*slf*-Halo parasites (see Materials and Methods). The depletion of SLF or CGP resulted in a significant defect in parasite invasion, as judged by the invasion rates dropping to 23.4% for CGP-depleted parasites and 8.4% for SLF-depleted parasites (Figure III-15). Since the presence of Ci A23187 could partially rescue the egress phenotype for *slf* cKO parasites, whether parasite invasion could be rescued after stimulation with Ci A23187 was interesting. The addition of Ci A23187 increased invasion slightly in *slf* cKO parasites compared to non-stimulated parasites (27.7% vs. 8.4%; Figure III-15B).

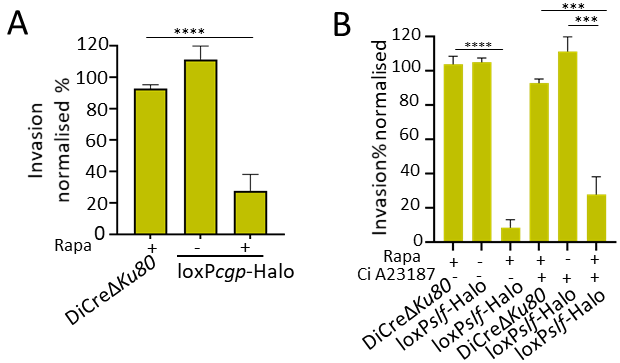

Figure III-15. CGP and SLF are involved in parasite invasion.

A) Invasion assay for loxP*cgp*-Halo. Invasion% was normalised to WT parasites. B) Invasion assay for loxP*slf*-Halo in the presence or absence of Ci 23187. Invasion% was normalised to WT parasites. Data are presented as mean + SD. P-values were calculated

by two-tailed unpaired Student's *t*-test. ns: non-significant; *p<0.05; **p< 0.01; ***p<0.001; ****p<0.0001. Rapa: 50 nM rapamycin.

Since host cell egress and invasion depend on the ability of the parasite to glide, parasites' gliding motility was analysed (see Materials and Methods). As a first assessment, a trail deposition assay was performed based on the detection of trails left by parasites capable of gliding. Many trails left by non-rapamycin-treated parasites were observed, whereas rapamycin-treated parasites barely left trails, suggesting a gliding defect (Figure III-16A). Quantitative analysis revealed that 35.5% of loxP*cgp*-Halo and 16.4% of loxP*slf*-mCherry parasites pre-treated with rapamycin were capable of gliding (Figure III-16B), which was significantly reduced when compared to DiCreΔ*ku80* parasites pre-incubated with rapamycin. Time-lapsed video revealed that once *cgp* cKO parasites settled down on the FCS-coated surface, the majority did not glide during the recording time, but some parasites could initiate gliding motility for a limited length (Figure III-16C; Movie 1). Parasites that managed to initiate gliding motility were manually tracked for more detailed gliding kinetics. This demonstrated that the trajectories for *cgp* cKO parasites were significantly reduced, as were the average and maximum gliding speeds (Figure III-16C). Unlike *cgp* cKO parasites, *slf* cKO parasites seemed unable to attach to the FCS-coated surface and could not initiate any type of gliding motility. In opposition, non-induced parasites moved normally (Movie 1). Notably, fewer than 20% of parasites (loxP*slf*-mCherry) were capable of gliding with the treatment of rapamycin, as evidenced by trail deposition assays (Figure III-16B). This might be explained by the incomplete KO efficiency of the

parasite population and the trails left by WT parasites. Some parasites with residual SLF signal were also observed by time-lapsed video to lose the ability to glide (data not shown). Since supplementation with Ci A23187 partially overcomes the invasion and egress phenotype, whether Ci A23187 can induce *slf* cKO parasites to glide was also assessed. In the presence of Ci A23187, there was an obvious increase in gliding trails left by induced KO parasites compared to those in the absence of Ci A23187 (Figure III-16A). Furthermore, live microscopy demonstrated that *slf* cKO parasites were well capable of gliding in the presence of Ci A23187 (Movie 2). Surprisingly, induced *slf* cKO parasites showed no difference in average speed or gliding length when compared to non-induced parasites (Figure III-16D), indicating that SLF is required to induce motility upstream of Ca^{2+} signalling.

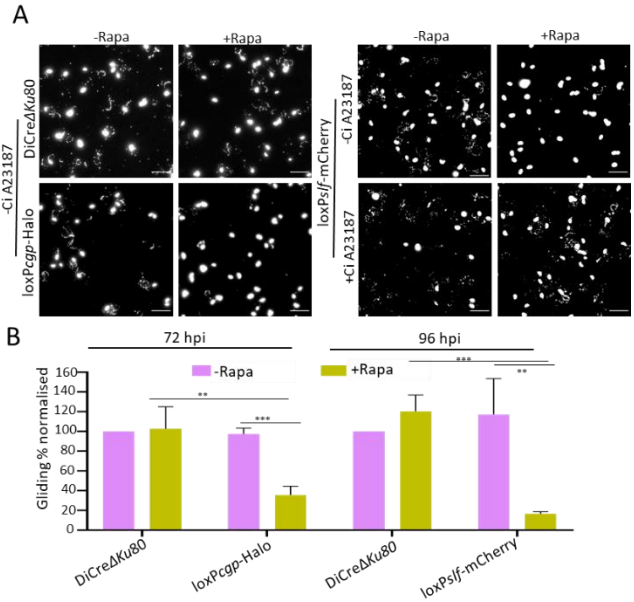

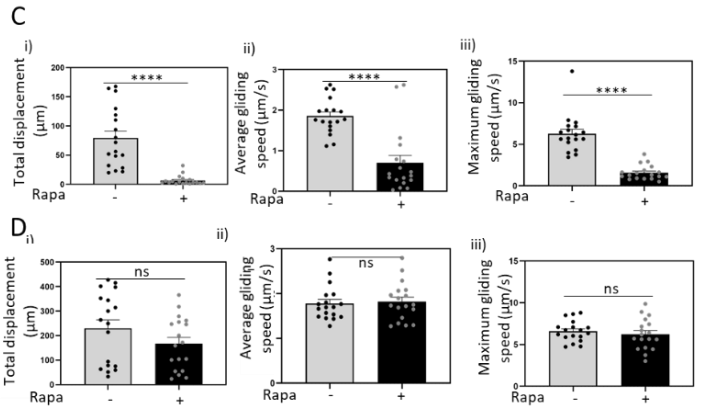

Figure III-16. CGP and SLF are involved in gliding motility.

A) Trail deposition assay of indicated parasite lines in the different conditions. LoxP*cgp*-Halo and loxP*slf*-mCherry parasites were pre-incubated ± 50 nM rapamycin for 72 hours or 96 hours, respectively, before the assays. B) Quantification in (A) in the absence of Ci A23187 treatment. The number of trails was counted and their percentages were calculated to reflect the ratio of gliding and immotile parasites. Data were normalised to the DiCre*Δku80* parasites. C–D) The gliding length, average gliding speed and maximum gliding speed of parasites were measured by 18 tracked parasites doing productive movements (helical and circular movements). P-values were calculated by two-tailed unpaired Student's *t*-test. ns: non-significant; *p<0.05; **p< 0.01; ***p<0.001; ****p<0.0001. Data are presented as mean ± SEM except in B (mean + SD). Rapa: 50 nM rapamycin. Scale bar: 30 µm.

2.5 Microneme secretion

Given the results obtained, it was worthwhile to test the parasites' microneme secretion ability because this is one of the factors that could affect parasite egress, invasion and motility. It has been reported to be regulated by the signalling cascades described. MIC2 was used as a marker for parasite microneme secretion ability, as previously described (Carruthers et al. 1999). To do this, parasites were mechanically released by syringing and resuspending them in an intracellular buffer, which mimics their intracellular conditions with a

high potassium concentration. To stimulate microneme secretion, inducers such as Ci A23187 and BIPPO were employed and released MIC2 in the supernatant (cleaved form) was quantified by Western blot. As a loading control, GRA1 was employed since it is a constitutively secreted protein (see Materials and Methods). As expected, the use of DMSO did not trigger MIC2 parasite secretion in WT parasites or non-induced KO parasites (loxP*cgp*-Halo and loxP*slf*-mCherry). On the other hand, the use of inducers induced MIC2 secretion. LoxP*cgp*-Halo parasites pre-incubated with rapamycin were comparable to non-rapamycin-treated conditions and WT parasites in terms of MIC2 secretion after stimulation with Ci A23187 (Figure III-17A and B). However, loxP*slf*-mCherry-induced KO parasites showed a significantly impacted secretion by using BIPPO (25.7%), which was partially rescued with Ci A23187 (45.5%). LoxP*slf*-mCherry non-rapamycin-induced parasites' MIC2 secretion was not impacted (Figure III-17A and B). Altogether, these results demonstrate that SLF but not CGP is involved in the regulation of microneme secretion.

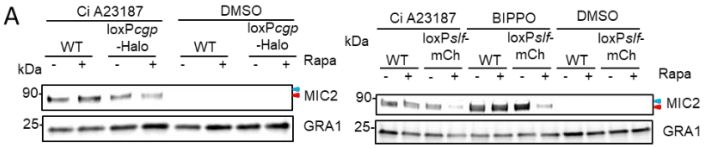

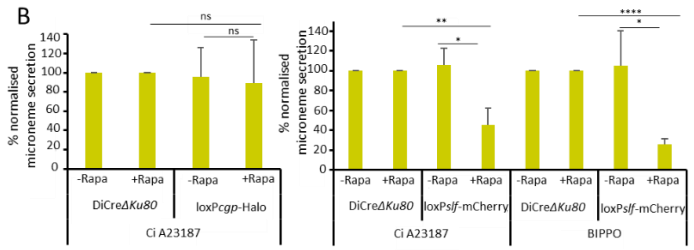

Figure III-17. The role of CGP and SLF in microneme secretion.

A) Representative Western blot images of microneme assays of loxP*cgp*-Halo and loxP*slf*-mCherry (loxP*slf*-mCh) strains in different conditions. α-MIC2 antibody and α-GRA1 antibody were used as primary antibodies. GRA1 is a constitutive secretion protein and is used as a loading control. Blue and red triangles indicate unprocessed and processed forms of MIC2, respectively. B) Quantification of MIC2 and GRA1 in (A). % normalised microneme secretion is the percentage of MIC2/GRA1 normalised to DiCre*Δku80* strain. Data are presented as mean + SD. P-values were calculated by two-tailed unpaired Student's *t*-test. ns: non-significant; *p<0.05; **p< 0.01; ***p<0.001; ****p<0.0001. Rapa: 50 nM rapamycin.

2.6 SLF and CGP effect on organelles

Since secretory organelles, micronemes and rhoptries are linked to parasite invasion and egress, it would be of interest to investigate the role of CGP and SLF in their biogenesis, particularly given that SLF-depleted parasites have a remarkably reduced MIC2 secretion. Microneme proteins are suggested to be arranged in different subsets and trafficked through different pathways. For instance, MIC3/8/11 are in a pathway that is Rab5A- and/or Rab5C-dependent, whereas MIC2/M2AP/AMA1 are in another pathway that is independent of Rab5A and Rab5C (Kremer et al. 2013). MIC2, MIC6 and MIC8 proteins were chosen to represent different microneme organelle subsets and trafficking routes to their destination after synthesis. IFA showing lacking CGP did not affect microneme protein synthesis and trafficking, as supported by different subsets of microneme proteins

having typical distribution at the apical region (Figure III-18A). This is in accordance with the microneme secretion assay, where *cgp* KO parasites were not impacted. SLF-lacking parasites showed normal MIC2 distribution, similar to non-induced KO parasites, which ruled out that MIC2 secretion defects result from incorrect formation and transportation (Figure III-18B). AMA1 also displayed the correct localisation, further demonstrating that SLF does not play a role in microneme protein trafficking.

Next, the role of CGP and SLF in rhoptries was analysed by checking soluble ROP1 and membrane-associated ROP2 and ROP4 (Bradley et al. 2005). Depletion of neither CGP nor SLF had an effect on rhoptry protein localisation as revealed by intracellular IFA probing ROP1 and ROP2-4 (Figure III-18C and D).

Finally, potential effects on other organelles that might be affected were also analysed. In the sCas9 screen, disruption of the *cgp* and *slf* genes did not affect apicoplast inheritance (data not shown). Here, antibody was used against CPN60 protein, an apicoplast resident protein (Agrawal et al. 2009). In good agreement with the results obtained in the sCas9 screen, apicoplasts remained unaffected (Figure III-18E and F).

All these results demonstrate the essential role of CGP and SLF proteins in both invasion and egress. However, secretory organelles and apicoplasts were not impacted by the absence of these proteins, although SLF plays an important role in microneme secretion.

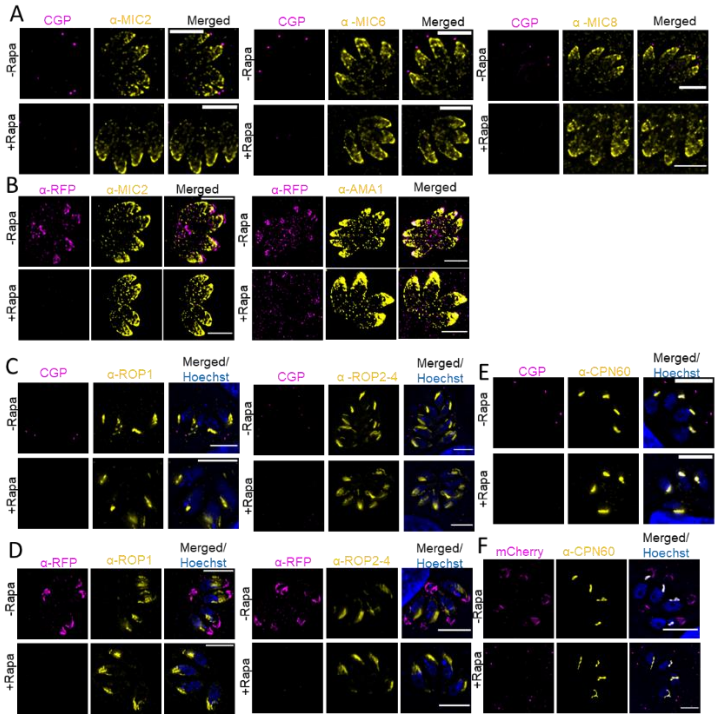

Figure III-18. Depletion of CGP and SLF does not affect microneme, rhoptry or apicoplast organelles.

A–B) Analysis of microneme proteins upon depletion of CGP and SLF after 72 hours post induction with ± 50 nM rapamycin using loxP*cgp*-Halo parasites line (A) and loxP*slf*-mCherry line (B). C–D) Analysis of rhoptry proteins upon depletion of CGP and SLF after 72 hours post induction with ± 50 nM rapamycin. LoxP*cgp*-Halo parasites (C) and loxP*slf*-mCherry parasites (D) were used. E–F) Analysis of apicoplast proteins upon depletion of CGP and SLF after 72 hours post induction with ± 50 nM rapamycin. LoxP*cgp*-Halo parasites (E) and loxP*slf*-mCherry parasites (F) were used. For induction KO, rapamycin was washed away after a 1-hour incubation with parasites. Halo Oregon Green was used to visualise CGP. Scale bar: 5 µm.

2.7 F-actin dynamics during egress

The adaption of Cb into *T. gondii* allows the visualisation of F-actin dynamics by fusing it to fluorescent tags, such as EmeraldFP (Periz et al. 2017). WT parasites transfected with CbEm showed that parasites

form an intensive F-actin network during intracellular replication, which collapses at an early step of parasite egress (Periz et al. 2017). To investigate SLF and CGP regulation of F-actin dynamics during parasite egress, CbEm, flanked by 5'UTR and 3'UTR of the *Tgdhfr* gene, was introduced into the *uprt* (*uracil phosphoribosyltransferase*) locus, which is a non-essential gene and has been commonly used to introduce cassettes in Δ*Ku80* parasites (Figure III-19; Shen et al. 2014, Hunt et al. 2019).

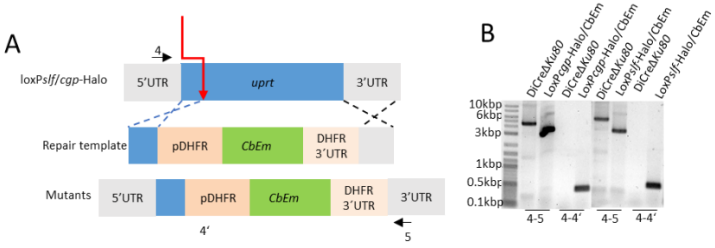

Figure III-19. The introduction of CbEm into loxP*cgp*-Halo and loxP*slf*-Halo strains.

A) Scheme for introducing CbEm in the *Tgdhfr* locus. The orange arrow indicates the targeted region by Cas9. Primer binding sequences are indicated by black arrows. B) Analytical PCRs for indicated strains. Primer binding sites are indicated in (A).

The typical F-actin network was observed as an intravacuolar network connecting individual parasites. For non-induced KO parasites upon treatment with BIPPO, the F-actin network disassembled, and the F-actin signal at the apicoplast and Golgi region decreased while the signal at the posterior area significantly increased over time. Motility was also initiated, and the parasites successfully escaped from the host cells (Figure III-20A and B, Movies 3 and 4). However, for *slf* cKO parasites, none of these steps occurred. F-actin was kept intact and the

signal at the apicoplast and Golgi region and the posterior end remained constant. Moreover, parasite motility was not initiated (Figure III-20A and B, Movie 3). Altogether, this result indicates that initiation of parasite egress was blocked, again pointing to a role of SLF in signalling in good agreement with the results obtained for gliding motility, egress and microneme secretion. However, live (Movie 3) and fixed microscopy demonstrated that treatment with Ci A23187 could partially rescue the F-actin dynamics during egress such that the initiation of disassembly of F-actin and posterior accumulation occurred in the majority of vacuoles. Of the vacuoles that remained confined within the PVs, 89.0% could disassemble the intravacuolar network, and 70.9% accumulated F-actin at the basal end after 5 minutes of induction with Ci A23187 (Figure III-21A and B).

When using propranolol for the induction of egress, *slf* cKO parasites remained in vacuoles. Although F-actin was disassembled, parasites seemed unable to initiate their motility. Notably, parasites' shapes rounded up (Movie 3). This effect was not observed in WT or *cgp* cKO parasites upon induction with propranolol.

F-actin in *cgp* cKO parasites behaved very differently when compared to *slf* cKO parasites. Although *cgp* cKO parasites were capable of disassembling the intravacuolar network, concomitant with the reduction of F-actin signal close to the apicoplast and Golgi region, no accumulation of posterior F-actin or activation of parasite motility was observed. Parasites remained in the host cell regardless of the inducer employed (Figure III-20A and B, Movie 4). These results are in good

agreement with the results obtained for gliding and invasion. They indicate that CGP plays a role in a later stage during the egress pathway, which is downstream of Ca^{2+} signalling and disassembly of the intravacuolar network.

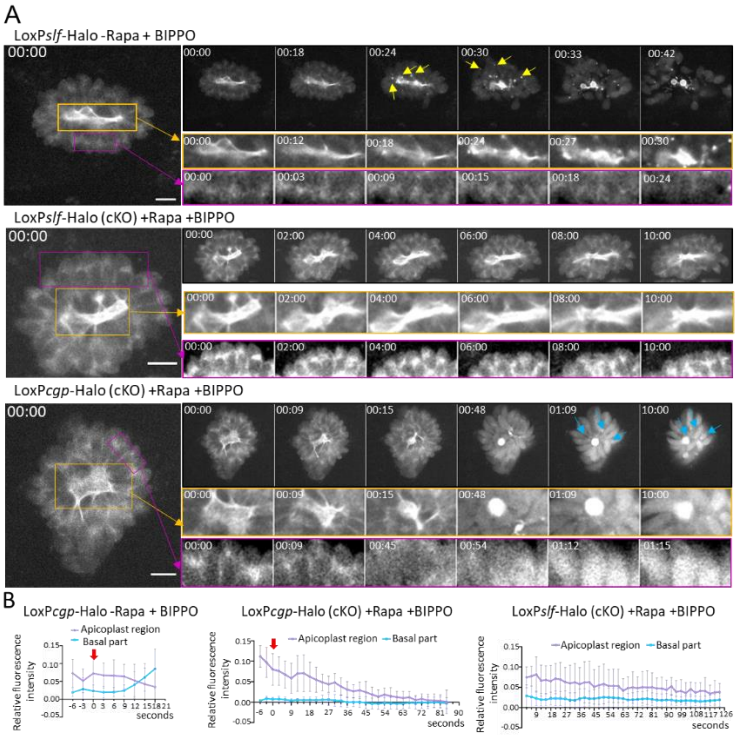

Figure III-20. F-actin dynamics upon induction of egress with BIPPO.

A) Upper, middle and bottom panels depict parasites stably expressing CbEm upon induction of egress in non-induced KO parasites (corresponding to Movie 3), SLF-depleted parasites (corresponding to Movie 3) and CGP-depleted parasites (corresponding to Movie 4), respectively. The F-actin intravacuolar network (orange box), F-actin polymerisation centre at the Golgi and apicoplast region (magenta box), and posterior end (indicated by yellow or blue arrows) are shown. Note: F-actin in

orange and magenta boxes is highly contrasted for better visualisation. Time is presented as minutes: seconds. Scale bar: 5 µm. B) Quantification of the average relative F-actin fluorescence in the apicoplast region and basal end after stimulation egress with BIPPO. The red arrow indicates the time F-actin starts to depolymerise and is set as 0.

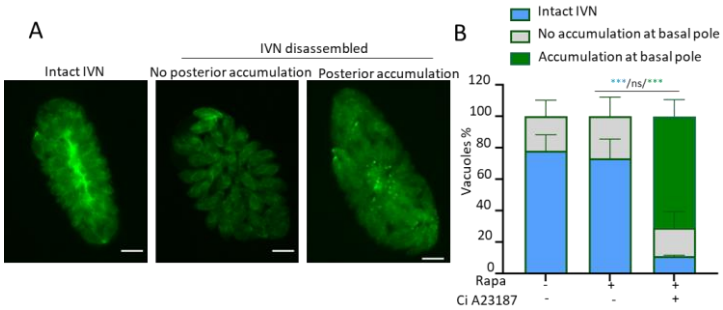

Figure III-21. F-actin disassembly in *slf* cKO parasites.

A) Egress assays were performed on loxP*slf*-Halo/CbEm parasites. Parasite egress was induced with ± Ci A23187 and fixed after 5 minutes. α-GFP Atto488 was used to amplify the F-actin signal. Parasite vacuoles with an intact intravacuolar network (IVN; left image) and disassembled IVN but no posterior accumulation of F-actin (middle image) and strong posterior accumulation (right image) are shown. B) Quantification of (A). Only parasites that failed to egress were counted. Data are presented as mean + SD. P-values were calculated by two-tailed unpaired Student's *t*-test. The colour of the asterisk represents the conditions analysed. ns: non-significant; *p<0.05; **p<0.01; ***p<0.001; ****p<0.0001. Rapa: 50 nM rapamycin. Scale bar: 5 µm.

2.8 Parasitophorous vacuole membrane integrity of parasites

During egress, the PV membrane (PVM) is lysed, probably concomitant with the disassembly of the IVN. To analyse the PVM integrity in *cgp* and *slf* cKO mutants, the surface protein SAG1 was transiently expressed where the GPI anchor was deleted, leading to its secretion into the PV. Therefore, a vector encoding *sag1* without the GPI anchor and fusing it to dsRed, driven by the tubulin promoter (*sag1*ΔGPI-dsRed), was employed (Striepen et al. 1998). The expression of *sag1*ΔGPI-dsRed leads to signal within the PVM in intracellular parasites. Once the PVM was ruptured, SAG1ΔGPI-

dsRed diffused into the host cell cytoplasm (Figure III-22; Movie 5). This was observed in both WT parasites and *cgp* cKO parasites (Figure III-22; Movie 5). However, no diffusion of SAG1ΔGPI-dsRed was observed in SLF-depleted parasites, indicating that the PVM was intact (Figure III-22; Movie 5). Overall, these results indicate that deletion of CGP did not affect the lysis of the PVM and SLF-lacking parasites had a defect in PVM lysis. This is in good agreement with their impaired microneme secretion since PLP1 (a microneme protein) is responsible for PVM rupture (Kafsack et al. 2009).

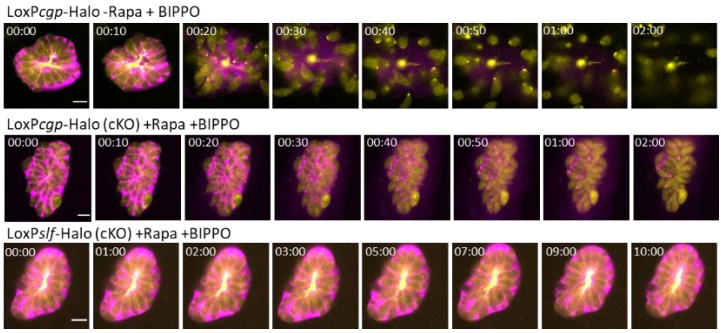

Figure III-22. Rupture of PVM in *cgp* cKO parasites but not in *slf* cKO parasites.

Parasites were stably expressing CbEm (yellow) and transiently expressing *sag1*ΔGPI-dsRed (magenta). Egress was induced upon treatment with BIPPO. Time is presented as minutes: seconds. Scale bar: 5 µm.

2.9 The SLF part of the GC signalling complex

A recent publication has shown that GC and its interactors, CDC50.1 and UGO, are important members of a signalling platform required for invasion, egress, gliding and microneme secretion (Bisio et al. 2019). Of relevance, SLF was identified as a potential interactor for GC. However, SLF was shown to be dispensable for the parasite lytic

cycle when using the AID system. The conditional AID system only allows downregulation of a POI, and it appears that the background expression of SLF was sufficient for maintaining the overall function of the signalling platform. In contrast, complete depletion of SLF using sCas9 or DiCre was deleterious for the parasite.

To analyse the role of SLF within this signalling platform, the following transgenic strains were generated (Table III-3), allowing co-localisation of SLF with the other components.

Table III-3. Parasite lines generated for analysing the SLF part of the GC signalling complex.

Strain	Description
LoxP*slf*-mCherry/*gc*-3HA	*gc* was tagged with triple HA in the loxP*slf*-mCherry line
LoxP*slf*-mCherry/*cdc50.1*-SYFP2	*cdc50.1* was tagged with SYFP2 in the loxP*slf*-mCherry line
LoxP*slf*-mCherry/*ugo*-3HA	*ugo* was tagged with triple HA in the loxP*slf*-mCherry line
LoxP*slf*-mCherry/*ugo*-SYFP2	*ugo* was tagged with SYFP2 in the loxP*slf*-mCherry line
cdc50.1-SYFP2/*slf*-Halo	*cdc50.1* was tagged with SYFP2 in the *slf*-Halo strain
ugo-SYFP2/*slf*-Halo	*ugo* was tagged with SYFP2 in the *slf*-Halo strain
gc-SYFP2/*slf*-Halo	*gc* was tagged with SYFP2 in the *slf*-Halo strain
LoxP*cdc50.1*-SYFP2/*slf*-Halo	*slf* was tagged with Halo, and *cdc50.1*-SYFP2 was floxed
LoxP*ugo*-SYFP2/*slf*-Halo	*slf* was tagged with Halo, and *ugo*-SYFP2 was floxed
LoxP*gc*-SYFP2/*slf*-Halo	*slf* was tagged with Halo, and *gc*-SYFP2 was floxed

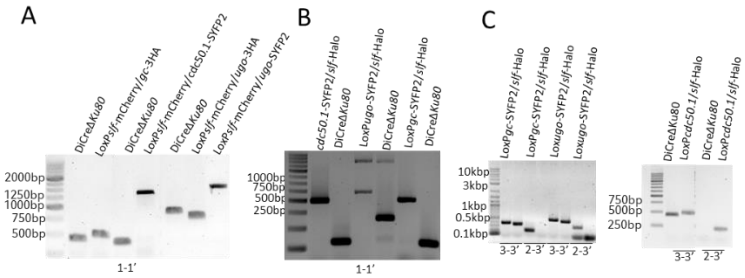

Figure III-23. Establishment of indicated strains.

A) Analytical PCRs for tagging GC, CDC50.1 and UGO in the loxP*slf*-mCherry strain. B) Analytical PCRs for tagging GC, CDC50.1 and UGO in the *slf*-Halo strain. C) Analytical PCRs for insertion of loxP sequence at 5' UTR in the *gc*-SYFP2/*slf*-Halo, *cdc50.1*-SYFP2/*slf*-Halo and *ugo*-SYFP2/*slf*-Halo strains. Primer binding areas are indicated in Figure III-6A and Figure III-9A. PCR products were purified and sent for sequencing to confirm the correct loxP integration.

Next, co-localisation analysis was performed using STED or confocal microscopy. SLF colocalised with GC, UGO and CDC50.1 in both the apical end and RB (Figure III-24A). Upon depletion of SLF, the other components of the signalling platform, GC, UGO and CDC50.1, did not localise to the apical pole and RB. Instead, they appeared to be retained in the ER (Figure III-24B). Conversely, depletion of GC, UGO and CDC50.1 resulted in the mislocalisation of SLF in the ER, and in the case of the CDC50.1-depleted parasite, some SLF could localise at the apical tip (Figure III-24C). All of these results indicate that SLF forms a complex with GC, CDC50.1 and UGO, and this complex is assembled early in the secretory pathway, probably in the ER, and then trafficked to the apical end and RB. Only if all factors are present can they arrive at their final destination.

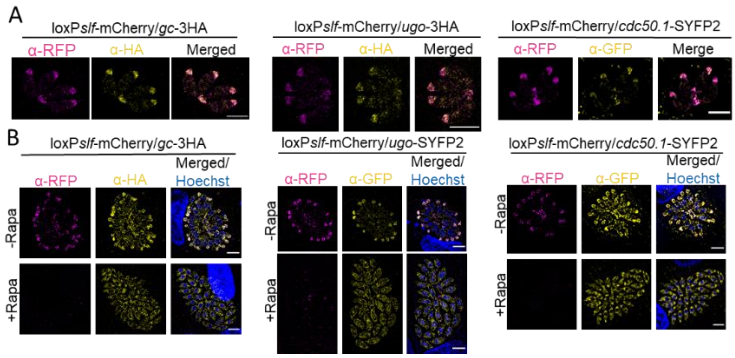

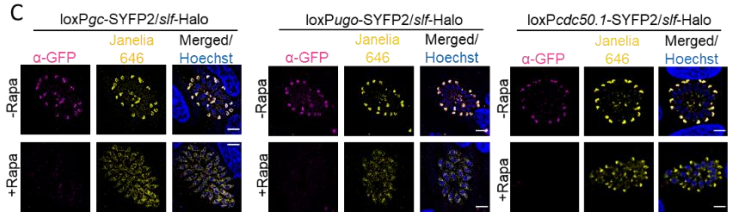

Figure III-24. SLF interacts with GC complex.

A) STED images depict SLF partially colocalised with GC (left panel) and UGO (middle panel). Confocal images of SLF partially colocalised with CDC50.1 (right panel). B) Mislocalisation of GC, UGO and CDC50.1 in SLF-depleted parasites. Parasites were fixed at 96 hours post induction. C) Depletion of either GC, UGO or CDC50.1 results in mislocalisation of SLF. Parasites were fixed at 96 hours post induction. Scale bar: 5 µm.

2.10 Assessment of SLF potential symporter properties

Because SLF was predicted to be a sodium neurotransmitter symporter, whether the transport of neurotransmitters could be part of the signalling transduced by this complex was interesting to test. In mammalian cells, γ-aminobutyric acid (GABA) is known to be a neurotransmitter that acts on GABA receptors and mediates signal transduction. *T. gondii* synthesises high levels of GABA (MacRae et al. 2012) and triggers infected cells to synthesise and secrete it (Bhandage et al. 2019). Furthermore, GABA has been reported to act as a messenger and modulator for dendritic cell migration (Fuks et al. 2012). This raised the questions of whether GABA could act as an egress signal for parasites and whether SLF acts as a GABA transporter. I reasoned that if I supplemented parasites with rich GABA, which weighs more than it syntheses, I would be able to rescue the SLF cKO phenotypes if other putative GABA transporters were present. To support this, as a first trial, plaque assays were performed in the presence of GABA. Equal numbers of parasites were

inoculated in each well and supplied with different concentrations of GABA ranging from 0 to 15 mM for 6 days. Unfortunately, *slf* cKO parasites did not survive because they barely made any plaque in any of the different GABA concentrations. These parasites behaved similarly when no GABA was supplemented or in our vehicle controls (Figure III-25A). Therefore, higher concentrations of GABA cannot rescue the SLF cKO phenotype.

Tested in parallel was gabapentin, a GABA analogue that is structurally related to GABA and used in the treatment of seizures (Mathieson et al. 2020). Theoretically, if SLF is the main GABA transporter, it could transport gabapentin and then cause impairment of the parasite lytic cycle. However, after the addition of gabapentin, parasite growth was not impacted even at a 5 mM concentration (Figure III-25B). These observations did not support the hypothesis that SLF is the main GABA transporter. Therefore, the substrate of SLF still remains to be determined.

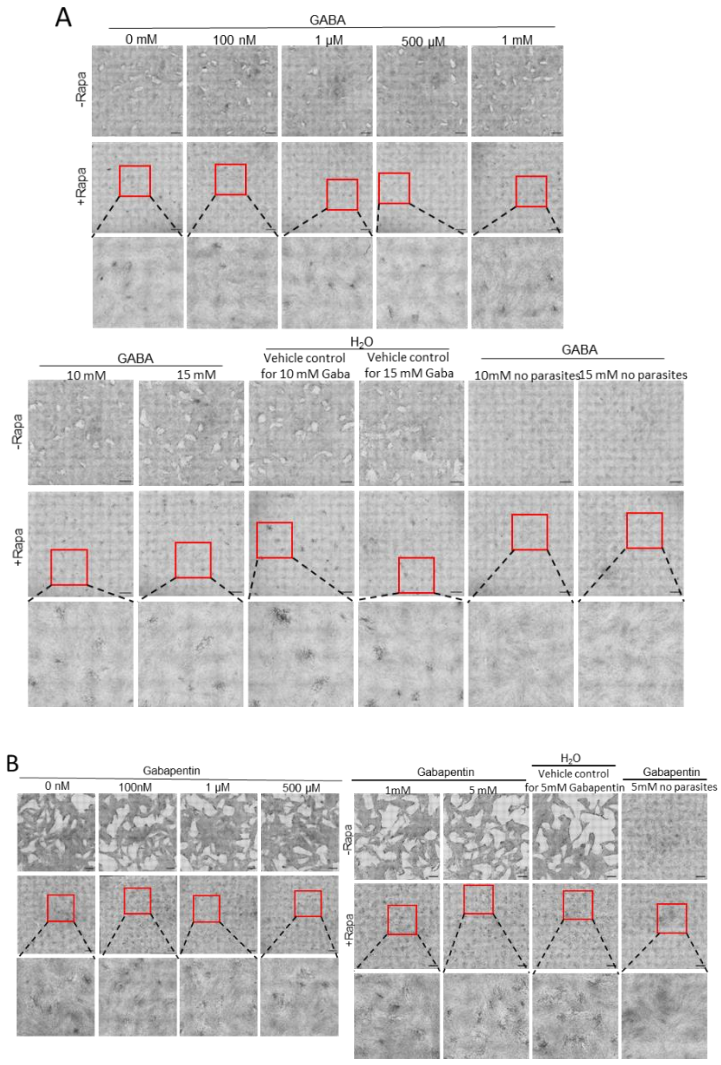

Figure III-25. SLF does not play a role in GABA signalling.

Plaque assays of lox*Pslf*-mCherry supplemented with different concentrations of GABA (A) and gabapentin (B). Each bottom panel is a magnified view of the area marked with a red rectangle. Scale bar: 1.5 mm.

3. A potential protein complex at the conoid complex revealed by BioID

3.1 CGP localisation within the apical complex

Wide-field microscopy has revealed that CGP is confined to the apical tip. Due to the limited resolution of wide-field microscopy and the small size of the apical complex, the exact localisation of CGP cannot be inferred. SAS6L, which localises at the conoid body, was C-terminally tagged, along with RNG2 protein, which localises at the APR2, closely associated with the conoid apical end in intracellular parasites (Koreny et al. 2021), as marker proteins to further pinpoint the localisation of CGP (Figure III-26A, Table III-4). STED microscopy indicated that CGP was anterior to both conoidal markers in intracellular parasites where the conoid stays retracted. In extracellular parasites whose conoids were protruded, CGP was above the RNG2 with a clear gap in between and remained at a similar distance from SAS6L to in retracted conoids (Figure III-27A). Together, these results suggest that CGP is a preconoidal protein.

Table III-4. An overview table of parasite lines generated and used in this section.

loxP*frm1*-mCherry strain was generated by Mirko Singer; loxP*akmt*-SYFP2 strain was generated by Elena Jimenez-Ruiz. Thanks to Peipei Qin for assistance with some vector clonings used for generation of strains here.

Strain	Genotype
loxP*cgp*-Halo/*rng2*-6HA	RH DiCre-T2A/Δku80/Δhx/CAT/loxP-cgp-Halo-loxP/rng2-6HA/dhfr
loxP*cgp*-Halo/*sas6l*-eGFP	RH DiCre-T2A/Δku80/Δhx/CAT/loxP-cgp-Halo-loxP/sas6l-eGFP/dhfr
loxP*cgp*-Halo/*myoh*-SYFP2	RH DiCre-T2A/Δku80/Δhx/CAT/loxP-cgp-Halo-loxP/myoh-SYFP2-loxP
loxP*cgp*-Halo/*frm1*-SNAP	RH DiCre-T2A/Δku80/Δhx/CAT/loxP-cgp-Halo-loxP/*frm1*-SNAP-loxP

loxP*frm1*-mCherry	RH DiCre-T2A/Δku80/Δhx/CAT/loxP-*frm1*-mCherry-loxP
loxP*frm1*-mCherry/*cgp*-Halo	RH DiCre-T2A/Δku80/Δhx/CAT/loxP-frm1-mCherry-loxP/*cgp*-Halo-loxP
cgp-TurboID/*frm1*-3HA	RH DiCre-T2A/Δku80/Δhx/CAT/cgp-TurboID-loxP/frm1-3HA-loxP
frm1-TurboID/loxP*cgp*-Halo	RH DiCre-T2A/Δku80/Δhx/CAT/loxP-cgp-Halo-loxP/frm1-TurboID-loxP
253440-SYFP2/loxP*cgp*-Halo	RH DiCre-T2A/Δku80/Δhx/CAT/loxP-cgp-Halo-loxP/253440-SYFP2-loxP
231160-SYFP2/loxP*cgp*-Halo	RH DiCre-T2A/Δku80/Δhx/CAT/loxP-cgp-Halo-loxP/231160-SYFP2
263070-SYFP2/loxP*cgp*-Halo	RH DiCre-T2A/Δku80/Δhx/CAT/loxP-cgp-Halo-loxP/263070-SYFP2-loxP
212780-3HA/loxP*cgp*-Halo	RH DiCre-T2A/Δku80/Δhx/CAT/loxP-cgp-Halo-loxP/212780-3HA-loxP
238170-SYFP2/loxP*cgp*-Halo	RH DiCre-T2A/Δku80/Δhx/CAT/loxP-cgp-Halo-loxP/238170-SYFP2-loxP
293480-SYFP2/loxP*frm1*-Halo	RH DiCre-T2A/Δku80/Δhx/CAT/loxP-frm1-Halo-loxP/293480-SYFP2-loxP
loxP*cgp*-Halo/*akmt*-SYFP2	RH DiCre-T2A/Δku80/Δhx/CAT/loxP-cgp-Halo-loxP/akmt-SYFP2-loxP
loxP*cgp*-Halo/*pckmt*-SYFP2	RH DiCre-T2A/Δku80/Δhx/CAT/loxP-cgp-Halo-loxP/pckmt-SYFP2-loxP
loxP*cgp*-Halo/*icap16*-SYFP2	RH DiCre-T2A/Δku80/Δhx/CAT/loxP-cgp-Halo-loxP/icap16-SYFP2-loxP
loxP*cgp*-Halo/*dap1*-SYFP2	RH DiCre-T2A/Δku80/Δhx/CAT/loxP-cgp-Halo-loxP/*dap1*-SYFP2-loxP
loxP*cgp-Halo/gac-SYFP2*	RH DiCre-T2A/Δku80/Δhx/CAT/loxP-cgp-Halo-loxP/gac-SYFP2-loxP
loxP*cgp-Halo/akmt-SYFP2*	RH DiCre-T2A/Δku80/Δhx/CAT/loxP-cgp-Halo-loxP/akmt-SYFP2-loxP
loxP*cgp*-Halo/*aamt*-sYFP2	RH DiCre-T2A/Δku80/Δhx/CAT/loxP-cgp-Halo-loxP/*aamt*-sYFP2-loxP
loxP*akmt*-SYFP2/*cgp*-Halo	RH DiCre-T2A/Δku80/Δhx/CAT/loxP-akmt-SYFP2-loxP/cgp-Halo-loxP
loxP*frm1*-Halo	RH DiCre-T2A/Δku80/Δhx/CAT/loxP-frm1-Halo-loxP
loxP*frm1*-Halo/*pckmt*-SYFP2	RH DiCre-T2A/Δku80/Δhx/CAT/loxP-frm1-Halo-loxP/pckmt-SYFP2-loxP
loxP*frm1*-Halo/*dap1*-SYFP2	RH DiCre-T2A/Δku80/Δhx/CAT/loxP-frm1-Halo-loxP/dap1-SYFP2-loxP
loxP*frm1*-Halo/*icap16*-SYFP2	RH DiCre-T2A/Δku80/Δhx/CAT/loxP-frm1-Halo-loxP/icap16-SYFP2-loxP
loxP*frm1*-Halo/*akmt*-SYFP2	RH DiCre-T2A/Δku80/Δhx/CAT/loxP-frm1-Halo-loxP/akmt-SYFP2-loxP
loxP*frm1*-Halo/*aamt*-SYFP2	RH DiCre-T2A/Δku80/Δhx/CAT/loxP-frm1-Halo-loxP/aamt-SYFP2-loxP

loxP*frm1*-Halo/*gac*-SYFP2	RH DiCre-T2A/Δku80/Δhx/CAT/loxP-frm1-Halo-loxP/gac-SYFP2-loxP
loxP*akmt*-SYFP2	RH DiCre-T2A/Δku80/Δhx/CAT/loxP-akmt-SYFP2-loxP
loxP*akmt*-SYFP2/*frm1*-Halo	RH DiCre-T2A/Δku80/Δhx/CAT/loxP-akmt-SYFP2-loxP/frm1-Halo-loxP
loxP*akmt*-SYFP2/*dap1*-Halo	RH DiCre-T2A/Δku80/Δhx/CAT/loxP-akmt-SYFP2-loxP/dap1-Halo-loxP
loxP*dap1*-SYFP2	RH DiCre-T2A/Δku80/Δhx/CAT/loxP-dap1-SYFP2-loxP
loxP*dap1*-SYFP2/*cgp*-Halo	RH DiCre-T2A/Δku80/Δhx/CAT/loxP-dap1-SYFP2-loxP/cgp-Halo-loxP
loxP*dap1*-SYFP2/*frm1*-Halo	RH DiCre-T2A/Δku80/Δhx/CAT/loxP-dap1-SYFP2-loxP/frm1-Halo-loxP
loxP*dap1*-SYFP2/*icap16*-Halo	RH DiCre-T2A/Δku80/Δhx/CAT/loxP-dap1-SYFP2-loxP/icap16-Halo-loxP
loxP*dap1*-SYFP2/*pckmt*-Halo	RH DiCre-T2A/Δku80/Δhx/CAT/loxP-dap1-SYFP2-loxP/pckmt-Halo-loxP
loxP*dap1*-SYFP2/*aamt*-Halo	RH DiCre-T2A/Δku80/Δhx/CAT/loxP-dap1-SYFP2-loxP/aamt-Halo-loxP

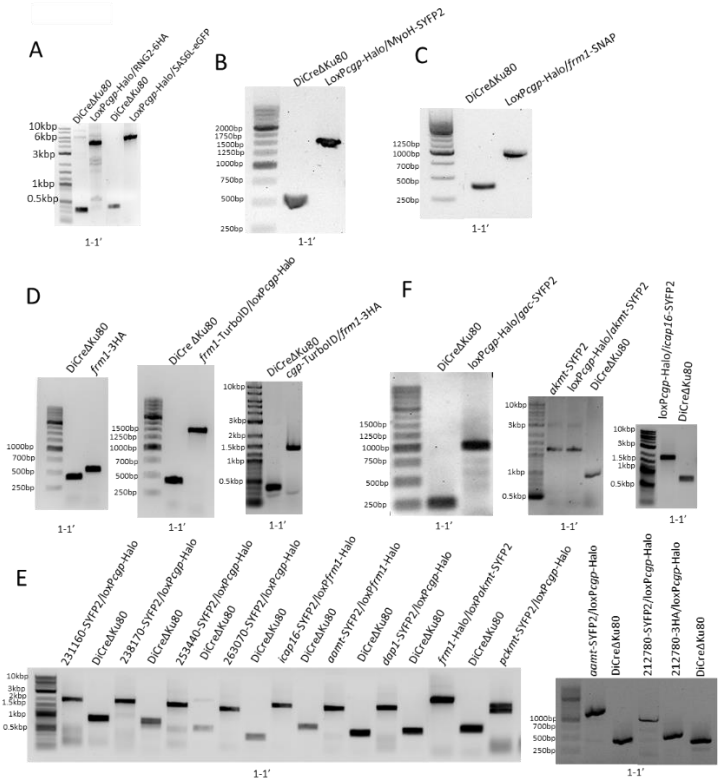
A
DiCreΔKu80
LoxPcgp-Halo/RNG2-6HA
DiCreΔKu80
LoxPcgp-Halo/SAS6L-eGFP
10kbp
6kbp
3kbp
1kbp
0.5kbp
1-1′
B
DiCreΔKu80
LoxPcgp-Halo/MyoH-SYFP2
2000bp
1750bp
1500bp
1250bp
1000bp
750bp
500bp
250bp
1-1′
C
DiCreΔKu80
LoxPcgp-Halo/frm1-SNAP
1250bp
1000bp
700bp
500bp
250bp
1-1′
D
DiCreΔKu80
frm1-3HA
DiCre ΔKu80
frm1-TurboID/loxPcgp-Halo
DiCreΔKu80
cgp-TurboID//frm1-3HA
1000bp
700bp
500bp
250bp
1500bp
1250bp
1000bp
700bp
500bp
250bp
10kbp
3kbp
2kbp
1.5kbp
1kbp
0.5kbp
1-1′
1-1′
1-1′
F
DiCreΔKu80
loxPcgp-Halo/gpc-SYFP2
akmt-SYFP2
loxPcgp-Halo/akmt-SYFP2
DiCreΔKu80
loxPcgp-Halo/icop16-SYFP2
DiCreΔKu80
1500bp
1250bp
1000bp
750bp
500bp
250bp
10kbp
3kbp
1kbp
0.5kbp
10kbp
3kbp
1.5kbp
1kbp
0.5kbp
1-1′
1-1′
1-1′
E
231160-SYFP2/loxPcgp-Halo
DiCreΔKu80
238170-SYFP2/loxPcgp-Halo
DiCreΔKu80
253440-SYFP2/loxPcgp-Halo
DiCreΔKu80
263070-SYFP2/loxPcgp-Halo
DiCreΔKu80
icap16-SYFP2/loxPcgp-Halo
DiCreΔKu80
aamt-SYFP2/loxPfrm1-Halo
DiCreΔKu80
ddp1-SYFP2/loxPcgp-Halo
DiCreΔKu80
frm1-Halo/loxPakmt-SYFP2
DiCreΔKu80
pckmt-SYFP2/loxPcgp-Halo
aamt-SYFP2/loxPcgp-Halo
DiCreΔKu80
212780-SYFP2/loxPcgp-Halo
212780-3HA/loxPcgp-Halo
DiCreΔKu80
10kbp
3kbp
2kbp
1.5kbp
1kbp
0.5kbp
1000bp
700bp
500bp
250bp
1-1′
1-1′

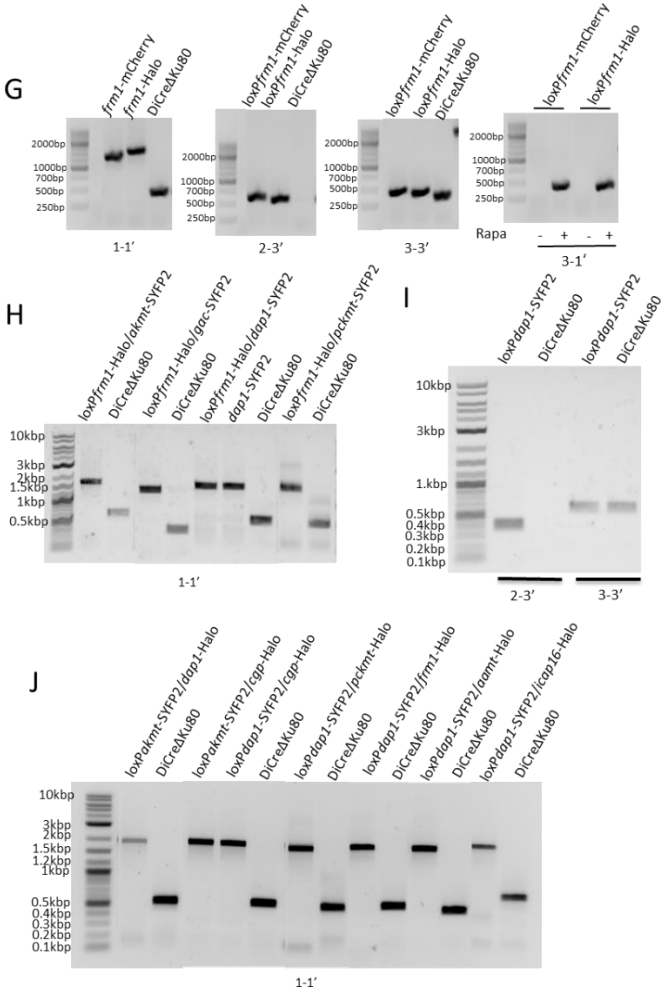

Figure III-26. Analytical PCRs for parasite lines generated in this section.

A) PCRs indicate successful tagging of RNG2 and SAS6L in the loxP*cgp*-Halo line. B) PCRs indicate successful tagging of MyoH with SYFP2 in the loxP*cgp*-Halo line. C) PCRs indicate successful tagging of FRM1 with SNAP in the loxP*cgp*-Halo line. D) Left: Analytical PCRs indicating successful tagging of FRM1 with 3HA in

DiCreΔKu80 strain. Middle and right panel: Successful tagging of FRM1 and CGP with TurboID in the loxP*cgp*-Halo and *frm1*-3HA strains, respectively. E) Analytical PCRs show the correct integration of tags in the floxed parasite lines. F) Analytical PCRs show the correct integration of tags in the floxed lines or DiCre*Δku*80 strains. G) Successful generation of loxP*frm1*-mCherry and loxP*frm1*-Halo strains indicated by genotyping PCR for tagging (1-1'), integration PCRs for 5'loxP (2-3' and 3-3') and excision PCRs (3-1'). Analytical PCR products (3-3' primers) were purified and sent for sequencing to confirm the correct loxP integration. H) Analytical PCRs show the correct integration of tags in the floxed lines or DiCreΔku80 strains. I) Analytical PCRs show the correct integration of 5'loxP in the *dap1*-SYFP2 strain. PCR products (3-3' primers) were purified and sent for sequencing to confirm the correct loxP integration. J) Analytical PCRs show the correct integration of tags in the floxed lines. The primer binding area is indicated in Figure III-6A and Figure III-9A.

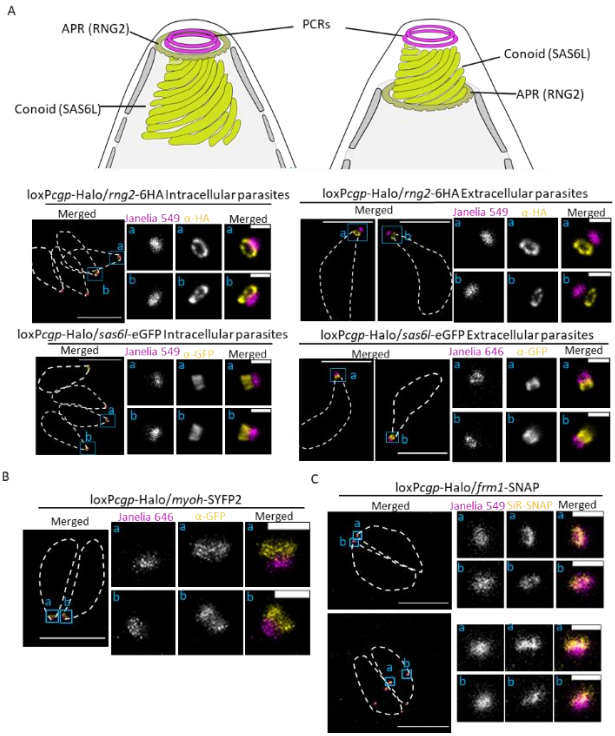

Figure III-27. STED images of CGP with different marker proteins.

A) STED imaging of CGP with SAS6L and RNG2 proteins in intracellular parasites with retracted conoids and extracellular parasites with protruded conoids. Parasites were intracellularly labelled with 200 nM Halo Janelia Fluro 549 or 646 for 1 hour before fixation. Top: Schematic of apical part of *T. gondii*. B–C) STED imaging of CGP with MyoH and FRM1 in intracellular parasites. In the case of loxP*cgp*-Halo/*myoh*-SYFP2 parasites, CGP was intracellularly labelled with 200 nM Halo Janelia Fluro 646 for 1 hour before fixation. LoxP*cgp*-Halo/*frm1*-SNAP parasites were first labelled with 1µM SNAP-Cell 647-SiR (also termed SiR-SNAP) for 1 hour and then labelled with 200 nM Halo Janelia Fluro 549 for 1 hour before fixation. White dashed line indicates parasite periphery. Scale bar: 5 µm for intracellular parasites, 3 µm for extracellular parasites. 0.5 µm for zoomed-in pictures.

The myosin MyoH and the actin nucleator FRM1 were previously described as factors involved in motility and localised in the conoidal region. KO of either MyoH or FRM1 phenocopies CGP KO mutants to a certain extent. Thus, it is interesting to colocalise CGP with both proteins. STED imaging showed that MyoH signal, which has been reported to localise at the tubular core of the conoid (Graindorge et al. 2016), was posterior to CGP (Table III-4, Figure III-26B, Figure III-27B). However, CGP colocalised with FRM1 in the conoids of both mature cells as well as in developing daughter cells (Table III-4, Figure III-26C, Figure III-27C).

Importantly, the lack of CGP had no impact on SAS6L, RNG2 and MyoH localisation, which indicates that CGP is not involved in maintaining conoid stability or transport of these proteins to the conoid (Figure III-28A-C). In contrast, depletion of CGP showed a loss of FRM1 signal in mature cells. Interestingly, FRM1 was still present in the forming daughter cells (Figure III-28D and E). In contrast, CGP was not lost in the absence of FRM1 (Table III-4, Figure III-28F). Given these observations, I hypothesised that CGP, FRM1 and potentially other proteins form a complex at the conoid

complex that could be key for motility initiation and thus critical for egress and invasion.

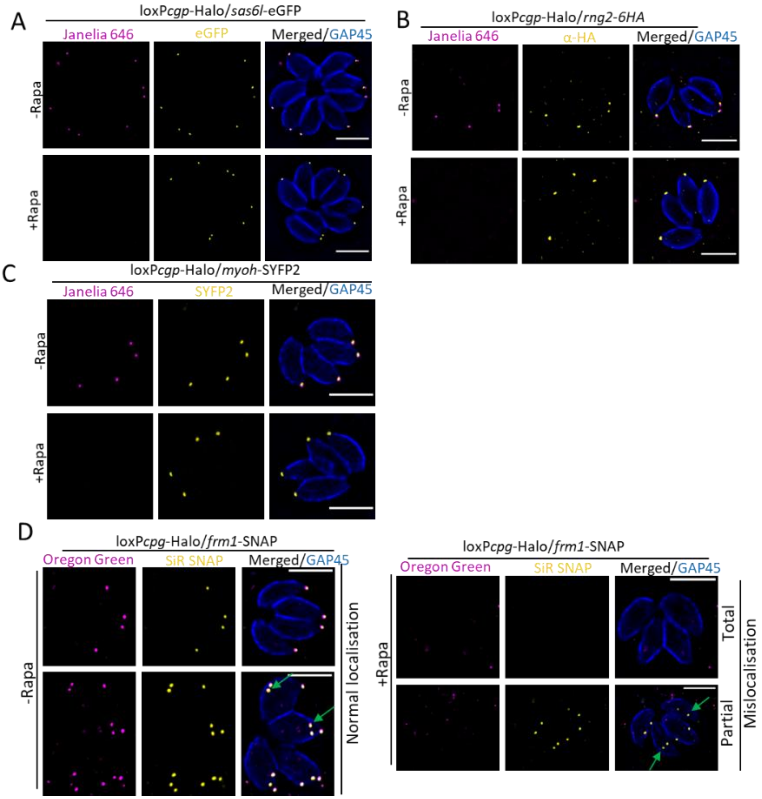

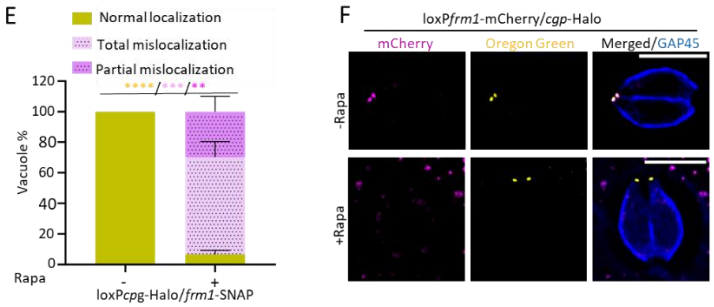

Figure III-28. Effect of CGP depletion on conoidal markers.

A) Upon depletion of CGP, SAS6L (A), RNG2 (B) and MyoH (C) were not affected in their apical localisation. D) Mislocalisation of FRM1 upon depletion of CGP. In non-induced parasites, FRM1 is correctly localised in the conoids in mature and budding daughter cells (left panels). Right panels show *cgp* cKO where no FRM1 signal was observed (referred to as 'total mislocalisation'; upper panel) or it was absent at the conoid of mother cells but still visible in the forming daughter cells (referred to as 'partial mislocalisation'; bottom panel). Parasites were induced with 50 nM rapamycin for 1 hour, and phenotypes were examined at 72 hours post induction. 100 nM Halo Oregon Green was used to label CGP and 1 µM SiR-SNAP was used to stain FRM1 for 1 hour, then washed away, followed by incubation with media for 1 hour before fixation at 72 hours post induction. E) Quantification of FRM1 correctly localised vacuoles and mislocalised vacuoles upon KO of *cgp* in (D). Only parasites lacking CGP were counted in the rapamycin-induced condition. FRM1 in the daughter cells is indicated by green arrows. F) Upon depletion of FRM1, CGP remained at the conoid. Images were taken 72 hours post induction. Scale bar: 5 µm. Data are presented as mean + SD. P-values were calculated by two-tailed unpaired Student's *t*-test. ns: non-significant; *p<0.05; **p<0.01; ***p<0.001; ****p<0.0001. The colour of the asterisk represents the conditions analysed. Rapa: 50 nM rapamycin.

3.2 Identification of potential interactors by BioID for CGP and FRM1

To identify additional interactors of CGP and FRM1, a proximity labelling method was chosen based on the promiscuous BirA enzyme for BioID of proteins that would interact with CGP and/or FRM1. This system has been successfully employed in *T. gondii* to label not only proteins that might be insoluble but also those with weak or transient interactions (Chen et al. 2015, Long et al. 2017, Branon et al. 2018).

A variant of this BirA enzyme is known as TurboID, with much greater labelling efficiency than BirA, being more robust and faster (Branon et al. 2018). The TurboID was fused to CGP and FRM1 at their C-termini (*cgp*-TurboID in the *frm1*-3xHA strain and *frm1*-TurboID in the loxP*cgp*-Halo strain; Table II-4, Figure III-26D). To examine whether the TurboID was functional in those parasites, intracellular parasites were treated with 150 µM biotin for 6 hours and then fixed by staining with Alexa Fluor 488 conjugated streptavidin (Alexa Fluor 488 Streptavidin), which has a very high affinity for biotinylated proteins. As expected, signals at the apicoplast region (and to a lesser degree in the mitochondria) were detected in both WT and TurboID strains since these organelles contain endogenously biotinylated proteins (Figure III-29A; Jelenska et al. 2001). Although WT parasites showed no biotinylated signals at the conoid, TurboID strains showed biotinylated signals at the conoid that overlapped with FRM1 and CGP, respectively (Figure III-29A).

Thus, *cgp*-TurboID/*frm1*-3HA, *frm1*-TurboID/loxP*cgp*-Halo and WT parasites pre-treated with 150 µM biotin for 6 hours were harvested. The parasite pellet was lysed and incubated with streptavidin-conjugated beads for 30 minutes to purify biotinylated proteins, after which the beads were washed and kept at -80 °C until they were sent for mass spectrometry analysis (see Materials and Methods). A sample of non-biotin-treated parasites, biotin-treated parasites and 5% of the streptavidin beads were analysed by Western blot. Additional bands were seen in TurboID-tagged parasites treated with elevated biotin in comparison with biotin untreated parasites. Additional bands could be

more clearly observed in the bead samples when compared to the WT (Figure III-29B).

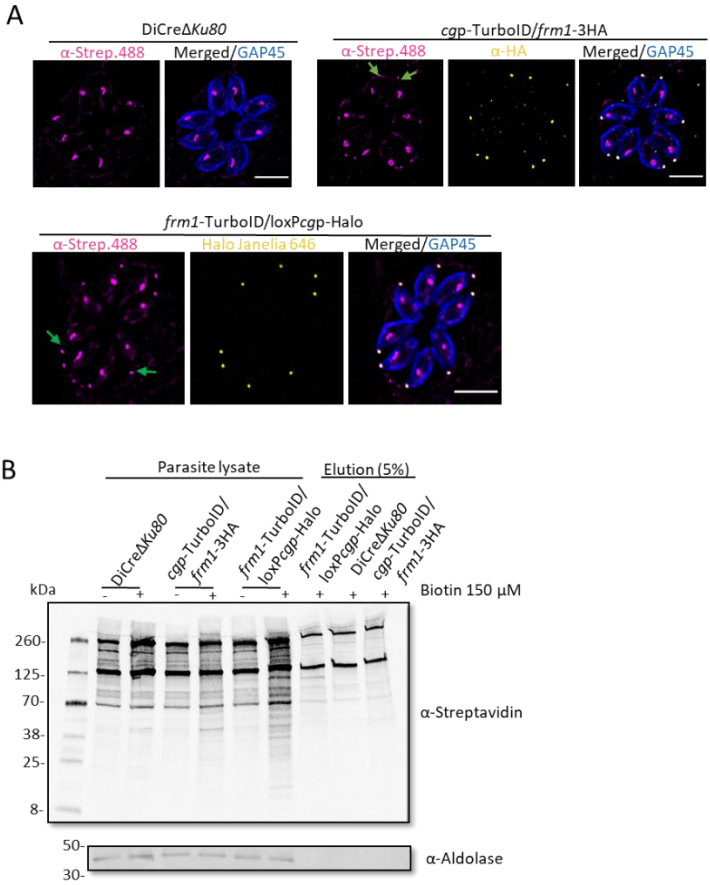

Figure III-29. Biotinylated proteins in parasites expressing TurboID.

A) IFA depicting WT parasites and parasites expressing TurboID stained with Alexa Fluor 488 Streptavidin (α-Strep.488) and apical marker proteins. Green arrows indicate biotinylated proteins at the apical tip. Parasites' periphery was visualised by labelling GAP45. Scale bar: 5 µm. B) WB showing the biotinylated proteins in the indicated parasite lines. After culturing the indicated parasite lines for 24 hours, the media was

supplemented with 150 µM biotin for 6 hours, followed by parasite harvesting. Parasite pellets were lysed and Western blotted, except for the last three lanes where proteins eluted from 5% streptavidin-conjugated beads after incubation with parasite lysate for 30 minutes. Anti-aldolase was used as a loading control.

Mass spectrometry identified around 200 hits that are displayed in the volcano plot (Figure III-30); 58 and 64 proteins were significantly enriched or substantially enriched, with a cut-off of difference of over 4.5 in *cgp*-TurboID and *frm1*-TurboID strains, respectively. Out of those enriched proteins, the candidate lists were filtered by adding the criteria of a phenotypic score of <-1 with an apical or unknown localisation according to the literature or as predicted by HyperLOPIT (Barylyuk et al. 2020). This process resulted in a total of 15 candidates (Table III-5) for further investigation. Of relevance, *cgp*-TuroID and *frm1*-TurboID BioID shared the majority of enriched candidates (Table III-5). Moreover, FRM1 was significantly enriched in *cgp*-TuroID and vice versa, suggesting that these two proteins interact with each other (Table III-5, Figure III-30).

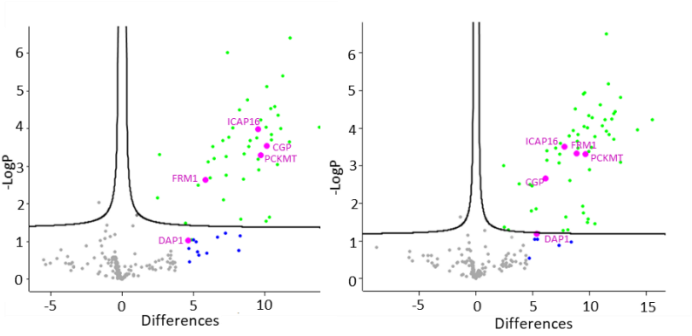

Figure III-30. Biotinylated proteins identified by mass spectrometry.

Volcano plots showing the relative enrichment of CGP (left panel) and FRM1 (right panel) revealed by differences, defined as the value of protein enrichment in TurboID-tagged parasite lines minus that in WT parasites. Each hit is presented as a circle. Significantly enriched hits are represented as green circles. Highly enriched (difference over 4.5) but not statistically significant hits are represented as blue circles. Proteins in magenta indicated with their names are those mislocalised when *cgp* was KO.

Table III-5. Selection of interesting candidates potentially interacting with CGP and FRM1.
NA, not applicable. ✓ indicates protein is enriched in BioID. × indicates protein is not enriched in BioID. Proteins enriched in both BioIDs are highlighted in green.

Gene ID (TGGT1-_)	Product	Phenotypic score	hyperLOPIT predicted localisation				Known localisation	Reference for localisation	Enrichment	
			Final probability	TAGM-MAP	TAGM-MCMC	Top probability			CGP	FRM1
240380	CGP	-3.85	0	PM - peripheral 2	PM - peripheral 2	0.996			✓	✓
462965	FRM 1	-2.8	N/A	N/A	N/A	N/A	Preconidal ring	(Dos Santos Pacheco et al. 2022)	✓	✓
292170	PCKMT	-4.83	N/A	N/A	N/A	N/A			✓	✓
284620	DAP1	-1.02	N/A	N/A	N/A	N/A	Conoid canopy ring	(Koreny et al. 2021)	✓	✓
212780	hypothetical protein	-5.33	N/A	N/A	N/A	N/A			✓	✓
210430	DnaJ domain–containing protein	-3.81	N/A	N/A	N/A	N/A			✓	✓
299190	B-box zinc finger domain–containing protein	-2.58	N/A	N/A	N/A	N/A			×	✓
310070	AAMT	-1.22	8.99E-20	cytosol	PM - peripheral 2	1	Apical annuli	(Engelberg et al. 2020)	✓	✓
216080	AKMT	-4.3	7.58E-21	cytosol	nucleolus	0.992	Apical complex	(Heaslip et al. 2011, Sivagurunathan et al. 2013)	✓	✓
238170	hypothetical protein	-5.06	N/A	N/A	N/A	N/A			✓	✓

293480	MoeA N-terminal region (domain I and II) domain–containing protein	-1.55	0.00164	nucleus - chromatin	nucleus - non-chromatin	0.827			×	✓
253440	putative cell-cycle-associated protein kinase SRPK	-3.09	0.971	nucleus - chromatin	nucleus - chromatin	0.987			✓	✓
202120	ICAP16	-2.1	0	nucleus - chromatin	PM - peripheral 2	0.985	Conoid canopy ring	(Sidik et al. 2016, Koreny et al. 2021)	✓	✓
230940	hypothetical protein	-4.92	0.667	nucleus - chromatin	nucleus - chromatin	0.928			×	✓
263070	CMGC kinase, CK2 family	-2.65	0.879	cytosol	cytosol	0.558			✓	×
231160	hypothetical protein	-1.6	7.05E-19	IMC	IMC	0.698			✓	✓
312630	GAC	-3.53	0.999	cytosol	cytosol	1	PCRs/Conoid+cytosol	(Jacot et al. 2016, Dos Santos Pacheco et al. 2022)	×	✓

3.3 Characterisation of potential interactors revealed by BioID

I attempted to determine the cellular localisation of these selected 15 proteins. Twelve candidate proteins were successfully tagged endogenously with SYFP2 or 3HA at the 3' end (Table III-4, Figure III-26E,F). These proteins localised in different subcellular compartments. Among them, TGGT1_253440, TGGT1_231160 and TGGT1_263070 are not apically localised proteins (Figure III-31A). Interestingly, in some vacuoles, TGGT1_263070 had accumulated signal close to the nucleus (Figure III-31A). Three proteins showed a cell cycle–dependent signal based on the detection of their signals only in some vacuoles in the clonal parasite lines: TGGT1_212780 and TGGT1_238170 were in close association with the nucleus, and TGGT1_293480 displayed an uneven cytosolic distribution and a faint signal at the conoid (Figure III-31B).

AKMT, as a conoid protein, has been described as essential for the parasite lytic cycle because of its role in invasion, egress and motility (Heaslip et al. 2011). Indispensable conserved apicomplexan protein 16 (ICAP16) was first reported from a genome-wide CRISPR screen. It is indispensable and involved in parasite invasion (Sidik et al. 2016). In this study, AKMT and ICAP16 were identified at the apical tip as previously described (Figure III-31C; Heaslip et al. 2011, Sidik et al. 2016). Two hypothetical proteins, TGGT1_292170, now named preconoidal lysine methyltransferase (PCKMT), and TGGT1_284620, now named dispensable apical protein 1 (DAP1), were present only at the conoid. This is in good agreement with DAP1 localised at the PCRs (Figure III-31C; Koreny et al. 2021). Notably, PCKMT was

recently found in our lab in a parallel sCas9 screen where an indicator strain (sCas9-CbEm-mCherry_αTubulin) was used to screen for factors involved in F-actin and microtubules, and disruption of PCKMT showed a strong F-actin phenotype (Jimenez-Ruiz et al., in preparation).

GAC and AAMT have also been previously described (Jacot et al. 2016, Engelberg et al. 2020). The localisation reported earlier, where the accumulated signal is located at the conoid, was confirmed (Figure III-31D). Interestingly, the GAC signal distribution appeared different in live imaging than after its fixation with PFA. In the case of live parasites, GAC exhibited a more accumulated signal in the apical region instead of only in the conoid region (Figure III-33D).

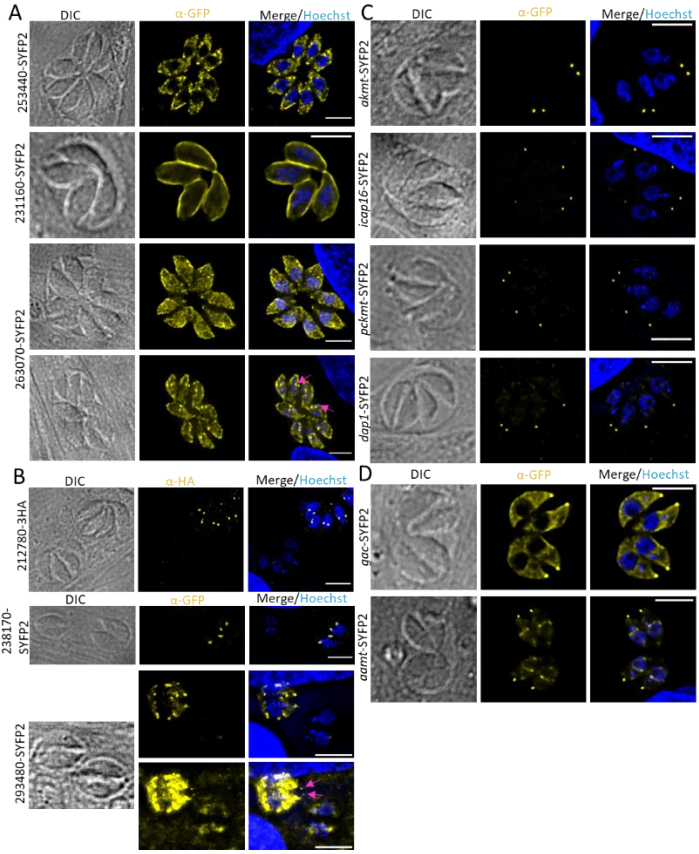

Figure III-31. Localisation of selected candidate proteins.

A) Candidate proteins showed non-conoidal localisations. Note: TGGT1_263070 showed accumulated signals close to the nucleus, indicated by purple arrows in some vacuoles. B) Candidate proteins with cell cycle–dependent signals. TGGT1_293480 in the bottom images is highly contrasted for better visualisation of the signal at the parasite apical tip, indicated by purple arrows. C) Proteins exclusively localised at the apex of parasites. D) Proteins not only localised at the apical tip but also in other cellular compartments. Scale bar: 5 µm.

Next, the fate of candidates with an apical localisation upon depletion of CGP was investigated since proteins apically localised are more

likely to interact directly with CGP. Thus, different C-terminally tagged proteins were generated in the *cgp* flox line (Table III-4, Figure III-26E and F). PCKMT, DAP1 and ICAP16 proteins emerged in the early endodyogeny before IMC1 appeared in daughter cells (Figure III-32A-C). Interestingly, PCKMT disappeared from the conoid in both mature and developing daughter cells upon deletion of CGP (Figure III-32A). Similarly, DAP1 failed to localise to the apical tip in mature cells when CGP was absent. However, this protein remained present in budding daughter cells (Figure III-32B).

Upon depletion of CGP, ICAP16 was only absent from the conoid in 43.6% of vacuoles (Figure III-32C and D). Examining closer the vacuoles that still had ICAP16 signal, 66% were forming daughter cells. In contrast, 100% of vacuoles without ICAP16 signal were not replicating, indicated by no emergence of daughter IMC1, although we cannot rule out the possibility that ICAP16 was also absent in daughter cells, which occurred before IMC1 emergence in them (Figure III-32E). Further experiments would be needed to elucidate the real function of ICAP16 at the conoid and potentially at the conoid assembly during cell division.

Regarding the other lysine methyltransferases that were found in the BioID assay, deletion of CGP did not result in changes in AKMT and AAMT apical localisations (Figure III-33A and B). Additionally, CGP remained at the conoid in the absence of AKMT (Table III-4, Figure III-26J, Figure III-33C).

Although GAC is not a significantly enriched hit in the *cgp*-TurboID experiment, whether depletion of CGP affects its distribution was analysed since GAC is reported to bind F-actin and is described as one of the crucial components for parasite gliding motility (Jacot et al. 2016). IFA showed that depletion of CGP did not cause a defect in GAC apical localisation (Figure III-33D). Although the intracellular localisation of AKMT, AAMT and GAC was unaffected in the absence of CGP, and since they change their localisation once they are extracellular, further investigating whether depletion of CGP affects their distribution in extracellular parasites would be worthwhile. However, this remains to be done in the future.

One cell cycle–dependent protein (TGGT1_212780) appeared as two dot signals that were closely associated with CGP in the forming daughter cells. Therefore, the fate of this protein upon KO of *cgp* was examined. Surprisingly, the localisation of this protein seemed unaffected, but high percentages of vacuoles displayed the morphology defects as revealed by GAP45 staining, whereas non-induced KO parasites barely had abnormal GAP45 staining (Figure III-33E). This is reminiscent of the similar phenotype observed in around 20% of the population of vacuoles resulting from *cgp* KO (Figure III-13), which is yet to be explained.

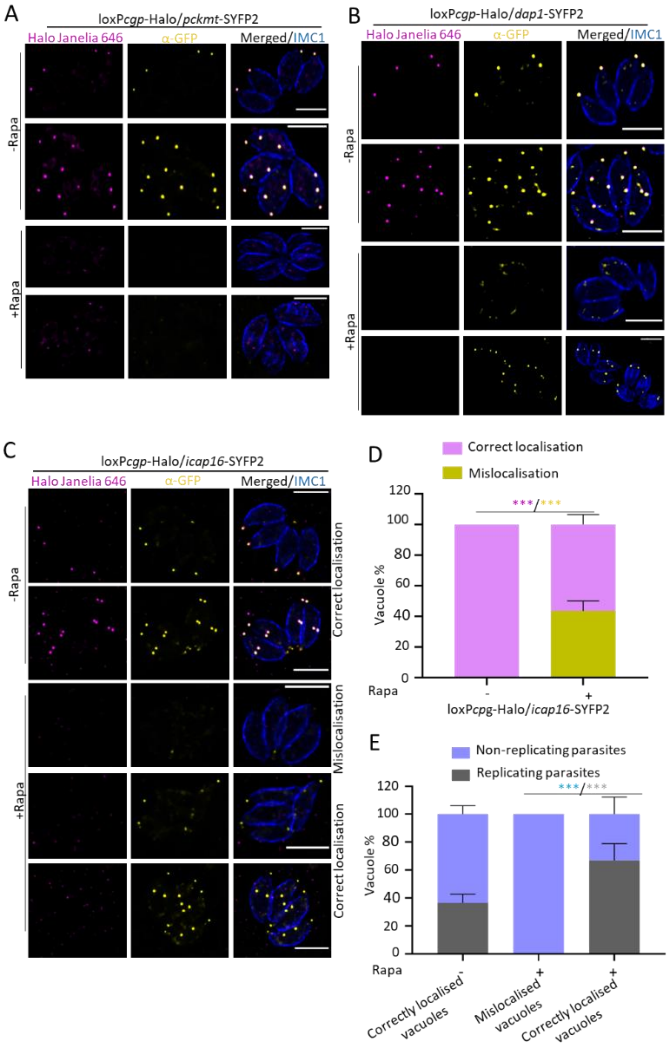

Figure III-32. CGP depletion affected PCKMT, DAP1 and ICAP16 localisation.

A) IFA depicting the absence of PCKMT in CGP-lacking parasites. B) IFA showing the absence of DAP1 in mature cells but not in daughter cells. C) Representative images

of non-mislocalised and mislocalised ICAP16 for treatment ± 50 nM rapamycin for 2 hours. Phenotypes were examined at 72 hours post induction. D) Quantification of (C). Only parasites lacking CGP were counted in the rapamycin-induced condition. E) Percentages of vacuoles containing replicating or non-replicating parasites. Note that in CGP-depleted vacuoles, ICAP16 mislocalised primarily in non-replicating cells, whereas it was still present in replicating parasites as shown in (C). Only parasites lacking CGP were counted in the rapamycin-induced condition. Data are presented as mean + SD. P-values were calculated by two-tailed unpaired Student's *t*-test. ns: non-significant; *p<0.05; **p< 0.01; ***p<0.001; ****p<0.0001. The colour of the asterisk represents the conditions analysed. Rapa: 50 nM rapamycin. Scale bar: 5 µm.

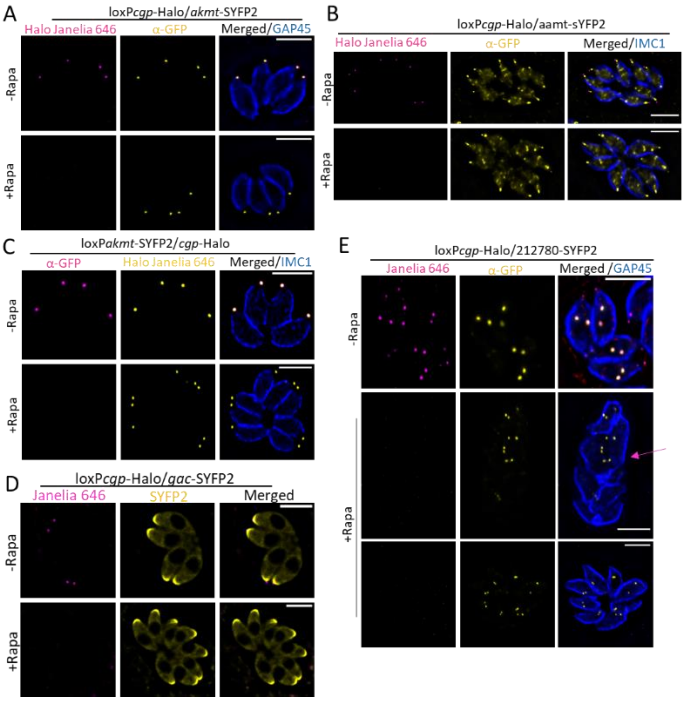

Figure III-33. Other candidate proteins were not affected by CGP depletion.

A) AKMT was unaffected in the absence of CGP. B) AAMT remained unchanged in CGP-depleted parasites. C) Depletion of AKMT, CGP apical localisation was also not impacted. D) GAC was not affected by CGP depletion by live imaging. E) Lack of CGP did not impact TGGT1_212780 localisation but caused defects in parasite morphology indicated by abnormal GAP45 staining (indicated by the arrow in magenta). Scale bar: 5 µm.

Confocal or STED images indicated that CGP colocalised with the other potential complex members: ICAP16, PCKMT, DAP1 and FRM1 (Figure III-27C, Figure III-34).

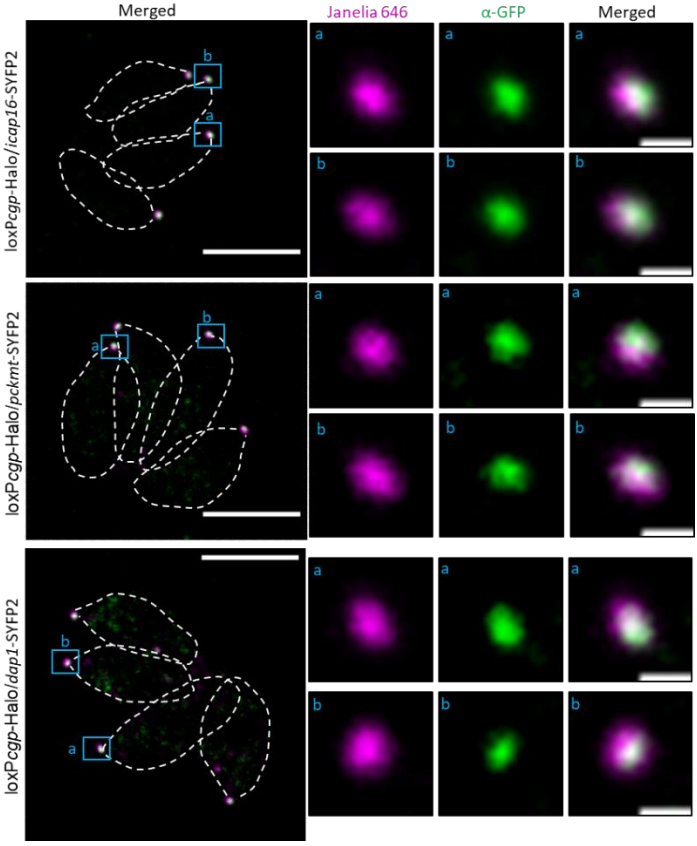

Figure III-34. Confocal images displaying CGP colocalisation with apical proteins that were affected when CGP was not present.

ICAP16, PCKMT and DAP1 showed overlapped signals with CGP. White dashed lines indicate parasite periphery. Scale bar: 5 µm for intracellular parasites, 0.5 µm for zoomed pictures.

Next, whether those apically localised proteins identified by BioID were affected upon depletion of FRM1 was tested. An FRM1 floxed line (loxP*frm1*-Halo) was generated in the DiCreΔ*ku80* background (Table III-4, Figure III-26G). PCKMT, DAP1, ICAP16, AKMT, AAMT and GAC in this strain were then C-terminally tagged (Table III-4, Figure III-26E and H). Upon induction of *frm1* KO, all of the tagged proteins remained localised at the conoid (Figure III-35A-F), indicating their localisation was independent of FRM1. Notably, FRM1 localisation was independent of AKMT since FRM1 signal remained in the conoid after depletion of AKMT (Table III-4, Figure III-26E, Figure III-35G).

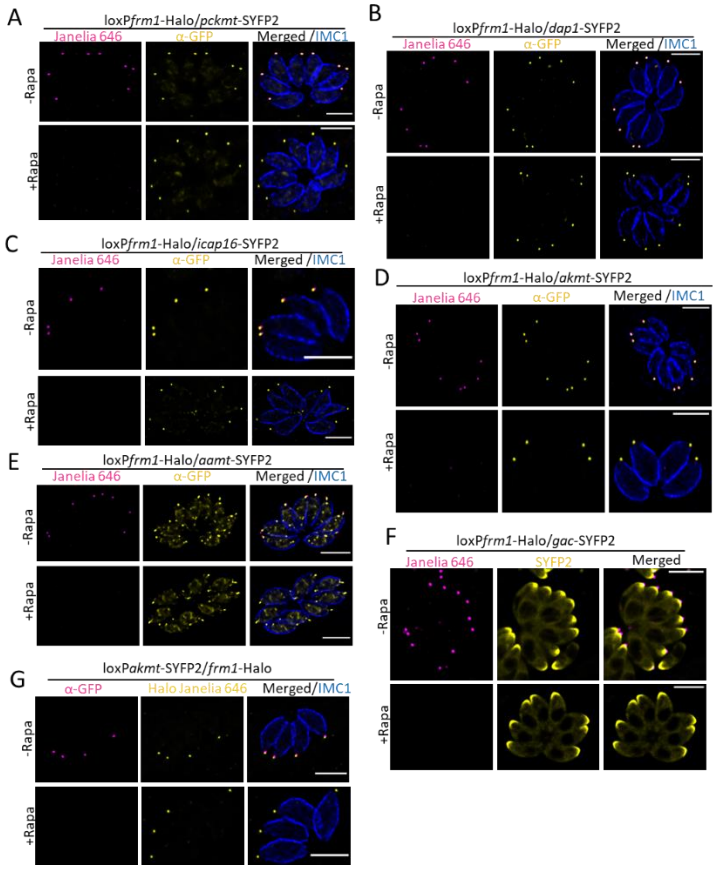

Figure III-35. Proteins (partially) localising at apical pole remained unaffected in the absence of FRM1.

A–C) Proteins that were affected by CGP depletion were unaffected by FRM1 depletion. PCKMT in (A), DAP1 in (B), ICAP16 in (C). D–E) Methyltransferase proteins remained unaffected by the loss of FRM1. AKMT in (D), AAMT in (E). F) Lack of FRM1 did not impact GAC apical localisation by live imaging. G) Depletion of AKMT did not cause FRM1 mislocalisation. Scale bar: 5 µm.

Dap1 were floxed, and the effect on other conoidal protein localisations were also analysed (Table III-4, Figure III-26I and J,

Figure III-36). IFA showed that in the absence of this protein, CGP and FRM1 were correctly positioned (Figure III-36A and B). Similar to FRM1 cKO parasites, ICAP16, PCKMT and AAMT localisation remained unchanged in DAP1-depleted parasites (Figure III-36C-E). Depletion of AKMT did not affect the localisation of DAP1 either (Table III-4, Figure III-26J, Figure III-36F).

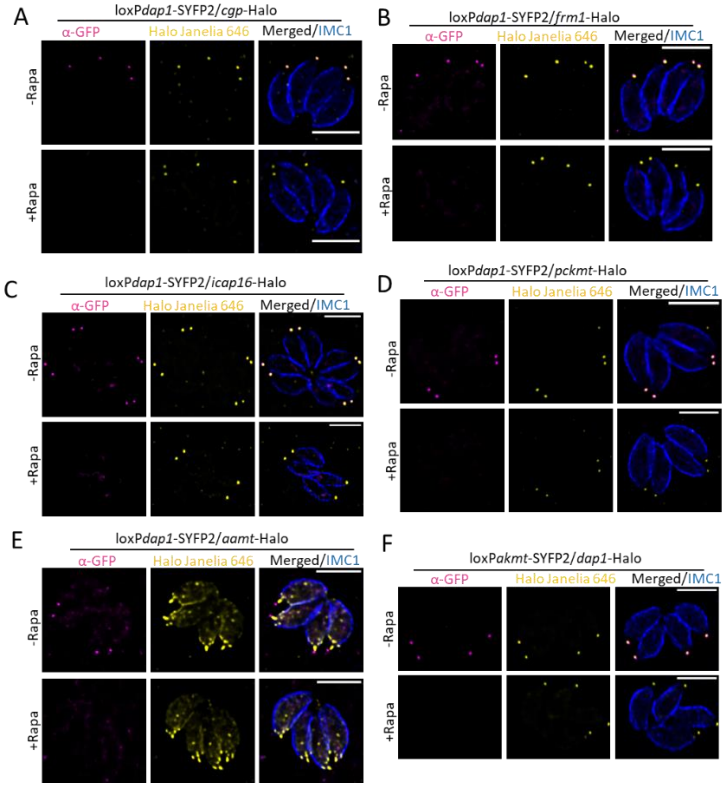

Figure III-36. Proteins (partially) localising at apical pole remain unaffected in the absence of DAP1.

A) CGP remained properly at the apical area. B–D) Proteins that were affected with depleted CGP, however, remained unaffected with the loss of DAP1. FRM1 in (B), ICAP16 in (C), PCKMT in (D). E) AAMT remained unaffected by the loss of DAP1. F) DAP1 localisation was independent of AKMT. Scale bar: 5 µm.

Lastly, the importance of DAP1 protein in the parasite's growth was assessed by carrying out a plaque assay. Without this protein, the parasites were capable of forming similar plaques to non-rapamycin-treated parasites (Figure III-37). Therefore, DAP1 is not critical for parasite survival.

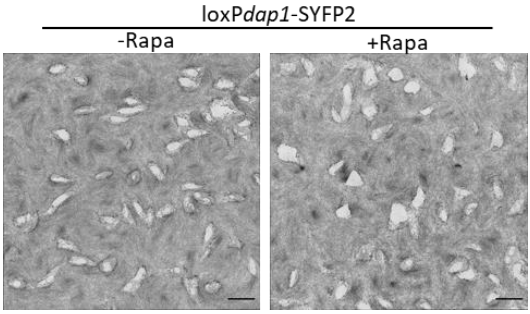

Figure III-37. Plaque assay indicates DAP1 is dispensable to parasite lytic cycle.

Parasites were grown in different conditions (± 50 nM rapamycin) and fixed after 6 days post infection. Scale bar: 1.5 mm. Rapa: 50 nM rapamycin.

IV. DISCUSSION

1. sCas9 is a powerful tool for phenotypic screens

The possibility to block parasite egress is a valid intervention strategy to control parasite dissemination and may lead the way to novel treatment strategies. Additionally, recent studies have revealed some novel players involved in the signalling cascade leading to host cell egress by the parasite, shedding some light on the involved mechanisms (Bisio et al. 2019). Uncertainty remains on some aspects of the egress process.

Since ~40% of genes in this organism are annotated as hypothetical, novel apicomplexan-specific genes may be involved in this process in *T. gondii*. To find proteins closely involved in egress, our lab carried out a phenotypic screen based on a newly established sCas9 system (Li et al. 2022). Around 7% of the clones exhibited a possible delay or block in egress. A second, more rigorous, examination, found 10 candidate genes that are involved in natural egress, and four genes displayed a delay in egress when induced with Ci A23187: ND6, radical S-adenosylmethionine (rSAM) domain–containing protein (TGGT1 252465), SLF and CGP.

Although I only focused on the detailed characterisation of two candidates, ND6 and TGGT1 252465 are also interesting genes that we identified in this screen and are briefly summarised here.

TgND6 was recently described as part of the rhoptry secretion system, revealing a role in parasite invasion (Aquilini et al. 2021). In the present research, ND6 also presented a decreased egress rate when

stimulated by Ci A23187 for 5 minutes. However, when Aquilini et al. (2021) knocked down the protein using the AID approach, parasites could still egress after 8 minutes of induction with Ci A23187, similarly to non-induced parasites. This discrepancy may be explained by the fact that ND6 was not degraded completely by the AID system and background levels (not detectable by IFA or WB) were sufficient to ensure parasite egress. In line with what they found, our research shows that ND6 is also important for parasite invasion.

The radical S-adenosylmethionine (rSAM) domain–containing protein (TGGT1 252465) presented an egress defect, probably due to a severe replication phenotype. rSAM family enzymes are capable of catalysing methylation reactions on other molecules such as proteins, lipids, DNA and RNA (Fujimori 2013, Padgett et al. 2018). Therefore, methylation affects a variety of subsequent biological processes. In *Toxoplasma*, two proteins of the rSAM superfamily are found on the outer mitochondrial membrane: elongator protein-3 (Elp3) and rRNA large subunit methyltransferase gene N (RlmN). Overexpression of either protein results in a substantial parasite replication deficiency (Padgett, Lentini et al. 2018). Similarly, TGGT1 252465 seems to be involved in parasite replication since parasites remained in the 2–8-stage vacuoles in a 24-hour replication.

The successful identification of novel egress factors via our sCas9 phenotypic screen demonstrates that sCas9 is a powerful tool for identifying genes involved in a particular process and for the analysis of gene functions. The screen acts directly on the DNA level, and the kinetics of protein depletion is presumably comparable to those of the

DiCre and TET systems but significantly slower than the AID system. The advantage of the sCas9-based screen is that, in principle, all genes can be targeted and conditionally disrupted without no background expression, including those where the corresponding protein has no access to the degradation machinery, such as secreted proteins or proteins residing in the organelles. Additionally, the existing gRNA library can be directly employed for functional screens. sCas9 can also be used for genome-wide dropout screens, and the advantage is that gene disruption can be temporally controlled (time course analysis of dropout). However, one of its pitfalls is that Cas9 activity causes DNA damage in a percentage of the population, making clearly interpreting nuclear and replication phenotypes difficult without further downstream analysis (Li et al., 2022). Recently, a high-throughput (HiT) CRSPR-mediated tagging method was established, which endogenously tags protein kinases with a minimal AID and fluorophore (Smith et al. 2022). On this basis, protein localisation can also be seen using fluorescent markers, POI expression is controlled by IAA, and phenotypic analysis may be conducted with minimal effort (Smith et al. 2022). By labelling and downregulating the *T. gondii* kinome, the researchers identified kinases involved in a range of activities, proving the efficiency of the approach. As with any other technology, the mAID-based screening approach offers both benefits and drawbacks. This novel method allows for the direct localisation, rapid regulation and temporal control of POI, but partial or inefficient protein knock-down is possible due to the inaccessibility of the targeted protein to the degradation machinery and the inability to functionally tag some proteins. Nevertheless, these phenotypic

screens are highly complementary and a great advance in the field that will improve the data obtained by other genome-wide screens (Sidik et al., 2016) where the function of the individual genes could not be inferred.

2. SLF and CGP act on different steps in the egress

Important cellular components for sensing signals, microneme secretion and initiating motility, which are critical for escape and invasion of host cells, are often located in the apical region of the parasite (see sections 2.2.3 and 3.3). Both proteins found in the sCas9 screen, SLF and CGP, are localised in this region and involved in egress and invasion. SLF also displays a localisation in the intravacuolar network that may be used for communication of the parasites inside the vacuoles to coordinate synchronised egress (Periz et al., 2017).

Although the genes were readily identified in the sCas9 screen, the DiCre system was used to validate the results since it allowed a complete excision of the gene, and parasites that failed to excise the gene could be excluded because each was endogenously tagged (Andenmatten et al. 2013). A 100% KO efficiency was not achieved in either *cgp* or *slf* floxed parasite lines, which might be due to their long gene sequences (*cgp*: 25,738 bp and *slf*: 11,200 bp). Longer distances between loxP sequences reduce the efficiency of Cre recombinase-mediated recombination, making it more difficult to excise floxed DNA (Zheng et al. 2000, Coppoolse et al. 2005). However, the phenotype of these two candidates were further explored.

2.1 SLF and CGP acting upstream and downstream of egress signalling cascade

Prior research has shown that SLF is dispensable for parasite growth (Bisio et al. 2019). The authors tagged SLF with AID to degrade the protein using IAA. Since overall parasite growth, as determined by plaque assays, was not affected upon the addition of IAA, which should lead to degradation of SLF, they concluded that SLF is not required for the parasite lytic cycle (Bisio et al. 2019). In contrast, using the sCas9 and DiCre systems resulted in an identical phenotype upon disruption or removal of *slf*. I suspect that SLF was not efficiently degraded using the AID system, probably due to the inaccessibility of the protein to the proteasome. This could be due to the AID domain being situated within the GC signalling complex or, since SLF is a transmembrane protein, the C-terminus domain could be in the extracellular portion of the plasma membrane and therefore not accessible to the proteasome. Hence, protein degradation may not be adequate to determine a phenotype for proteins such as SLF (Armstrong et al. 2007, Brown et al. 2018). In contrast, the DiCre system allows the total excision of the gene of interest, and it was verified that SLF is essential for parasite growth. This is consistent with a strong negative phenotypic score (Sidik et al. 2016). In the *slf*-cKO, invasion, gliding and egress were demonstrated considerably blocked. Furthermore, plaques were barely observed in the growth assay, and the failure to isolate a *slf*-KO clone further supports that SLF is essential for parasite survival. Similar to SLF, isolating a *cgp* cKO clone was failed, and phenotypic assays (invasion, gliding and egress assays) further highlight its essentiality.

In the past, egress has been divided into several steps: signalling to start egress, disassembly of intravacuolar filaments and initiation of motility. We observed that SLF was required for initiation of the signalling cascade, whereas CGP was not. The use of distinct egress inducers led to different behaviours in SLF-depleted parasites but did not affect CGP-depleted parasites. For *slf* cKO parasites, the treatment of Ci A23187 partly rescued the phenotype, where the parasites exhibited a complete block in egress, invasion, motility, microneme secretion and PVM rupture. These findings suggest that SLF acts directly downstream of the signal stimulation of the signalling cascade. In the case of CGP, all steps until initiation of motility appeared to be normal since the IVN was fully disassembled and the PVM lysed. However, egress was blocked since the initiation of motility failed, placing CGP downstream of the signalling cascade.

Notably, when propranolol, an inhibitor of PA phosphatase and positioned downstream of the Ca^{2+} signalling cascade, is applied, the egress defect is comparable to BIPPO induction rather than being rescued in *slf* cKO parasites, which is similar to GC KD parasites (Bisio et al. 2019). It has been claimed that GC directly or indirectly affects PA synthesis, which stimulates microneme secretion detected by APH on the microneme surface. In the GC-KD, PA production decreased significantly (Yang et al. 2019). Therefore, depletion of SLF may affect PA production due to mislocalised GC (see below section 3) and other components, resulting in a block in microneme secretion defect that cannot be bypassed by propranolol because of the low production of PA and thus no rescue of egress. We also discovered

that propranolol caused a noticeable rounding of *slf* cKO parasites, which was not seen in wildtype parasites or *cgp* cKO parasites. This may indicate an osmolarity alteration after propranolol induction, probably due to interference with another unknown signalling pathway involving the GC signalling complex, which is only activated during the egress process. However, further experiments are required to test this hypothesis.

2.2 Posterior accumulation of F-actin is lost in the absence of CGP, whereas no changes in F-actin dynamics occur in the absence of SLF

In this work, CbEm was introduced to examine the dynamics of F-actin in SLF and CGP conditional KO mutants during egress. Similar to what has been reported before, time-lapsed video revealed that F-actin disintegrated, motility initiated and parasites escaped the host cell (Periz et al. 2017). Upon induction with BIPPO, the F-actin network remained intact only in *slf* cKO mutants, again indicating that SLF is an early actor in the signalling cascade, whereas CGP acts downstream in the egress signalling cascade (Figure IV-1). Even though *cgp* cKO can disassemble the filaments connecting the parasites, they remained trapped in the cell. This suggests that CGP has a role in motility initiation, potentially due to defects in F-actin polymerisation at the apical tip of the parasite. During the egress of WT parasites, the F-actin signal in the actin polymerisation centres at the Golgi and apicoplast area was significantly decreased, indicating a reduction or turn-off of FRM2 activity that resides close to the Golgi complex. In *cgp* cKO parasites, reduced signal at the Golgi and apicoplast area occurs as for WT parasites, indicating that FRM2

activity regulation is independent of motility initiation. In addition, we detected a notable increase in posterior F-actin signal in WT parasites, whereas no posterior F-actin was detected in CGP-depleted parasites. The lack of F-actin accumulation in the basal pole might be a consequence of FRM1-dependent actin apical-basal flow, as described in earlier studies (Stortz et al. 2019, Tosetti et al. 2019). Indeed, our subsequent experiments demonstrated that FRM1 was missing from the apical tip in CGP-depleted parasites. However, whether FRM1 is degraded or just mislocalised remains unclear. Since FRM1 expression is low, instead of being degraded, FRM1 likely has a distributed pattern within the parasite cytosol, resulting in no detectable FRM1 signal through IFA. To address this point, further studies comparing the expression levels of FRM1 in *cgp* cKO and WT strains will be needed.

In contrast to *cgp* cKO parasites, SLF-deficient parasites induced by BIPPO for egress exhibited no posterior actin accumulation and no reduction of signal in the Golgi and apicoplast area, indicating no change in FRM1 or FRM2 activity. Since SLF is a critical component of the GC signalling complex, it is reasonable that SLF-absent parasites are incapable of detecting signals required for the initiation of egress. Upon Ci A23187 induction that bypasses the signalling transduced by the GC signalling complex, F-actin depolymerisation and posterior accumulation still occurred in most *slf* cKO parasites, despite impaired microneme secretion ability, indicating that F-actin depolymerisation could also be triggered in a separate signalling pathway that operates independently to microneme secretion.

Similarly, apico-basal F-actin flux is not affected in transporter facilitator protein (TFP1)-depleted parasites, which abolishes microneme secretion (Hammoudi et al. 2018, Tosetti et al. 2019).

Previous research has shown that in the presence of BIPPO, extracellular parasites exhibit an apical-basal flow, resulting in posterior F-actin accumulation. This suggests that cGMP signalling is responsible for F-actin flux (Del Rosario et al. 2019, Tosetti et al. 2019). Similar to these findings, we observed that following BIPPO treatment, an accumulation of F-actin signal occurred at the basal pole of WT parasites. When *slf* is depleted, no change occurs in the F-actin network, which may be explained by the low concentration of cGMP since deletion of SLF results in the mislocalisation of GC, whose function is the generation of cGMP (Bisio et al. 2019). Previous research indicates that Ca^{2+} signalling also regulates F-actin flow (Del Rosario et al. 2019, Tosetti et al. 2019). We found that Ci A23187 caused F-actin disassembly and a strong posterior F-actin accumulation even before gliding was initiated, indicating that Ca^{2+} signalling regulates F-actin dynamics.

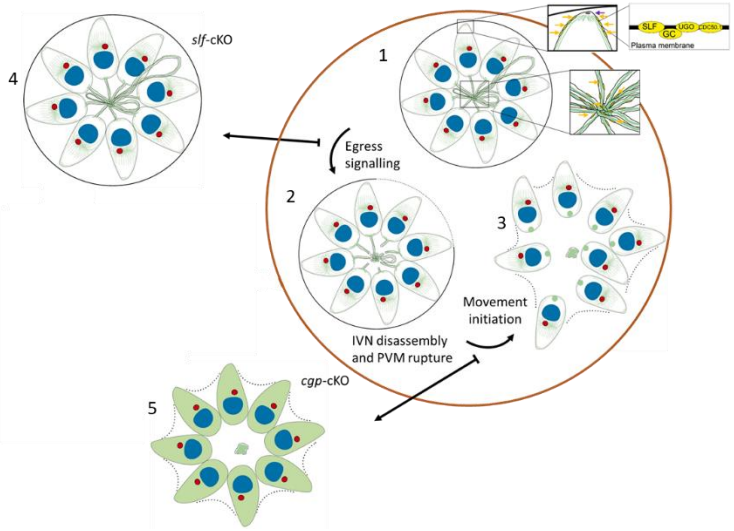

Figure IV-1. Block of egress is associated with the disassembly of the F-actin in CGP- and SLF-lacking parasites.

1–3) Egress steps in WT parasites. 1) The GC signalling complex consisting of GC, CDC50.1, UGO and SLF, which is localised at the apical tip and IVN on the plasma membrane, is responsible for initiating the egress signalling cascade. Magnified boxes: The location of the components of the signalling platform at the apical tip and RB are indicated by yellow arrows. The location of CGP in the parasite's conoid is indicated by the purple arrow. 2) Disassembly of the IVN and lysis of the PVM. 3) Accumulation of F-actin at the parasite's basal pole and initiation of gliding motility. 4) Without SLF, components of the signalling platform mislocalise, resulting in an early egress block. No IVN disintegration or PVM lysis occurs. 5) Absence of CGP leads to a late egress block. Disintegration of the IVN and lysis of the PVM occur, but F-actin cannot relocate to the basal pole, and motility is not initiated. Image from (Li et al. 2022).

3. SLF forms a complex with GC signalling complex, and its substrate remains unknown

At the last step of endodyogeny, the daughter cells hatch out from the mother, inheriting the plasma membrane, which occurs after IMC formation; mitochondria enter daughter cells; and daughter cells mature from mother cells (Anderson-White et al. 2012, Gubbels et al.

2020). Since SLF localisation at the apical cap area was not observed in forming daughter cells, only on mature parasites, SLF is probably a plasma membrane protein. Co-localisation analysis of SAG1 and GC provides further evidence that SLF resides on the plasma membrane.

In this study, we discovered that SLF is also a component of the GC signalling complex, which is consistent with a previous report that identified SLF as a significant hit in a GC co-immunoprecipitation experiment (Bisio et al. 2019). We demonstrated that SLF colocalises with other components of the GC signalling complex and that depletion of SLF leads to the mislocalisation of these other components. Similarly, the depletion of one of the components of GC/CDC50.1/UGO results in the entire or partial sequestration of SLF in the secretory pathway, most likely in the ER compartment. However, microneme and rhoptry proteins display normal localisations, indicating that they are successfully transported to their destinations. These findings suggest that the trafficking of the GC/CDC50.1/UGO/SLF complex depends on the presence of all its components during the transport through the secretory pathway. Consistent with this, GC was mislocalised in the secretory route in parasites lacking CDC50.1 or UGO, whereas micronemes and rhoptry protein were not impacted (Bisio et al. 2019). These results may suggest a quality control system for trafficking of the GC signalling complex that must be assembled at the very early start of transport (in the ER). This is similar to some microneme complexes, such as MIC1/4/6 (Reiss et al. 2001), that need to be fully assembled during their transport through the secretory system of the parasite.

DISCUSSION

Neurotransmitter transporters were classified into two types. One is vesicular neurotransmitter transporters, responsible for packing synaptic vesicles with neurotransmitters, and the other is plasma membrane neurotransmitter transporters, which function at the plasma membrane (Borowsky et al. 1995, Fei et al. 2008). Two families of plasma membrane neurotransmitter transporters, Na^+/Cl^- dependent neurotransmitter transporters and glutamate transporters, are present in mammalian cells and are structurally and mechanistically different (Amara et al. 1993, Borowsky et al. 1995). The glutamate transporters are Na^+-dependent transporters with 8–10 transmembrane domains. In Na^+/Cl^--dependent neurotransmitter transporters, the majority co-transport Na^+ and Cl^- to transport neurotransmitter molecules against their concentration gradient into the cell (Shi et al. 2008). Proteins in this family have a similar structure of 12 presumable transmembrane helices and comprise transporters such as the GABA transporter (Pramod et al. 2013). SLF is annotated as having an SNF-like domain and belonging to the sodium: neurotransmitter symporter family. Additionally, SLF has 12 transmembrane domains. We thus hypothesised that SLF may be a symporter protein.

GABA is one of the substrates of neurotransmitter symporters. GABA and GABA signalling are ubiquitously present in mammalian cells, plants and even prokaryotes (Bouché et al. 2003, Ramesh et al. 2017). *T. gondii* can metabolise and synthesise GABA (MacRae et al. 2012). Therefore, I hypothesised that GABA may be a possible substrate of SLF and serve as an egress signal, with the activation of the GABA signalling cascade resulting in parasite egress when the level of

GABA is over the threshold. However, our plaque assay supplemented with different concentrations of GABA could not rescue the SLF depletion phenotype. This indicates that it is unlikely that SLF is a GABA transporter, although we cannot rule out the possibility that SLF is the sole GABA transporter found in *Toxoplasma* and that GABA cannot thus rescue the SLF depletion phenotype. Indeed, searching in the database, we found a paralog of SLF in *Toxoplasma* (TGGT1_208410) that also contains a putative SNF-like domain with a negative phenotypic score (-0.88), indicating that this paralog protein could potentially function as a GABA transporter synergistically with SLF. Overall, SLF is not likely to be a GABA transporter. The substrates of this protein are still unknown. One approach to find the substrate would be to heterologously express SLF protein in *Xenopus laevis* oocytes, incubate it with radiolabelled components (amino acids, ions, etc.) and then monitor the amount of radioactivity in the oocytes (Rajendran et al. 2017). Additionally, several questions remain unanswered regarding the GC complex, such as how exactly the components of the complex interact with each other and their individual roles within the complex. Based on the results presented here, only the structural role of SLF for the assembly and transport of the whole GC complex was demonstrated, and whether SLF plays a more direct role in signalling remains to be seen.

4. CGP forms a potential complex with other proteins at the preconoidal rings

Our STED images show that CGP has a preconoidal ring localisation and colocalises well with FRM1, a protein localising at PCRs,

revealed by expansion microscopy (Dos Santos Pacheco et al. 2022). CGP has a TPR-like domain, which is a structural motif for mediating protein–protein interaction and often the assembly of multiprotein complexes (Das et al. 1998). Interestingly, FRM1 also possesses two TPR domains (Stortz et al. 2019), and depletion of CGP leads to the mislocalisation of FRM1 at the mature apical tip. These results suggest that both proteins form a complex at the PCRs. Notably, FRM1 and CGP are not among the top hits in the *cgp*-TurboID and *frm1*-TurboID assays based on proximity labelling. This may be because FRM1 and CGP are relatively lowly expressed proteins, as shown by RNA-seq transcription and ribosome profiling data (Hassan et al. 2017). However, proximity labelling uncovers a list of proteins that may interact with CGP and FRM1. Altogether, this study also demonstrates that BioID is a reliable tool for identifying possible interactors, particularly for large and poorly expressed proteins that are difficult to detect using conventional co-immunoprecipitation assays.

Recent literature suggests that GAC, AKMT and FRM1 serve as a platform for actin polymerisation and glideosome assembly for motility (Dos Santos Pacheco et al. 2022). Given CGP involvement in motility and localisation at PCRs, I hypothesised that CGP, AKMT, GAC and FRM1 must be coupled to carry out their roles in gliding motility. However, neither *cgp* nor *frm1* cKO affected the localisation of GAC and AKMT in intracellular parasites. In addition, AKMT depletion did not affect the apical localisation of CGP or FRM1. This suggests that GAC and AKMT do not interact directly with CGP to

achieve gliding motility and potentially act downstream of CGP/FRM1. Given that after egress and motility activation, AKMT and GAC localisation changes, it is worthwhile to investigate in extracellular parasites whether depletion of CGP and FRM1 affects their relocalisation ability.

How GAC, FRM1, AKMT, CGP and other proteins coordinate parasite movement is uncertain. A newly proposed model described GAC, AKMT and FRM1 as important key players in motility initiation in *T. gondii* (Dos Santos Pacheco et al. 2022). During extrusion of the conoid, powered by MyoH, a space is created and allows F-actin, polymerised by FRM1 at the PCRs, to be pushed into the pellicle compartment, where it is translocated by MyoH and MyoA. This drives the translocation of adhesions (micronemal proteins) that are connected to actin by GAC, which results in parasite movement (Dos Santos Pacheco et al. 2022). AKMT seems to contribute to the accumulation of GAC at PCRs. Combined with our finding, CGP might provide a structure for anchoring FRM1 at the PCRs to fulfil their function for the initiation of motility.

Interestingly, one methyltransferase, PCKMT, was shown to be absent in parasites lacking CGP. Similar to CGP, PCKMT is crucial to the parasite lytic cycle and is involved in motility, invasion and egress (Jimenez-Ruiz et al. unpublished data). The depletion of PCKMT also causes mislocalisation of FRM1 in mature cells but not in daughter cells, identical to *cgp* cKO parasites. It is also significantly enriched in both *cgp*-TurboID and *frm1*-TurboID bioID assays. Additionally, PCKMT has a TPR domain. Hence, it is highly probable that CGP,

FRM1, and PCKMT form a complex through their TPR domains. Similar to FRM1 depletion, PCKMT depletion does not affect CGP localisation (Jimenez-Ruiz et al. unpublished data), which further indicates that CGP might provide the structural basis for this complex. PCKMT also possesses the ankyrin repeat and SET domains. Whether these domains are essential for PCKMT activities and what roles they play in motility are yet unknown. Recent research indicates that proteins on PCRs are highly methylated (Dos Santos Pacheco et al. 2022). Our group is currently investigating the activity of PCKMT as a SET methyltransferase and the potential substrates of this protein.

DAP1 is another potential member of this protein complex (CGP/FRM1/PCKMT/DAP1) at PCRs. The deletion of CGP results in the absence of this protein at the apical tip while it is independent of the presence of FRM1. However, this protein is dispensable in the lytic cycle. This result is consistent with the depletion of DAP1; its absence did not affect any essential conoidal proteins investigated in this study, such as CGP, FRM1 or PCKMT. DAP1 has an RNI domain. A mammalian protein containing an RNI domain is cytoplasmic and could bind to pancreatic-type ribonucleases to prevent their activity (Shapiro 2001). However, the function of DAP1 remains unclear. Since it is non-essential, it might act as an accessory protein in this complex for gliding motility.

ICAP16 is conserved in Apicomplexa and possesses a PH domain that is known to bind phosphoinositide in cell membranes (Yao et al. 1994, Cullen et al. 2001). Through these interactions, PH domains play a role in recruiting proteins to different membranes, and some PH

domains are implicated in the regulation of other domains' activities (Lemmon et al. 2002). Previous reports have indicated the essentiality of ICAP16 in parasite growth and its role in invasion but without further functional characterisation. In our study, the depletion of CGP resulted in a partial mislocalisation of ICAP16, whereas in the FRM1 or PCKMT cKOs, ICAP16 remained unaffected. Thus, ICAP16 also might act as another accessory protein that is present in this complex. However, whether ICAP16 is essential for recruiting FRM1, CGP, PCKMT and DAP1 to the conoid is unknown and remains to be investigated in future studies.

Although our findings suggest that CGP, FRM1, PCKMT, ICAP16 and DAP1 form a complex at the PCRs that I have called the gliding initiation complex (GIC), one might argue that the observed phenotypes in the *cgp* cKO parasites, i.e. the loss of FRM1, PCKMT, DAP1 and ICAP16, might be due to CGP depletion or impaired PCRs. The latter is less likely. However, to determine whether the PCRs are affected, I would mark them by co-tagging the recently discovered structural proteins Pcr4 and Pcr5 (Dos Santos Pacheco et al. 2022). Since depletion of Pcr4 or Pcr5 resulted in the loss of PCRs, which causes the loss of AKMT and GAC at the PCR region, it is possible that in Pcr4- or Pcr5-depleted parasites, the GIC will also be lost, and thus the initiation of motility is lost. In addition, in our study, GAC and AKMT remained present at the apical area, acting downstream of the initiation of motility, as we suspected. The depletion of the alveolin network proteins AC9 and AC10 causes the loss of conoid, which occurs during the late stages of cell division. Thus, conoid

resident proteins that appear early in the endodyogeny are not detectable at the apical conoid region in mature parasites; however, they are still present in daughter cells. In contrast, late-appearing conoid proteins are lacking in both mother and daughter cells (Tosetti et al. 2020). In our case, the proper localisation of MyoH and RNG2 ruled out the possibility of conoid loss. Additionally, proteins in this complex, some were lost in both mature and daughter cells, and some were only lost in mature cells, indicating intact PCRs, since those proteins appeared in the early endodyogeny. Therefore, we concluded that the likelihood of PCRs being affected by deletion of CGP was small. To corroborate this notion, however, additional TEM comparison of PCRs in *cgp* cKO and WT should be performed. Additionally, even if the depletion of CGP affected PCRs, this would not rule out the formation of a complex. AlphaFold and other computational techniques may also be used to estimate their interaction, although no structural information on these proteins in *T. gondii* was found in the AlphaFold Protein Structure Database. Collectively, our data strongly imply that CGP, FRM1, PCKMT, ICAP16 and DAP1 form a large complex at the PCRs that is essential for parasite gliding motility, and within the complex, CGP, FRM1 and PCKMT are essential components for motility, whereas ICAP16 and DAP1 are accessory components (Figure IV-2).

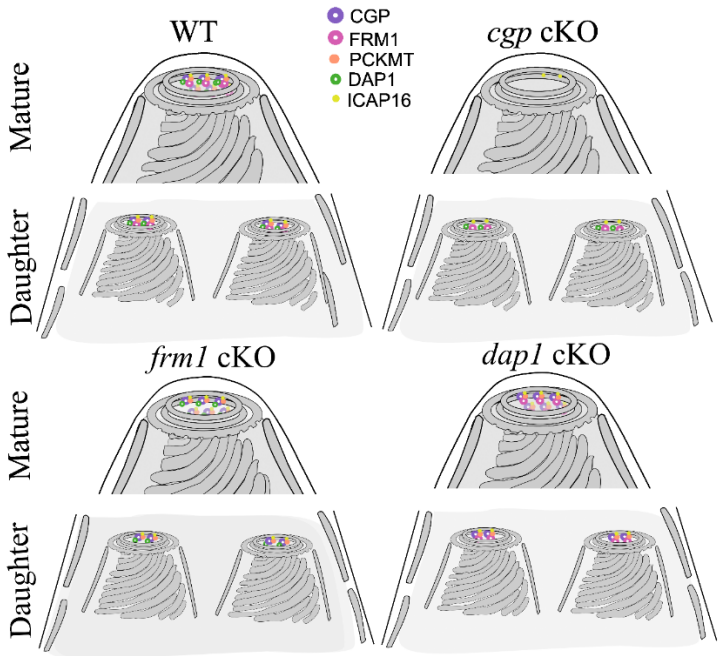

Figure IV-2. Potential protein complex involving CGP at the PCRs is important for the parasite lytic cycle.

Based on our results, CGP, FRM1, PCKMT, ICAP16 and DAP1 likely form a complex (GIC) at the PCRs. CGP, FRM1 and PCKMT are core components, whereas ICAP16 and DAP1 might be accessory proteins in this complex.

Apart from GIC, several other components affecting gliding motility or conoid stability, such as Pcr2, Pcr4, Pcr5 and Pcr6, have been identified in independent studies (Dos Santos Pacheco et al. 2022, Lopez et al. 2022). However, the coordination and integration of all these complexes remain unclear and require further studies. My work indicated that GIC appears to have no effect on conoid stability and formation, but it is required to be present at the conoid to initiate gliding motility via the function of FRM1 and potentially PCKMT.

5. Investigation of CGP and SLF in other Apicomplexa parasites

Given that both CGP and SLF are conserved in *Plasmodium* spp., investigating their homologs in this pathogen is worthwhile since they might serve as effective drug targets. With a phenotypic score of -2.87, the homolog of SLF in *P. falciparum* (PF3D7_0209600) annotated as a putative transporter is likewise predicted to be essential. Go Term analysis indicates that this homolog has the same function as SLF, suggesting possible functional conservation. In addition, transcription data indicated that its expression level rose significantly throughout the late trophozoite and schizont stages, suggesting a possible involvement in controlling schizont egress during the asexual blood stage (Otto et al. 2010). The homolog of CGP (PF3D7_1313600) is also found in *P. falciparum*, with a predicted negative phenotypic score (-0.53) and the same Clu domain and TPR-like domain as CGP. Furthermore, transcriptional data indicated that its expression is significantly elevated in late trophozoite and schizonts stages (Otto et al. 2010). Therefore, this protein in *P. falciparum* is likely involved in schizont egress. Future research on the homolog proteins in *P. falciparum* is worthwhile for malaria control; I tried and fail to obtain inducible Pf*slf* parasites.

V. SUMMARY

Characterisation of two essential proteins for host cell egress and invasion identified by phenotypic screening in *Toxoplasma gondii*

The apicomplexan parasite *T. gondii* is an obligate intracellular parasite that can infect almost all warm-blooded animals, including humans. Egress from host cells is the prerequisite for its dissemination. However, the exact steps that lead to egress are still poorly understood. During replication, the parasites establish an intravacuolar F-actin network that connects individual parasites and is essential for synchronous replication and material exchange between parasites. During egress, this network rapidly disintegrates before parasite motility and egress are activated, indicating a tight regulation of F-actin disassembly and activation of the motility machinery for egress.

To identify novel factors involved in this regulation, a pooled gRNA library, which targets 320 genes predicted to be fitness-conferring according to a recent genome-wide *in vitro* screen, was transfected into a parasite line that expresses a regulatable Cas9 (sCas9). We successfully identified genes required for egress during the asexual life cycle. Further characterisation of two of these candidates indicated that they are essential for invasion and egress from host cells and that they act at distinct time points during this process. The signalling linking factor (SLF), an essential component of the guanylate cyclase (GC) signalling complex, is essential for the early induction of egress, acting upstream of Ca^{2+} signalling. The depletion of SLF led to no changes in F-actin upon induction with BIPPO. Whether SLF acts as a symporter is still uncertain. In contrast, the new conoidal protein

named conoid gliding protein (CGP) acts at a later step in egress, downstream of Ca^{2+} signalling, and is necessary for the activation of gliding motility. Upon egress induction, F-actin networks disassemble but without F-actin accumulation at the basal pole. Furthermore, CGP might form a complex at the preconoidal rings, revealed by proximity-dependent biotin identification (BioID). Within this complex, here named gliding initiation complex (GIC), a novel methyltransferase (PCKMT), an actin nucleator formin1 (FRM1) and CGP are the core components. Dispensable protein 1 (DAP1) and indispensable conserved apicomplexan protein 16 (ICAP16) might serve as accessory proteins.

Collectively, this study revealed that SLF and CGP are crucial for the lytic cycle of parasites, and their role in egress broadens our understanding of the egress mechanism. The discovery of a new preconoidal complex incorporating CGP lays a foundation for future mechanistic research establishing their specific function in motility.

VI. ZUSAMMENFASSUNG

Charakterisierung zweier für die Invasion und Reinvasion essentieller Proteine für den Austritt und die Invasion von Wirtszellen, identifiziert durch phänotypisches Screening in *Toxoplasma gondii*

T. gondii gehört zum Stamm der Apicomplexa und ist ein obligat intrazellulärer Parasit, der fast alle warmblütigen Tiere einschließlich des Menschen infizieren kann. Der Austritt aus der Wirtszelle ist die Voraussetzung für die Verbreitung dieses Parasiten. Die genauen Faktoren, die zum Austritt aus der Wirtszelle führen, sind jedoch noch kaum bekannt. Während der intrazellulären Replikation baut *T. gondii* ein intravakuoläres F-Aktin-Netzwerk auf, das die Parasiten in der parasitophoren Vakuole miteinander verbindet und für die synchrone Replikation sowie den Materialaustausch zwischen den einzelnen Parasiten unerlässlich ist. Kurz bevor die Parasiten die Wirtszelle aktiv verlassen, zerfällt dieses Aktin-basierte Netzwerk zwischen den einzelnen Parasiten. Anschließend bewegt sich der Parasit aktiv aus der Zelle, wobei diese Motilität auf der Polymerisation von F-Aktin beruht. Diese streng orchestrierte Regulierung von F-Aktin sowohl in der parasitophoren Vakuole als auch im Parasiten selbst, weist darauf hin, dass Aktin eine zentrale Rolle beim Austritt aus der Wirtszelle spielt.

Um neue Faktoren zu identifizieren, die an dieser Regulation beteiligt sind, wurde eine gRNA-Bibliothek erstellt. Diese zielt auf insgesamt 320 Gene ab, welche laut einem kürzlich durchgeführten genomweiten *in vitro*-Screen als essentielle Gene indetifiziert wurden.

Diese gRNA-Bibliothek wurde in eine spezielle Parasitenlinie transfiziert, die eine regulierbare Cas9 Endonuclease (sCas9) exprimiert. Mit diesem Vorgehen wurden erfolgreich Gene identifiziert, die während des asexuellen Lebenszyklus für den Austritt des Parasiten aus der Wirtszelle wichtig sind. Die genauere Charakterisierung von zwei dieser Kandidaten-Gene zeigte, dass diese für die Invasion und den Austritt aus Wirtszellen wesentlich sind. Zudem zeigte sich, dass sie während dieses Prozesses zu unterschiedlichen Zeitpunkten wirken. Der Signalling Linking Factor (SLF) ist ein wesentlicher Bestandteil der GC-Signalkaskade. Dieser ist für die frühe Induktion des Austritts unerlässlich, da er der Ca2+-Signalübertragung vorgeschaltet ist. Ein Knockout von SLF führte zu keinen Veränderungen von F-Aktin nach Induktion mit BIPPO. Ob SLF als Symporter fungiert, ist noch ungewiss. Im Gegensatz dazu zeigte die Charakterisierung des zweiten Gens, dass dieses zu einem späteren Zeitpunkt des Zellaustritts, nach der Ca2+-Signalgebung wirkt und für die Aktivierung der Motilität des Parasiten notwendig ist. Dieses Conoid-Protein wurde als Conoid-Gliding-Protein (CGP) benannt. Bei Induktion des Austritts wird das F-Aktin-Netzwerk zerlegt, dies geschieht jedoch ohne F-Aktin-Akkumulation am Basalpol der Parasiten. Durch proximitätsabhängige Biotinidentifikation (BioID) zeigte sich, dass CGP wahrscheinlich Bestandteil eines Komplexes an den präkonoidalen Ringen ist. Innerhalb dieses Komplexes, der als Gliding Initiation Complex (GIC) benannt wurde, bildet die neuartige Methyltransferase (PCKMT) zusammen mit dem Aktin-Nukleator FRM1 (Formin1) und CGP die Kernkomponenten des Komplexes, während DAP1 (Dispensable

Protein 1) und ICAP16 (Indispensable Conserved Apicomplexan Protein 16) wahrscheinlich als akzessorische Proteine dienen.

Zusammenfassend zeigt diese Studie, dass SLF und CGP für den lytischen Zyklus von *T. gondii* entscheidende Faktoren sind. Ihre zeitliche Regulation beim Austritt des Parasiten aus der Zelle erweitert unser Verständnis des Austrittsmechanismus per se. Die Entdeckung eines neuen präkonoidalen Komplexes, der CGP enthält, bildet die Grundlage für zukünftige Studien, die dessen spezifische Funktion im Rahmen der Motilität des Parasiten aufdecken.

VII. REFERENCE

Agrawal, S., G. G. van Dooren, W. L. Beatty and B. Striepen (2009). "Genetic Evidence that an Endosymbiont-derived Endoplasmic Reticulum-associated Protein Degradation (ERAD) System Functions in Import of Apicoplast Proteins*." Journal of Biological Chemistry 284(48): 33683-33691.

Alexander, D. L., J. Mital, G. E. Ward, P. Bradley and J. C. Boothroyd (2005). "Identification of the moving junction complex of Toxoplasma gondii: a collaboration between distinct secretory organelles." PLoS Pathog 1(2): e17.

Alkema, M., I. J. Reuling, G. M. de Jong, K. Lanke, L. E. Coffeng, G. J. van Gemert, *et al.* (2021). "A Randomized Clinical Trial to Compare Plasmodium falciparum Gametocytemia and Infectivity After Blood-Stage or Mosquito Bite-Induced Controlled Malaria Infection." J Infect Dis 224(7): 1257-1265.

Allen, M. L., J. M. Dobrowolski, H. Muller, L. D. Sibley and T. E. Mansour (1997). "Cloning and characterization of actin depolymerizing factor from Toxoplasma gondii." Mol Biochem Parasitol 88(1-2): 43-52.

Amara, S. G. and J. L. Arriza (1993). "Neurotransmitter transporters: three distinct gene families." Current Opinion in Neurobiology 3(3): 337-344.

Andenmatten, N., S. Egarter, A. J. Jackson, N. Jullien, J. P. Herman and M. Meissner (2013). "Conditional genome engineering

in Toxoplasma gondii uncovers alternative invasion mechanisms." Nat Methods 10(2): 125-127.

Anderson-White, B., J. R. Beck, C. T. Chen, M. Meissner, P. J. Bradley and M. J. Gubbels (2012). "Cytoskeleton assembly in Toxoplasma gondii cell division." Int Rev Cell Mol Biol 298: 1-31.

Aquilini, E., M. M. Cova, S. K. Mageswaran, N. Dos Santos Pacheco, D. Sparvoli, D. M. Penarete-Vargas, *et al.* (2021). "An Alveolata secretory machinery adapted to parasite host cell invasion." Nat Microbiol 6(4): 425-434.

Armstrong, C. M. and D. E. Goldberg (2007). "An FKBP destabilization domain modulates protein levels in Plasmodium falciparum." Nat Methods 4(12): 1007-1009.

Arrizabalaga, G. and J. C. Boothroyd (2004). "Role of calcium during Toxoplasma gondii invasion and egress." Int J Parasitol 34(3): 361-368.

Attias, M., D. E. Teixeira, M. Benchimol, R. C. Vommaro, P. H. Crepaldi and W. De Souza (2020). "The life-cycle of Toxoplasma gondii reviewed using animations." Parasit Vectors 13(1): 588.

Barylyuk, K., L. Koreny, H. Ke, S. Butterworth, O. M. Crook, I. Lassadi, *et al.* (2020). "A Comprehensive Subcellular Atlas of the Toxoplasma Proteome via hyperLOPIT Provides Spatial Context for Protein Functions." Cell Host Microbe 28(5): 752-766.e759.

Beck, J. R., I. A. Rodriguez-Fernandez, J. C. de Leon, M. H. Huynh, V. B. Carruthers, N. S. Morrissette, *et al.* (2010). "A novel

family of Toxoplasma IMC proteins displays a hierarchical organization and functions in coordinating parasite division." PLoS Pathog 6(9): e1001094.

Bednarek, A., S. Wiek, K. Lingelbach and F. Seeber (2003). "Toxoplasma gondii: analysis of the active site insertion of its ferredoxin-NADP(+)-reductase by peptide-specific antibodies and homology-based modeling." Exp Parasitol 103(1-2): 68-77.

Bhandage, A. K. and A. Barragan (2019). "Calling in the Ca(V)alry-Toxoplasma gondii Hijacks GABAergic Signaling and Voltage-Dependent Calcium Channel Signaling for Trojan horse-Mediated Dissemination." Front Cell Infect Microbiol 9: 61.

Bisio, H., M. Lunghi, M. Brochet and D. Soldati-Favre (2019). "Phosphatidic acid governs natural egress in Toxoplasma gondii via a guanylate cyclase receptor platform." Nat Microbiol 4(3): 420-428.

Bisio, H. and D. Soldati-Favre (2019). "Signaling Cascades Governing Entry into and Exit from Host Cells by Toxoplasma gondii." Annu Rev Microbiol 73: 579-599.

Blader, I. J., B. I. Coleman, C. T. Chen and M. J. Gubbels (2015). "Lytic Cycle of Toxoplasma gondii: 15 Years Later." Annu Rev Microbiol 69: 463-485.

Boothroyd, J. C. and J. F. Dubremetz (2008). "Kiss and spit: the dual roles of Toxoplasma rhoptries." Nat Rev Microbiol 6(1): 79-88.

REFERENCES

Borowsky, B. and B. J. Hoffman (1995). Neurotransmitter Transporters: Molecular Biology, Function, and Regulation. International Review of Neurobiology. R. J. Bradley and R. A. Harris, Academic Press. 38: 139-199.

Bouché, N., B. Lacombe and H. Fromm (2003). "GABA signaling: a conserved and ubiquitous mechanism." Trends Cell Biol 13(12): 607-610.

Bradley, P. J., C. Ward, S. J. Cheng, D. L. Alexander, S. Coller, G. H. Coombs, *et al.* (2005). "Proteomic analysis of rhoptry organelles reveals many novel constituents for host-parasite interactions in Toxoplasma gondii." J Biol Chem 280(40): 34245-34258.

Branon, T. C., J. A. Bosch, A. D. Sanchez, N. D. Udeshi, T. Svinkina, S. A. Carr, *et al.* (2018). "Efficient proximity labeling in living cells and organisms with TurboID." Nat Biotechnol 36(9): 880-887.

Brown, K. M., S. Long and L. D. Sibley (2018). "Conditional Knockdown of Proteins Using Auxin-inducible Degron (AID) Fusions in Toxoplasma gondii." Bio Protoc 8(4):e2728.

Bullen, H. E., Y. Jia, Y. Yamaryo-Botté, H. Bisio, O. Zhang, N. K. Jemelin, *et al.* (2016). "Phosphatidic Acid-Mediated Signaling Regulates Microneme Secretion in Toxoplasma." Cell Host Microbe 19(3): 349-360.

Caldas, L. A. and W. de Souza (2018). "A Window to Toxoplasma gondii Egress." Pathogens 7(3):69.

REFERENCES

Carruthers, V. and J. C. Boothroyd (2007). "Pulling together: an integrated model of Toxoplasma cell invasion." Curr Opin Microbiol 10(1): 83-89.

Carruthers, V. B. (2019). "Interrupting Toxoplasma's Regularly Scheduled Program of Egress." Trends Parasitol 35(5): 338-340.

Carruthers, V. B., O. K. Giddings and L. D. Sibley (1999). "Secretion of micronemal proteins is associated with toxoplasma invasion of host cells." Cell Microbiol 1(3): 225-235.

Chaudhry, S. A., N. Gad and G. Koren (2014). "Toxoplasmosis and pregnancy." Can Fam Physician 60(4): 334-336.

Chen, A. L., E. W. Kim, J. Y. Toh, A. A. Vashisht, A. Q. Rashoff, C. Van, *et al.* (2015). "Novel components of the Toxoplasma inner membrane complex revealed by BioID." mBio 6(1): e02357-02314.

Chylinski, K., K. S. Makarova, E. Charpentier and E. V. Koonin (2014). "Classification and evolution of type II CRISPR-Cas systems." Nucleic Acids Res 42(10): 6091-6105.

Coleman, B. I., S. Saha, S. Sato, K. Engelberg, D. J. P. Ferguson, I. Coppens, *et al.* (2018). "A Member of the Ferlin Calcium Sensor Family Is Essential for Toxoplasma gondii Rhoptry Secretion." mBio 9(5).

Collins, C. R., S. Das, E. H. Wong, N. Andenmatten, R. Stallmach, F. Hackett, *et al.* (2013). "Robust inducible Cre recombinase activity in the human malaria parasite Plasmodium falciparum enables efficient gene deletion within a single

asexual erythrocytic growth cycle." Mol Microbiol 88(4): 687-701.

Coppoolse, E. R., M. J. de Vroomen, F. van Gennip, B. J. Hersmus and M. J. van Haaren (2005). "Size does matter: cre-mediated somatic deletion efficiency depends on the distance between the target lox-sites." Plant Mol Biol 58(5): 687-698.

Cova, M. M., M. H. Lamarque and M. Lebrun (2022). "How Apicomplexa Parasites Secrete and Build Their Invasion Machinery." Annu Rev Microbiol 76:619-640.

Cullen, P. J., G. E. Cozier, G. Banting and H. Mellor (2001). "Modular phosphoinositide-binding domains--their role in signalling and membrane trafficking." Curr Biol 11(21): R882-893.

Daher, W., N. Klages, M. F. Carlier and D. Soldati-Favre (2012). "Molecular characterization of Toxoplasma gondii formin 3, an actin nucleator dispensable for tachyzoite growth and motility." Eukaryot Cell 11(3): 343-352.

Daher, W., F. Plattner, M. F. Carlier and D. Soldati-Favre (2010). "Concerted action of two formins in gliding motility and host cell invasion by Toxoplasma gondii." PLoS Pathog 6(10): e1001132.

Das, A. K., P. W. Cohen and D. Barford (1998). "The structure of the tetratricopeptide repeats of protein phosphatase 5: implications for TPR-mediated protein-protein interactions." Embo j 17(5): 1192-1199.

Das, S., J. F. Stortz, M. Meissner and J. Periz (2021). "The multiple functions of actin in apicomplexan parasites." Cell Microbiol: e13345.

REFERENCES

de Leon, J. C., N. Scheumann, W. Beatty, J. R. Beck, J. Q. Tran, C. Yau, *et al.* (2013). "A SAS-6-like protein suggests that the Toxoplasma conoid complex evolved from flagellar components." Eukaryot Cell 12(7): 1009-1019.

Del Rosario, M., J. Periz, G. Pavlou, O. Lyth, F. Latorre-Barragan, S. Das, *et al.* (2019). "Apicomplexan F-actin is required for efficient nuclear entry during host cell invasion." EMBO Rep 20(12): e48896.

Dobrowolski, J. M., I. R. Niesman and L. D. Sibley (1997). "Actin in the parasite Toxoplasma gondii is encoded by a single copy gene, ACT1 and exists primarily in a globular form." Cell Motil Cytoskeleton 37(3): 253-262.

Donahue, C. G., V. B. Carruthers, S. D. Gilk and G. E. Ward (2000). "The Toxoplasma homolog of Plasmodium apical membrane antigen-1 (AMA-1) is a microneme protein secreted in response to elevated intracellular calcium levels." Mol Biochem Parasitol 111(1): 15-30.

Donald, R. G., J. Allocco, S. B. Singh, B. Nare, S. P. Salowe, J. Wiltsie, *et al.* (2002). "Toxoplasma gondii cyclic GMP-dependent kinase: chemotherapeutic targeting of an essential parasite protein kinase." Eukaryot Cell 1(3): 317-328.

Dos Santos Pacheco, N., L. Brusini, R. Haase, N. Tosetti, B. Maco, M. Brochet, *et al.* (2022). "Conoid extrusion regulates glideosome assembly to control motility and invasion in Apicomplexa." Nat Microbiol 7(11): 1777-1790.

Dos Santos Pacheco, N., N. Tosetti, L. Koreny, R. F. Waller and D. Soldati-Favre (2020). "Evolution, Composition, Assembly,

and Function of the Conoid in Apicomplexa." Trends Parasitol 36(8): 688-704.

Dubey, J. P. (2009). "Toxoplasmosis in sheep--the last 20 years." Vet Parasitol 163(1-2): 1-14.

Dubey, J. P., F. H. A. Murata, C. K. Cerqueira-Cézar, O. C. H. Kwok and Y. R. Yang (2020). "Public Health Significance of Toxoplasma gondii Infections in Cattle: 2009-2020." J Parasitol 106(6): 772-788.

Dubois, D. J. and D. Soldati-Favre (2019). "Biogenesis and secretion of micronemes in Toxoplasma gondii." Cell Microbiol 21(5): e13018.

Egarter, S., N. Andenmatten, A. J. Jackson, J. A. Whitelaw, G. Pall, J. A. Black, *et al.* (2014). "The toxoplasma Acto-MyoA motor complex is important but not essential for gliding motility and host cell invasion." PLoS One 9(3): e91819.

Endo, T., K. K. Sethi and G. Piekarski (1982). "Toxoplasma gondii: calcium ionophore A23187-mediated exit of trophozoites from infected murine macrophages." Exp Parasitol 53(2): 179-188.

Engelberg, K., C. T. Chen, T. Bechtel, V. Sánchez Guzmán, A. A. Drozda, S. Chavan, *et al.* (2020). "The apical annuli of Toxoplasma gondii are composed of coiled-coil and signalling proteins embedded in the inner membrane complex sutures." Cell Microbiol 22(1): e13112.

Fei, H., A. Grygoruk, E. S. Brooks, A. Chen and D. E. Krantz (2008). "Trafficking of vesicular neurotransmitter transporters." Traffic 9(9): 1425-1436.

REFERENCES

Francia, M. E., J. F. Dubremetz and N. S. Morrissette (2015). "Basal body structure and composition in the apicomplexans Toxoplasma and Plasmodium." Cilia 5: 3.

Francia, M. E. and B. Striepen (2014). "Cell division in apicomplexan parasites." Nat Rev Microbiol 12(2): 125-136.

Frénal, K., J. F. Dubremetz, M. Lebrun and D. Soldati-Favre (2017). "Gliding motility powers invasion and egress in Apicomplexa." Nat Rev Microbiol 15(11): 645-660.

Frénal, K., D. Jacot, P. M. Hammoudi, A. Graindorge, B. Maco and D. Soldati-Favre (2017). "Myosin-dependent cell-cell communication controls synchronicity of division in acute and chronic stages of Toxoplasma gondii." Nat Commun 8: 15710.

Frénal, K., V. Polonais, J. B. Marq, R. Stratmann, J. Limenitakis and D. Soldati-Favre (2010). "Functional dissection of the apicomplexan glideosome molecular architecture." Cell Host Microbe 8(4): 343-357.

Freppel, W., D. J. P. Ferguson, K. Shapiro, J. P. Dubey, P. H. Puech and A. Dumètre (2019). "Structure, composition, and roles of the Toxoplasma gondii oocyst and sporocyst walls." Cell Surf 5: 100016.

Fruth, I. A. and G. Arrizabalaga (2007). "Toxoplasma gondii: induction of egress by the potassium ionophore nigericin." Int J Parasitol 37(14): 1559-1567.

Fujimori, D. G. (2013). "Radical SAM-mediated methylation reactions." Current opinion in chemical biology 17(4): 597-604.

REFERENCES

Fuks, J. M., R. B. Arrighi, J. M. Weidner, S. Kumar Mendu, Z. Jin, R. P. Wallin, *et al.* (2012). "GABAergic signaling is linked to a hypermigratory phenotype in dendritic cells infected by Toxoplasma gondii." PLoS Pathog 8(12): e1003051.

Gaji, R. Y., D. E. Johnson, M. Treeck, M. Wang, A. Hudmon and G. Arrizabalaga (2015). "Phosphorylation of a Myosin Motor by TgCDPK3 Facilitates Rapid Initiation of Motility during Toxoplasma gondii egress." PLoS Pathog 11(11): e1005268.

Gaskins, E., S. Gilk, N. DeVore, T. Mann, G. Ward and C. Beckers (2004). "Identification of the membrane receptor of a class XIV myosin in Toxoplasma gondii." J Cell Biol 165(3): 383-393.

Graindorge, A., K. Frénal, D. Jacot, J. Salamun, J. B. Marq and D. Soldati-Favre (2016). "The Conoid Associated Motor MyoH Is Indispensable for Toxoplasma gondii Entry and Exit from Host Cells." PLoS Pathog 12(1): e1005388.

Gras, S., A. Jackson, S. Woods, G. Pall, J. Whitelaw, J. M. Leung, *et al.* (2017). "Parasites lacking the micronemal protein MIC2 are deficient in surface attachment and host cell egress, but remain virulent in vivo." Wellcome Open Res 2: 32.

Gras, S., E. Jimenez-Ruiz, C. M. Klinger, K. Schneider, A. Klingl, L. Lemgruber, *et al.* (2019). "An endocytic-secretory cycle participates in Toxoplasma gondii in motility." PLoS Biol 17(6): e3000060.

Griffith, M. B., C. S. Pearce and A. T. Heaslip (2022). "Dense granule biogenesis, secretion, and function in Toxoplasma gondii." J Eukaryot Microbiol: e12904.

REFERENCES

Gubbels, M. J., C. D. Keroack, S. Dangoudoubiyam, H. L. Worliczek, A. S. Paul, C. Bauwens, *et al.* (2020). "Fussing About Fission: Defining Variety Among Mainstream and Exotic Apicomplexan Cell Division Modes." Front Cell Infect Microbiol 10: 269.

Guérin, A., R. M. Corrales, M. L. Parker, M. H. Lamarque, D. Jacot, H. El Hajj, *et al.* (2017). "Efficient invasion by Toxoplasma depends on the subversion of host protein networks." Nat Microbiol 2(10): 1358-1366.

Günay-Esiyok, Ö., U. Scheib, M. Noll and N. Gupta (2019). "An unusual and vital protein with guanylate cyclase and P4-ATPase domains in a pathogenic protist." Life Sci Alliance 2(3):e201900402.

Gustafson, P. V., H. D. Agar and D. I. Cramer (1954). "An electron microscope study of Toxoplasma." Am J Trop Med Hyg 3(6): 1008-1022.

Gutiérrez-Expósito, D., M. C. Arnal, D. Martínez-Durán, J. Regidor-Cerrillo, M. Revilla, D. L Fernández de Luco, *et al.* (2016). "The role of wild ruminants as reservoirs of Besnoitia besnoiti infection in cattle." Veterinary Parasitology 223: 7-13.

Hakimi, M. A., P. Olias and L. D. Sibley (2017). "Toxoplasma Effectors Targeting Host Signaling and Transcription." Clin Microbiol Rev 30(3): 615-645.

Hammoudi, P. M., B. Maco, S. K. Dogga, K. Frénal and D. Soldati-Favre (2018). "Toxoplasma gondii TFP1 is an essential

transporter family protein critical for microneme maturation and exocytosis." Mol Microbiol 109(2):225-244.

Harding, C. R., S. Egarter, M. Gow, E. Jiménez-Ruiz, D. J. Ferguson and M. Meissner (2016). "Gliding Associated Proteins Play Essential Roles during the Formation of the Inner Membrane Complex of Toxoplasma gondii." PLoS Pathog 12(2): e1005403.

Hartmann, J., K. Hu, C. Y. He, L. Pelletier, D. S. Roos and G. Warren (2006). "Golgi and centrosome cycles in Toxoplasma gondii." Mol Biochem Parasitol 145(1): 125-127.

Hassan, M. A., J. J. Vasquez, C. Guo-Liang, M. Meissner and T. Nicolai Siegel (2017). "Comparative ribosome profiling uncovers a dominant role for translational control in Toxoplasma gondii." BMC Genomics 18(1): 961.

Heaslip, A. T., M. Nishi, B. Stein and K. Hu (2011). "The motility of a human parasite, Toxoplasma gondii, is regulated by a novel lysine methyltransferase." PLoS Pathog 7(9): e1002201.

Herm-Götz, A., C. Agop-Nersesian, S. Münter, J. S. Grimley, T. J. Wandless, F. Frischknecht, *et al.* (2007). "Rapid control of protein level in the apicomplexan Toxoplasma gondii." Nat Methods 4(12): 1003-1005.

Hill, D. and J. P. Dubey (2002). "Toxoplasma gondii: transmission, diagnosis and prevention." Clin Microbiol Infect 8(10): 634-640.

Hoff, E. F. and V. B. Carruthers (2002). "Is Toxoplasma egress the first step in invasion?" Trends Parasitol 18(6): 251-255.

REFERENCES

Hu, K., J. Johnson, L. Florens, M. Fraunholz, S. Suravajjala, C. DiLullo, *et al.* (2006). "Cytoskeletal components of an invasion machine--the apical complex of Toxoplasma gondii." PLoS Pathog 2(2): e13.

Hu, K., T. Mann, B. Striepen, C. J. Beckers, D. S. Roos and J. M. Murray (2002). "Daughter cell assembly in the protozoan parasite Toxoplasma gondii." Mol Biol Cell 13(2): 593-606.

Hunt, A., M. R. G. Russell, J. Wagener, R. Kent, R. Carmeille, C. J. Peddie, *et al.* (2019). "Differential requirements for cyclase-associated protein (CAP) in actin-dependent processes of Toxoplasma gondii." Elife 8:e50598.

Hunter, C. A. and L. D. Sibley (2012). "Modulation of innate immunity by Toxoplasma gondii virulence effectors." Nat Rev Microbiol 10(11): 766-778.

Huynh, M. H. and V. B. Carruthers (2009). "Tagging of endogenous genes in a Toxoplasma gondii strain lacking Ku80." Eukaryot Cell 8(4): 530-539.

Jacot, D., N. Tosetti, I. Pires, J. Stock, A. Graindorge, Y. F. Hung, *et al.* (2016). "An Apicomplexan Actin-Binding Protein Serves as a Connector and Lipid Sensor to Coordinate Motility and Invasion." Cell Host Microbe 20(6): 731-743.

Jelenska, J., M. J. Crawford, O. S. Harb, E. Zuther, R. Haselkorn, D. S. Roos, *et al.* (2001). "Subcellular localization of acetyl-CoA carboxylase in the apicomplexan parasite Toxoplasma gondii." Proc Natl Acad Sci U S A 98(5): 2723-2728.

Jullien, N., F. Sampieri, A. Enjalbert and J. P. Herman (2003). "Regulation of Cre recombinase by ligand-induced

complementation of inactive fragments." Nucleic Acids Res 31(21): e131.

Kafsack, B. F., J. D. Pena, I. Coppens, S. Ravindran, J. C. Boothroyd and V. B. Carruthers (2009). "Rapid membrane disruption by a perforin-like protein facilitates parasite exit from host cells." Science 323(5913): 530-533.

Katris, N. J., G. G. van Dooren, P. J. McMillan, E. Hanssen, L. Tilley and R. F. Waller (2014). "The apical complex provides a regulated gateway for secretion of invasion factors in Toxoplasma." PLoS Pathog 10(4): e1004074.

Kessler, H., A. Herm-Götz, S. Hegge, M. Rauch, D. Soldati-Favre, F. Frischknecht, *et al.* (2008). "Microneme protein 8--a new essential invasion factor in Toxoplasma gondii." J Cell Sci 121(Pt 7): 947-956.

Khan, A., J. S. Shaik and M. E. Grigg (2018). "Genomics and molecular epidemiology of Cryptosporidium species." Acta Trop 184: 1-14.

Konstantinovic, N., H. Guegan, T. Stäjner, S. Belaz and F. Robert-Gangneux (2019). "Treatment of toxoplasmosis: Current options and future perspectives." Food Waterborne Parasitol 15: e00036.

Koreny, L., M. Zeeshan, K. Barylyuk, E. C. Tromer, J. J. E. van Hooff, D. Brady, *et al.* (2021). "Molecular characterization of the conoid complex in Toxoplasma reveals its conservation in all apicomplexans, including Plasmodium species." PLoS Biol 19(3): e3001081.

REFERENCES

Kremer, K., D. Kamin, E. Rittweger, J. Wilkes, H. Flammer, S. Mahler, *et al.* (2013). "An overexpression screen of Toxoplasma gondii Rab-GTPases reveals distinct transport routes to the micronemes." PLoS Pathog 9(3): e1003213.

Kur, J., L. Holec-Gasior and E. Hiszczyńska-Sawicka (2009). "Current status of toxoplasmosis vaccine development." Expert Rev Vaccines 8(6): 791-808.

Lemmon, M. A., K. M. Ferguson and C. S. Abrams (2002). "Pleckstrin homology domains and the cytoskeleton." FEBS Lett 513(1): 71-76.

Lentini, G., R. Ben Chaabene, O. Vadas, C. Ramakrishnan, B. Mukherjee, V. Mehta, *et al.* (2021). "Structural insights into an atypical secretory pathway kinase crucial for Toxoplasma gondii invasion." Nat Commun 12(1): 3788.

Leung, J. M., Y. He, F. Zhang, Y.-C. Hwang, E. Nagayasu, J. Liu, *et al.* (2017). "Stability and function of a putative microtubule-organizing center in the human parasite Toxoplasma gondii." Molecular biology of the cell 28(10): 1361-1378.

Leung, J. M., J. Liu, L. A. Wetzel and K. Hu (2019). "Centrin2 from the human parasite Toxoplasma gondii is required for its invasion and intracellular replication." J Cell Sci 132(13).

Leung, J. M., M. A. Rould, C. Konradt, C. A. Hunter and G. E. Ward (2014). "Disruption of TgPHIL1 alters specific parameters of Toxoplasma gondii motility measured in a quantitative, three-dimensional live motility assay." PLoS One 9(1): e85763.

REFERENCES

Li, W., J. Grech, J. F. Stortz, M. Gow, J. Periz, M. Meissner, *et al.* (2022). "A splitCas9 phenotypic screen in Toxoplasma gondii identifies proteins involved in host cell egress and invasion." Nat Microbiol 7(6): 882-895.

Long, S., B. Anthony, L. L. Drewry and L. D. Sibley (2017). "A conserved ankyrin repeat-containing protein regulates conoid stability, motility and cell invasion in Toxoplasma gondii." Nat Commun 8(1): 2236.

Long, S., K. M. Brown, L. L. Drewry, B. Anthony, I. Q. H. Phan and L. D. Sibley (2017). "Calmodulin-like proteins localized to the conoid regulate motility and cell invasion by Toxoplasma gondii." PLoS Pathog 13(5): e1006379.

López-Osorio, S., J. J. Chaparro-Gutiérrez and L. M. Gómez-Osorio (2020). "Overview of Poultry Eimeria Life Cycle and Host-Parasite Interactions." Front Vet Sci 7: 384.

Lopez, J. M., I. F. Tengganu, J. Liu, J. Murray, L. F. Arias Padilla, Y. Zhang, *et al.* (2022). "An apical protein, Pcr2, is required for persistent movement by the human parasite Toxoplasma gondii." PLoS Pathog 18(8): e1010776.

Los, G. V., L. P. Encell, M. G. McDougall, D. D. Hartzell, N. Karassina, C. Zimprich, *et al.* (2008). "HaloTag: a novel protein labeling technology for cell imaging and protein analysis." ACS Chem Biol 3(6): 373-382.

Lourido, S., J. Shuman, C. Zhang, K. M. Shokat, R. Hui and L. D. Sibley (2010). "Calcium-dependent protein kinase 1 is an essential regulator of exocytosis in Toxoplasma." Nature 465(7296): 359-362.

REFERENCES

MacRae, J. I., L. Sheiner, A. Nahid, C. Tonkin, B. Striepen and M. J. McConville (2012). "Mitochondrial metabolism of glucose and glutamine is required for intracellular growth of Toxoplasma gondii." Cell Host Microbe 12(5): 682-692.

Mallo, N., J. Ovciarikova, E. S. Martins-Duarte, S. C. Baehr, M. Biddau, M. L. Wilde, *et al.* (2021). "Depletion of a Toxoplasma porin leads to defects in mitochondrial morphology and contacts with the ER." J Cell Sci 134(20):jcs255299

Mann, T. and C. Beckers (2001). "Characterization of the subpellicular network, a filamentous membrane skeletal component in the parasite Toxoplasma gondii." Mol Biochem Parasitol 115(2): 257-268.

Mathieson, S., C. C. Lin, M. Underwood and S. Eldabe (2020). "Pregabalin and gabapentin for pain." Bmj 369: m1315.

Mazumdar, J., H. W. E, K. Masek, A. H. C and B. Striepen (2006). "Apicoplast fatty acid synthesis is essential for organelle biogenesis and parasite survival in Toxoplasma gondii." Proc Natl Acad Sci U S A 103(35): 13192-13197.

McCoy, J. M., L. Whitehead, G. G. van Dooren and C. J. Tonkin (2012). "TgCDPK3 regulates calcium-dependent egress of Toxoplasma gondii from host cells." PLoS Pathog 8(12): e1003066.

McDonald, C., D. Smith, M. Di Cristina, G. Kannan, Z. Dou and V. B. Carruthers (2020). "Toxoplasma Cathepsin Protease B and Aspartyl Protease 1 Are Dispensable for Endolysosomal Protein Digestion." mSphere 5(1):e00869-19

REFERENCES

McFadden, G. I. and E. Yeh (2017). "The apicoplast: now you see it, now you don't." Int J Parasitol 47(2-3): 137-144.

Mehta, S. and L. D. Sibley (2010). "Toxoplasma gondii actin depolymerizing factor acts primarily to sequester G-actin." J Biol Chem 285(9): 6835-6847.

Meissner, M., D. Schlüter and D. Soldati (2002). "Role of Toxoplasma gondii myosin A in powering parasite gliding and host cell invasion." Science 298(5594): 837-840.

Moudy, R., T. J. Manning and C. J. Beckers (2001). "The loss of cytoplasmic potassium upon host cell breakdown triggers egress of Toxoplasma gondii." J Biol Chem 276(44): 41492-41501.

Nagamune, K., W. L. Beatty and L. D. Sibley (2007). "Artemisinin induces calcium-dependent protein secretion in the protozoan parasite Toxoplasma gondii." Eukaryot Cell 6(11): 2147-2156.

Nagamune, K., L. M. Hicks, B. Fux, F. Brossier, E. N. Chini and L. D. Sibley (2008). "Abscisic acid controls calcium-dependent egress and development in Toxoplasma gondii." Nature 451(7175): 207-210.

Nagy, A. (2000). "Cre recombinase: the universal reagent for genome tailoring." Genesis 26(2): 99-109.

Nair, S. C., C. F. Brooks, C. D. Goodman, A. Sturm, G. I. McFadden, S. Sundriyal, *et al.* (2011). "Apicoplast isoprenoid precursor synthesis and the molecular basis of fosmidomycin resistance in Toxoplasma gondii." J Exp Med 208(7): 1547-1559.

REFERENCES

Nicolle, C. and L. Manceaux (1908). "Sur une infection á corps de Leishman (ou organismes voisons) du gondi."

Nishi, M., K. Hu, J. M. Murray and D. S. Roos (2008). "Organellar dynamics during the cell cycle of Toxoplasma gondii." J Cell Sci 121(Pt 9): 1559-1568.

Otto, T. D., D. Wilinski, S. Assefa, T. M. Keane, L. R. Sarry, U. Böhme, *et al.* (2010). "New insights into the blood-stage transcriptome of Plasmodium falciparum using RNA-Seq." Mol Microbiol 76(1): 12-24.

Padgett, L. R., J. M. Lentini, M. J. Holmes, K. L. Stilger, D. Fu and W. J. Sullivan, Jr. (2018). "Elp3 and RlmN: A tale of two mitochondrial tail-anchored radical SAM enzymes in Toxoplasma gondii." PLoS One 13(1): e0189688.

Peng, D. and R. Tarleton (2015). "EuPaGDT: a web tool tailored to design CRISPR guide RNAs for eukaryotic pathogens." Microb Genom 1(4): e000033.

Periz, J., M. Del Rosario, A. McStea, S. Gras, C. Loney, L. Wang, *et al.* (2019). "A highly dynamic F-actin network regulates transport and recycling of micronemes in Toxoplasma gondii vacuoles." Nat Commun 10(1): 4183.

Periz, J., J. Whitelaw, C. Harding, S. Gras, M. I. Del Rosario Minina, F. Latorre-Barragan, *et al.* (2017). "Toxoplasma gondii F-actin forms an extensive filamentous network required for material exchange and parasite maturation." Elife 6: e24119.

Pieperhoff, M. S., G. S. Pall, E. Jiménez-Ruiz, S. Das, C. Melatti, M. Gow, *et al.* (2015). "Conditional U1 Gene Silencing in Toxoplasma gondii." PLoS One 10(6): e0130356.

REFERENCES

Portes, J., E. Barrias, R. Travassos, M. Attias and W. de Souza (2020). "Toxoplasma gondii Mechanisms of Entry Into Host Cells." Front Cell Infect Microbiol 10: 294.

Pramod, A. B., J. Foster, L. Carvelli and L. K. Henry (2013). "SLC6 transporters: structure, function, regulation, disease association and therapeutics." Molecular aspects of medicine 34(2-3): 197-219.

Rajendran, E., S. V. Hapuarachchi, C. M. Miller, S. J. Fairweather, Y. Cai, N. C. Smith, *et al.* (2017). "Cationic amino acid transporters play key roles in the survival and transmission of apicomplexan parasites." Nat Commun 8: 14455.

Ramesh, S. A., S. D. Tyerman, M. Gilliham and B. Xu (2017). "γ-Aminobutyric acid (GABA) signalling in plants." Cell Mol Life Sci 74(9): 1577-1603.

Reiss, M., N. Viebig, S. Brecht, M. N. Fourmaux, M. Soete, M. Di Cristina, *et al.* (2001). "Identification and characterization of an escorter for two secretory adhesins in Toxoplasma gondii." J Cell Biol 152(3): 563-578.

Ren, J., L. Wen, X. Gao, C. Jin, Y. Xue and X. Yao (2009). "DOG 1.0: illustrator of protein domain structures." Cell Res 19(2): 271-273.

Robert-Gangneux, F. and M. L. Dardé (2012). "Epidemiology of and diagnostic strategies for toxoplasmosis." Clin Microbiol Rev 25(2): 264-296.

Rorman, E., C. S. Zamir, I. Rilkis and H. Ben-David (2006). "Congenital toxoplasmosis--prenatal aspects of Toxoplasma gondii infection." Reprod Toxicol 21(4): 458-472.

REFERENCES

Saadatnia, G. and M. Golkar (2012). "A review on human toxoplasmosis." Scand J Infect Dis 44(11): 805-814.

Sahoo, N., W. Beatty, J. Heuser, D. Sept and L. D. Sibley (2006). "Unusual kinetic and structural properties control rapid assembly and turnover of actin in the parasite Toxoplasma gondii." Mol Biol Cell 17(2): 895-906.

Salamun, J., J. P. Kallio, W. Daher, D. Soldati-Favre and I. Kursula (2014). "Structure of Toxoplasma gondii coronin, an actin-binding protein that relocalizes to the posterior pole of invasive parasites and contributes to invasion and egress." Faseb j 28(11): 4729-4747.

Sander, J. D. and J. K. Joung (2014). "CRISPR-Cas systems for editing, regulating and targeting genomes." Nat Biotechnol 32(4): 347-355.

Sato, S. (2011). "The apicomplexan plastid and its evolution." Cell Mol Life Sci 68(8): 1285-1296.

Serpeloni, M., E. Jiménez-Ruiz, N. M. Vidal, C. Kroeber, N. Andenmatten, L. Lemgruber, *et al.* (2016). "UAP56 is a conserved crucial component of a divergent mRNA export pathway in Toxoplasma gondii." Mol Microbiol 102(4): 672-689.

Shapiro, R. (2001). "Cytoplasmic ribonuclease inhibitor." Methods Enzymol 341: 611-628.

Shen, B., K. M. Brown, T. D. Lee and L. D. Sibley (2014). "Efficient gene disruption in diverse strains of Toxoplasma gondii using CRISPR/CAS9." mBio 5(3): e01114-01114.

REFERENCES

Shen, B., K. M. Brown, T. D. Lee and L. D. Sibley (2014). "Efficient gene disruption in diverse strains of Toxoplasma gondii using CRISPR/CAS9." mBio 5(3): e01114.

Shen, B., J. S. Buguliskis, T. D. Lee and L. D. Sibley (2014). "Functional analysis of rhomboid proteases during Toxoplasma invasion." mBio 5(5): e01795-01714.

Shi, L., M. Quick, Y. Zhao, H. Weinstein and J. A. Javitch (2008). "The mechanism of a neurotransmitter:sodium symporter--inward release of Na+ and substrate is triggered by substrate in a second binding site." Molecular cell 30(6): 667-677.

Shortt, E., C. G. Hackett, R. V. Stadler, G. E. Ward and S. Lourido (2022). "CDPK2A and CDPK1 form a signaling module upstream of Toxoplasma motility." bioRxiv: 2022.2007.2019.500742.

Sidik, S. M., C. G. Hackett, F. Tran, N. J. Westwood and S. Lourido (2014). "Efficient genome engineering of Toxoplasma gondii using CRISPR/Cas9." PLoS One 9(6): e100450.

Sidik, S. M., M. A. Hortua Triana, A. S. Paul, M. El Bakkouri, C. G. Hackett, F. Tran, *et al.* (2016). "Using a Genetically Encoded Sensor to Identify Inhibitors of Toxoplasma gondii Ca2+ Signaling." J Biol Chem 291(18): 9566-9580.

Sidik, S. M., D. Huet, S. M. Ganesan, M. H. Huynh, T. Wang, A. S. Nasamu, *et al.* (2016). "A Genome-wide CRISPR Screen in Toxoplasma Identifies Essential Apicomplexan Genes." Cell 166(6): 1423-1435.e1412.

REFERENCES

Sidik, S. M., D. Huet and S. Lourido (2018). "CRISPR-Cas9-based genome-wide screening of Toxoplasma gondii." Nat Protoc 13(1): 307-323.

Singer, M., K. Simon, I. Forné and M. Meissner (2023). " A central CRMP complex essential for invasion in Toxoplasma gondii." PLoS Biol 21(1): e3001937.

Sivagurunathan, S., A. Heaslip, J. Liu and K. Hu (2013). "Identification of functional modules of AKMT, a novel lysine methyltransferase regulating the motility of Toxoplasma gondii." Mol Biochem Parasitol 189(1-2): 43-53.

Smith, T. A., G. S. Lopez-Perez, A. L. Herneisen, E. Shortt and S. Lourido (2022). "Screening the Toxoplasma kinome with high-throughput tagging identifies a regulator of invasion and egress." Nature Microbiology 7(6):868-881.

Song, R., Q. Wang, F. Guo, X. Liu, S. Song, C. Chen, *et al.* (2018). "Detection of Babesia spp., Theileria spp. and Anaplasma ovis in Border Regions, northwestern China." Transbound Emerg Dis 65(6): 1537-1544.

Sponseller, J. K., J. K. Griffiths and S. Tzipori (2014). "The evolution of respiratory Cryptosporidiosis: evidence for transmission by inhalation." Clin Microbiol Rev 27(3): 575-586.

Stelzer, S., W. Basso, J. Benavides Silván, L. M. Ortega-Mora, P. Maksimov, J. Gethmann, *et al.* (2019). "Toxoplasma gondii infection and toxoplasmosis in farm animals: Risk factors and economic impact." Food Waterborne Parasitol 15: e00037.

REFERENCES

Stommel, E. W., K. H. Ely, J. D. Schwartzman and L. H. Kasper (1997). "Toxoplasma gondii: dithiol-induced Ca2+ flux causes egress of parasites from the parasitophorous vacuole." Exp Parasitol 87(2): 88-97.

Stortz, J. F., M. Del Rosario, M. Singer, J. M. Wilkes, M. Meissner and S. Das (2019). "Formin-2 drives polymerisation of actin filaments enabling segregation of apicoplasts and cytokinesis in Plasmodium falciparum." Elife 8: e49030.

Straub, K. W., S. J. Cheng, C. S. Sohn and P. J. Bradley (2009). "Novel components of the Apicomplexan moving junction reveal conserved and coccidia-restricted elements." Cell Microbiol 11(4): 590-603.

Striepen, B., C. Y. He, M. Matrajt, D. Soldati and D. S. Roos (1998). "Expression, selection, and organellar targeting of the green fluorescent protein in Toxoplasma gondii." Mol Biochem Parasitol 92(2): 325-338.

Suarez, C., G. Lentini, R. Ramaswamy, M. Maynadier, E. Aquilini, L. Berry-Sterkers, *et al.* (2019). "A lipid-binding protein mediates rhoptry discharge and invasion in Plasmodium falciparum and Toxoplasma gondii parasites." Nat Commun 10(1): 4041.

Sweeney, K. R., N. S. Morrissette, S. LaChapelle and I. J. Blader (2010). "Host cell invasion by Toxoplasma gondii is temporally regulated by the host microtubule cytoskeleton." Eukaryot Cell 9(11): 1680-1689.

REFERENCES

Tardieux, I. and J. Baum (2016). "Reassessing the mechanics of parasite motility and host-cell invasion." J Cell Biol 214(5): 507-515.

Tosetti, N., N. Dos Santos Pacheco, E. Bertiaux, B. Maco, L. Bournonville, V. Hamel, *et al.* (2020). "Essential function of the alveolin network in the subpellicular microtubules and conoid assembly in Toxoplasma gondii." Elife 9: e56635.

Tosetti, N., N. Dos Santos Pacheco, D. Soldati-Favre and D. Jacot (2019). "Three F-actin assembly centers regulate organelle inheritance, cell-cell communication and motility in Toxoplasma gondii." Elife 8: e42669.

Tyanova, S., T. Temu, P. Sinitcyn, A. Carlson, M. Y. Hein, T. Geiger, *et al.* (2016). "The Perseus computational platform for comprehensive analysis of (prote)omics data." Nat Methods 13(9): 731-740.

Van Duyne, G. D. (2015). "Cre Recombinase." Microbiol Spectr 3(1): Mdna3-0014-2014.

Vartak, S. V., H. A. Swarup, V. Gopalakrishnan, V. K. Gopinatha, V. Ropars, M. Nambiar, *et al.* (2018). "Autocyclized and oxidized forms of SCR7 induce cancer cell death by inhibiting nonhomologous DNA end joining in a Ligase IV dependent manner." Febs j 285(21): 3959-3976.

Venugopal, K. and S. Marion (2018). "Secretory organelle trafficking in Toxoplasma gondii: A long story for a short travel." Int J Med Microbiol 308(7): 751-760.

Vinayak, S., M. C. Pawlowic, A. Sateriale, C. F. Brooks, C. J. Studstill, Y. Bar-Peled, *et al.* (2015). "Genetic modification of the

diarrhoeal pathogen Cryptosporidium parvum." Nature 523(7561): 477-480.

Waldman, B. S., D. Schwarz, M. H. Wadsworth, 2nd, J. P. Saeij, A. K. Shalek and S. Lourido (2020). "Identification of a Master Regulator of Differentiation in Toxoplasma." Cell 180(2): 359-372.e316.

Wang, J.-L., S.-Y. Huang, M. S. Behnke, K. Chen, B. Shen and X.-Q. Zhu (2016). "The Past, Present, and Future of Genetic Manipulation in Toxoplasma gondii." Trends in Parasitology 32(7): 542-553.

Whitelaw, J. A., F. Latorre-Barragan, S. Gras, G. S. Pall, J. M. Leung, A. Heaslip, *et al.* (2017). "Surface attachment, promoted by the actomyosin system of Toxoplasma gondii is important for efficient gliding motility and invasion." BMC Biol 15(1): 1.

Yang, L., A. D. Uboldi, S. Seizova, M. L. Wilde, M. J. Coffey, N. J. Katris, *et al.* (2019). "An apically located hybrid guanylate cyclase-ATPase is critical for the initiation of Ca(2+) signaling and motility in Toxoplasma gondii." J Biol Chem 294(22): 8959-8972.

Yao, L., Y. Kawakami and T. Kawakami (1994). "The pleckstrin homology domain of Bruton tyrosine kinase interacts with protein kinase C." Proc Natl Acad Sci U S A 91(19): 9175-9179.

Zetsche, B., S. E. Volz and F. Zhang (2015). "A split-Cas9 architecture for inducible genome editing and transcription modulation." Nat Biotechnol 33(2): 139-142.

REFERENCES

Zeytuni, N. and R. Zarivach (2012). "Structural and functional discussion of the tetra-trico-peptide repeat, a protein interaction module." Structure 20(3): 397-405.

Zheng, B., M. Sage, E. A. Sheppeard, V. Jurecic and A. Bradley (2000). "Engineering mouse chromosomes with Cre-loxP: range, efficiency, and somatic applications." Molecular and cellular biology 20(2): 648-655.

Zintl, A., G. Mulcahy, H. E. Skerrett, S. M. Taylor and J. S. Gray (2003). "Babesia divergens, a bovine blood parasite of veterinary and zoonotic importance." Clin Microbiol Rev 16(4): 622-636.

VIII. APPENDIX

1. Supplementary Information for movies.

Movie 1. CGP and SLF gliding motility revealed by time-lapsed microscopy. a-c) Motility of non-induced KO and CGP-depleted parasites. a) CGP non-induced KO parasites showing a normal gliding. b) CGP-lacking parasites was not capable of gliding. c) CGP-depleted parasites showing a minimal displacement. d-f) Motility of non-induced KO and SLF-depleted parasites. d) SLF non-induced KO parasites showing a normal gliding. e) SLF-depleted parasite attached badly to the FCS-coated surface. f) An example of SLF cKO parasites showed no movement but attached to the surface. Time displayed as minute: second. Scale bar: 5 µm.

Movie 2. Motility of SLF cKO parasite in the presence of Ci A23187. a) loxP*slf*-Halo parasite gliding in the presence of Ci A23187. b) An example of SLF cKO parasite was able to glide. Time displayed as minute: second. Scale bar: 5 µm.

Movie 3. Egress of loxP*slf*-Halo parasites expressing CbEm (loxP*slf*-Halo/CbEm). a-c) loxP*slf*-Halo/CbEm parasites stimulated egress with BIPPO (a), Ci A23187 (b), and propranolol (c) caused parasite efficient egress. d-g) SLF cKO parasites stimulated egress with BIPPO (d), Ci A23187 (e-f), and propranolol (g). d) SLF-lacking parasite showing a defect in egress with intact F-actin network. e) SLF cKO were able to egress with collapsed F-actin network. f) SLF-depleted parasites fail to escape from host cells although with

depolymerised F-actin network. g) SLF-lacking parasites showing a defect in egress stimulated with propranolol. Time displayed as minute: second. Scale bar: 5 μm.

Movie 4. Egress of loxP*cgp*-Halo parasites expressing CbEm (loxP*cgp*-Halo/CbEm). a-c) loxP*cgp*-Halo/CbEm parasites stimulated egress with BIPPO (a), Ci A23187 (b), and propranolol (c) caused parasite efficient egress. d-f) CGP cKO parasites stimulated egress with BIPPO (d), Ci A23187 (e) and propranolol (f) showed parasites were not able to leave host cells although F-actin networks disassembled. Time displayed as minute: second. Scale bar: 5 μm.

Movie 5. PVM integrity of parasites transiently expressing SAG1ΔGPI-dsRed triggered with BIPPO. a-b) Non-rapamycin-induced parasites showing an egress with dsRed signal (magenta) diffused to host cell cytoplasm indicating lysis of PVM. c) CGP cKO parasites lysed the PVM as illustrated by diffusion of dsRed signal. d) SLF cKO parasites PVM remained intact revealed by dsRed signal trapped within PVM. F-actin: yellow. SAG1ΔGPI-dsRed: magenta. Time displayed as minute: second. Scale bar: 5 μm.

IX. ACKNOWLEDGEMENT

To all of the people who have helped and supported me in any way throughout my bittersweet PhD studies in Germany, I am so grateful to finally be able to write this acknowledgement, despite the fact that the words cannot adequately express how much gratitude and respect I feel for you all. In particular, so many thanks to:

Prof. Markus Meissner for allowing me to work in this lab and for providing enough money to make this research possible. As a supervisor, he gives me lots of guidance and constructive suggestions on the projects, as well as thesis writing and revision. In addition, his encouragement helps me overcome difficulties and make progress. I admire his scientific thinking, academic attitude, and broad knowledge. This influence will be with me throughout my life.

Dr. Elena Jimenez-Ruiz for supervising my experiments, data analysis, project guidance and my dissertation revision. As my second supervisor, she makes every effort to guide me, which propels me forward. I appreciate this very much.

All people in Experimental parasitology. Thanks to Mirko Singer, Simon Gras, Javier Periz, Sujaan Das, Matthew Gow, Maresa Watzlowik, Mirjam Wagner, and Julia von Knoerzer-Suckow, Kathrin Simon who gave me assistance and advice on my project. Thanks to Janessa Grech, Miriam Rafajlovic, PeiPei Qin and Yuan Song, for your love, care, and assistance with lab work. Thank you, Marzena Broniszewska, for providing me with host cells and for being a

mother-like presence in Germany. Thanks, Adelheid Ackermann and Derschum Angelika for helping administrative issues.

China Scholarship Council (CSC) for supporting my stay here in Germany. Without this support, I won't be able to live in Germany for my PhD studies.

My parents, my love and my friends who back me up in pursuing my PhD in Germany. Your encouragement and support always make me feel strong and bold enough to tackle any difficulty, which fuels me to keep going. Thanks for their endless love.